Fall 2012

Real-time analysis of brain tumor cell dynamics: Novel thermoelectric detection of L-glutamate and cell metabolism using microfluidics

Siva Mahesh Tangutooru

REAL-TIME ANALYSIS OF BRAIN TUMOR CELL DYNAMICS:

NOVEL THERMOELECTRIC DETECTION OF

L-GLUTAMATE AND CELL

METABOLISM USING

MICROFLUIDICS

by

Siva Mahesh Tangutooru, B. E.

A Dissertation Presented in Partial Fulfillment
of the Requirements of the Degree
Doctor of Philosophy

COLLEGE OF ENGINEERING AND SCIENCE
LOUISIANA TECH UNIVERSITY

November, 2012

UMI Number: 3534293

UMI®

Dissertation Publishing

ProQuest®

LOUISIANA TECH UNIVERSITY

THE GRADUATE SCHOOL
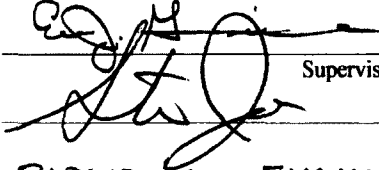
September 17, 2012
_____
Date

We hereby recommend that the thesis prepared under our supervision

by Siva Mahesh Tangutooru, B.E.
_____

entitled _____

Real-Time Analysis of Brain Tumor Cell Dynamics: Novel

Thermoelectric Detection of L-Glutamate and Cell Metabolism

using Microfluidics

_____

be accepted in partial fulfillment of the requirements for the Degree of

Doctor of Philosophy in Biomedical Engineering

_____
Supervisor of Thesis Research

_____
Head of Department

BIOMEDICAL ENGINEERING
_____
Department

Recommendation concurred in:

_____

_____

Advisory Committee

Approved:

_____
Director of Graduate Studies

Approved:

_____
Dean of the Graduate School

_____
Dean of the College

ABSTRACT

This study describes the design, fabrication and applications of a novel thermoelectric microfluidic bio-sensor. The bio-sensor is used for real time detection of the L-glut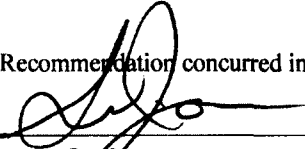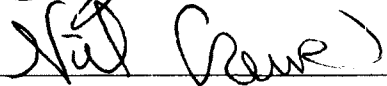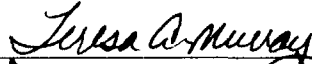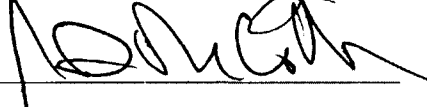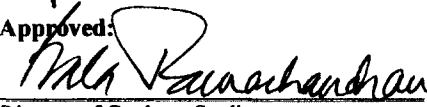amate (L-glu) dynamics and metabolism for brain tumor cells immobilized in a microfluidic device. The microfluidic device is fabricated using a polymer/glass laminating technique (Xurography). An antimony-bismuth thin-film thermopile (primary sensing element) is integrated to the microfluidic device. The brain tumor cells are immobilized over the thermopile covering measuring and reference junctions of the thermopile using a poly-l-lysine coating layer. L-glutamate oxidase (L-GLOD) is immobilized over the measuring junctions of the thermopile prior to the immobilization of the cells using Layer-by-layer self-assembly. The thermoelectric L-glu sensor measures the heat produced due to the reaction of L-glu released from immobilized brain tumor cells in the presence of L-GLOD. The immobilized brain tumor cells are stimulated using potassium chloride (kcl) and ionomycin to study the dynamics of L-glu release from the cells. The stimulators increase the release of L-glu from the brain cells, which mimics pathological conditions. The thermoelectric sensor is also used to measure the heat produced by normal metabolic activity of the brain tumor cells. The metabolism from the cells is measured by detecting the decrease in the metabolic rate followed by stopping the glucose supply.

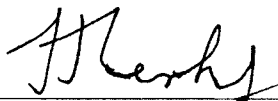The novel design of the microfluidic biosensor has two inlets, in which the fluid from one inlet is hydro dynamically focused by the fluid from the other inlet. The width of the focused fluid depends on the ratio of the inlet's flow rates. This way the hydro dynamically focused fluid flows only over measuring junctions of the thermopile without controlling the temperature of the reference junctions (the thermopile has measuring and reference junctions). Hence, the reaction zone in the microfluidic device is limited to the measuring junctions of the thermopile.

The measured sensitivity of the thermopile is 7 mV $(^\circ C)^{-1}$ and the heat sensitivity of the biosensor device is 0.165 W $(^\circ C)^{-1}$ or 23.57 W $(V)^{-1}$. The thermoelectric L-glu sensor system is calibrated by injecting known concentrations of L-glu samples. The effect of multiple layers of immobilized L-GLOD layers is studied. Two layers of L-GLOD produced a higher response than one layer of L-GLOD. The sensitivity of the thermoelectric L-glu sensor is 0.6 μVs (mg dL^{-1})$^{-1}$ in the linear range of 0.1-50 mg dL^{-1} with an R^2 value of 0.9998. The lowest detection limit of the L-glu sensor is 0.1 mg dL^{-1}. The L-glu sensor detected the release of L-glu from the cultured brain tumor cells after stimulating with 50 mM potassium chloride. The cells released L-glu for 30 seconds after the stimulus was applied. The release and uptake of 1.22 mg dL^{-1} L-glu concentration is detected. The results of L-glu released from the cells were also compared with the fluorescence-based assay tests. Experiments were also performed to detect the heat from brain tumor cell metabolism. The heat production of the brain tumor cells metabolism in anaerobic conditions detected by the thermoelectric metabolism sensor is 54 pW per cell. The developed thermoelectric biosensor sensor that employs simple fabrication, is highly sensitive, and operates at low sample volumes.

APPROVAL FOR SCHOLARLY DISSEMINATION

The author grants to the Prescott Memorial Library of Louisiana Tech University

the right to reproduce, by appropriate methods, upon request, any or all portions of this

Dissertation. It is understood that "proper request" consists of the agreement, on the part

of the requesting party, that said reproduction is for his personal use and that subsequent

reproduction will not occur without written approval of the author of this Dissertation.

Further, any portions of the Dissertation used in books, papers, and other works must be

appropriately referenced to this Dissertation.

Finally, the author of this Dissertation reserves the right to publish freely, in the

literature, at any time, any or all portions of this Dissertation.

Author _____

Date _____

DEDICATION

To my

Mother, Hemalatha Tangutooru;

Father, Viswanatham Tangutooru;

Sister, Swathi Tangutooru;

Aunt, Saradamma Tangutooru;

Uncle, Prakasham Panthulu Tangutooru

and

Grandparents.

TABLE OF CONTENTS

LIST OF FIGURES

LIST OF TABLES

ACKNOWLEDGMENTS

Vishwa Priya. She helped me to concentrate on completing this research and supported me mentally during the course of this work. Without her help and encouragement, this study would not have been completed.

CHAPTER 1

INTRODUCTION

1.1 Goal

The goal of this project was to develop a sensing device with the sensitivity, stability and response time needed to detect real time dynamics of metabolic activity and L-glu release from immobilized brain tumor cell cultures.

1.2 Rationale

L-glu is an important excitatory neurotransmitter which plays a key role in normal brain cell processes such as learning and memory. A growing number of neuroscientists believe that evidence supports the theory that perturbations in systems using the excitatory amino acid L-glu may underlie the pathogenic mechanisms of Alzheimer's disease (AD), hypoxia-ischemia, epilepsy, and Huntington's disease. Cerebral ischemia, head and spinal cord injury, and prolonged seizure activity cause excessive L-glu release into the extracellular space and subsequent neurotoxicity. There is also evidence that impairment of intracellular energy metabolism increases neuronal vulnerability to L-glu which when present even at physiological levels can damage neurons (slow excitotoxicity) [1]. Because almost all neurons in the central nervous system carry the N-methyl-D-aspartate (NMDA) subtype of ionotropic L-glu receptors, which can mediate post-synaptic Ca^{2+} influx, excitotoxicity resulting from excessive activation of NMDA

1

receptors may enhance the vulnerability of the neurons in a way consistent with AD neuropathology [2]. Scientists need an improved L-glu biosensor that is capable of monitoring rapid L-glu dynamics to understand the role L-glu plays in the normal and pathological spatial and temporal dynamics of brain cell and network excitation and communication to help discover new treatments and preventions. As an excitatory signal agent, it is important to remove L-glu from the synapse after release so that the next signal may be perceived before cells uptake L-glu. Astrocytes surrounding the synapse are most important in L-glu removal due to their active L-glu transporter [3]. The dynamics of L-glu release (signal on) and L-glu removal (signal off) can be dynamically controlled with a microfluidic device, and a biosensor capable of measuring these dynamics would greatly aid our understanding of normal brain cell function.

The heat production is an important parameter to determine the metabolism of any living cell line. Metabolic activity is an indicator of the viability of cells, in general. Cancer cells have higher metabolism and produce higher heat compared to normal cells. The stage of the cancer can be determined by the amount of the heat produced [4]. Early treatment of cancer minimizes the patient's post treatment time and minimizes the chance of death if cancer is diagnosed earlier. Therefore, a thermoelectric biosensor to detect the heat production due to the metabolism changes by the cells would greatly aid in understanding different cancer stages.

1.3 Hypothesis and Specific Aims

Our hypothesis is that the thermoelectric biosensor has the necessary sensitivity and response time needed to measure the heat generated by the L-glu deamination of the L-glu released by brain tumor cells or to measure the heat generated by the metabolism of

the brain tumor cells. To prove our hypothesis, a series of experiments were conducted and guided by the following set of specific aims:

1. Design and fabricate a microfluidic device to perform the chemical reaction. The objective of this aim is to fabricate the device using an inexpensive method.

2. Design and fabricate a thermopile to detect the heat from the chemical reaction. The objective of this aim is to fabricate the thermopile on the outer surface of the lower channel wall of the microfluidic device. The thermopile should have high sensitivity and response time needed to measure rapidly changing temperature due to the chemical reaction.

3. Calibrate the fabricated thermopile by applying known amounts of heat to the thermopile. The objective of this aim is to incorporate a thin nichrome wire heater on the measuring junctions of the thermopile and heat it in a controlled way. The Seebeck coefficient must be high for the thermopile to have high sensitivity.

4. Build a measuring system to collect and store the voltage data obtained from the thermoelectric biosensor. The objective of this aim is to have a high signal to noise ratio by eliminating thermal and electrical noise.

5. Calibrate the thermoelectric biosensor developed with the combination of Aims 1 and 2 by generating known amounts of heat in the microfluidic device. The objective of this aim is to incorporate a thin nichrome wire heater in the microfluidic device and heat it in a controlled way.

6. Investigate and develop a method to immobilize L-glutamate oxidase (L-GLOD) on the inner surface of the lower channel wall of the microfluidic device over the measuring junctions of the thermopile. The objective of this aim is to immobilize

the enzyme in high concentration. The enzyme should retain its activity after a few days of storage and continuous flow.

7. Measure the activity of the L-GLOD immobilized on the coverslip using a standard procedure. The objective of this aim is to perform the assay tests and quantify the amount of immobilized L-GLOD required to carry out the L-glu reaction.

8. Perform preliminary experiments to obtain a calibration curve for samples of known concentration of L-glu injected into the microfluidic device using the thermoelectric L-glu sensor developed with the combination of aim 1, 2 and 6. The objective of this aim is to inject various concentrations of L-glu ranging from 0 - 100 mg dL^{-1} in the microfluidic devices with single and multiple layers of immobilized L-GLOD. This allows measurement of the lowest L-glu detection limit for the thermoelectric L-glu sensor.

9. Investigate and develop a method to immobilize brain tumor cells on the inner surface of the lower channel wall of the microfluidic device. The objective of this aim is to immobilize cells in the region of interest either at a location on the thermopile or a location upstream of the thermopile.

10. Measure the viability and density of the cells immobilized on the lower channel wall of the microfluidic device. The objective of this aim is to stain the cells and demonstrate that the density of viable cells immobilized is large enough to detect the dynamic release of L-glutamate by the thermoelectric biosensor.

11. Perform control experiments to measure the metabolism of immobilized brain tumor cells using the thermoelectric metabolism sensor developed with the

combination of Aims 1, 2 and 9. The objective of this aim is to detect the heat released by the cells after stimulating them using the stimuli 50 mM kcl or 2 μM ionomycin.

12. Perform experiments to measure the dynamics of L-glu release from immobilized brain tumor cells using the thermoelectric L-glu sensor developed with the combination of Aims 1, 2, 6, and 9. The objective of this aim is to stimulate immobilized cells for L-glu release by using the stimuli 50 mM KCL or 2 μM ionomycin.

13. Measure the metabolism of immobilized brain tumor cells using the thermoelectric metabolism sensor developed with the combination of Aims 1, 2 and 9. The objective of this aim is to measure the amount of heat released by the tumor cells using Locke's solution without glucose.

1.4   Background

1.4.1   L-glutamate (L-glu)

L-glu is an amino acid neurotransmitter of the central nervous system and is responsible for most of the signal transduction that occurs in the brain. The chemical structure is shown in Figure 1.1. Neurochemical transmitters can be divided into two different classes, namely excitatory and inhibitory transmitters.
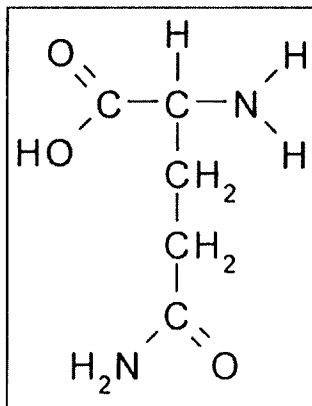
Figure 1.1: Chemical structure of L-glu

Excitatory neurotransmitters stimulate neurons by depolarizing the postsynaptic neuron, whereas inhibitory transmitters hyperpolarize and inhibit the excitation of the postsynaptic neurons. The major excitatory neurotransmitters are L-glu and aspartate. Other excitatory neurotransmitters are homocysteic acid, quinolinic acid, and N-acetyl-L-aspartyl-L-glutamic acid [5, 6]. The inhibitory neurotransmitters are GABA, glycine and taurine [5, 7]. The brain contains more L-glu than any other amino acid.

1.4.1.1   Role of L-glu in Brain Functions

L-glu plays a major role in the development and plasticity of the central nervous system (CNS), including the migration, differentiation and death of cells. L-glu is involved in many major brain functions such as memory, cognition, and learning. The release and uptake of L-glu by brain cells results in dynamic changes in L-glu concentration in cerebral spinal fluid. Cellular mechanisms underlying learning and memory such as long-term depression and long term potentiation are associated with glutamatergic synapses connectivity strength [8]. The extent of signal stimulation is determined by the L-glu concentration in the extracellular fluid [9].

Excitatory synaptic transmission is mediated by L-glu. Neurons generally (at resting state) have a higher intracellular concentration of potassium ions as against sodium ions which are more available in the extracellular space. Upon stimulation, the neuronal cell membrane depolarizes and generates an action potential by reversing the membrane potential. Following the action potential, the membrane is permeable to extracellular sodium ions until the membrane potential reaches its threshold value. Therefore, the reversal of membrane polarity generates an action potential that travels through the axon and to another neuron subsequently causing synaptic transmission. L-glu is secreted out of the presynaptic terminals via a calcium dependent process when the impulse (action potential) travels down the axon. L-glu then binds to the post synaptic receptors in turn changing their permeability properties and hence causing depolarization. Thus, the neuronal impulses are transmitted.

In neurotransmission, the neurotransmitter is released from a pre-synaptic neuron onto the receptors of a post-synaptic neuron. This allows the passage of an electrical signal through the neuron axon following the transmission of an action potential. Subsequent to its release from glutamatergic neurons into the synaptic cleft and activation of different subclasses of receptors, L-glu is taken up by a high affinity uptake system. The uptake system is comprised of various transporter proteins located on the surrounding neurons or astrocytes [10]. Such release and uptake cycles are modulated in a highly regulated glutamate – glutamine pathway between neurons and astrocytes via glutamine synthease and glutaminase. High affinity sodium dependent excitatory-amino acid transporters (EAAT): EAAT1, EAAT2, EAAT3, EAAT4 and EAAT5, and various ionotrophic receptors have also been identified on neuronal and glial surfaces. The L-glu

released bind to these transporters and receptors during synaptic transmission causing post synaptic depolarization of neurons. The EAATs are responsible for the removal of L-glu from the extracellular space to prevent hyper excitability and neurotoxicity, thus playing a highly crucial role in the normal functioning of the CNS [11]. These ionotrophic receptors can be subdivided into three groups N-methyl-D-aspartic acid (NMDA) and kainate receptors. Extracellular L-glu concentrations changes as observed in the neurons and the astrocytes release and reuptake L-glu are shown in Figure 1.2.
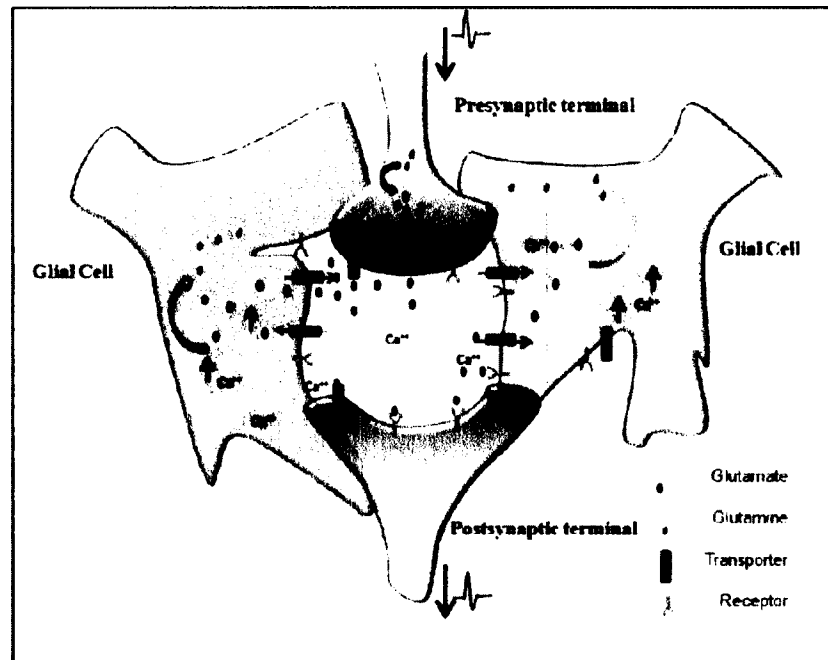
Figure 1.2: Diagrammatic representation of a glutamatergic synapse and concurrent events following excitation [10]

1.4.1.2   Patho-physiology of L-glu

The concentrations of L-glu in the extracellular fluid of the brain and cerebrospinal fluid (CSF) are about 3-4 μM and 10 μM, respectively. During pathological conditions the concentration may increase to 350 μM. The extracellular L-glu is

maintained at low concentrations because high concentrations of L-glu increase the signal stimulations which lead to neurological disorders [9].

Alzheimer's Disease (AD) is a progressive brain disease that produces mental deterioration. Its general cause is the accumulation of a protein, Beta-Amyloid either in between the spaces of the nerve cells (plaques) or inside the nerve cells (tangles). Accumulated Beta-Amyloid protein in the brain causes the neurotoxic effects of the L-glu. Beta-Amyloid inhibits the L-glu recycling (uptake). Excess L-glu inhibits signal transmission and signal detection. AD, the most frequent cause of cognitive deficit in the aging, affects over 5 million Americans over the age of 65 (one in every eight individuals). The average survival following diagnosis with AD is four to eight years with some individuals living as long as 20 years; 40% of this time is spent in the most severe stage of the disease and often in nursing homes. The annual cost of caring for those with AD is estimated to be $183 billion with profound implications for government costs ($37 billion is paid by Medicaid and $93 billion is paid by Medicare). Unless new treatments and preventive measures are discovered, the cost of treating individuals with AD is estimated to increase to over $1.1 trillion by 2050. The emotional and physical toll on caregivers contributes to the societal impact of AD. AD and dementia caregivers had $7.9 billion in additional health care costs in 2010 and more than 60% of family caregivers report high levels of stress with 33% reporting symptoms of depression [12].

Parkinson's Disease is a chronic, progressive, and degenerative disorder of the nervous system. It occurs due to the death of neural cells in basal ganglia. People suffering from Parkinson's Disease have abnormal mitochondria in the substantia nigra [9]. Mitochondria cannot provide enough energy as it partially loses a subunit, complex-

1. Due to insufficient energy, the cell cannot produce enough free radical scavengers. This increases the level of free radicals dangerously. L-glu receptors generally increase the free radical load. The blocking of L-glu transmitters would decrease the free radicals and hence reduce the toxic effect.

1.4.2   Brain Tumor Cells

Besides neurons, glia are a second type of cell in the brain and they play essential roles in the CNS and glutamatergic neurotransmission [13]. Glia have various subclasses based on their morphological properties and functions. They are categorized as microglia that are responsible for the immune system, as oligodendrocytes which play a critical role in axon myelination, and as astrocytes that reflect the majority of glia in the CNS [14]. Astrocytes are the type of glia that play an important role in glutamatergic neurotransmission and neuronal depolarization. A high ratio of astrocytes to neurons, 1.4:1, is found in the human cortex compared to a lower ratio in lower mammals, e.g. rats and mice [15, 16]. Astrocytes' roles are divided into providing neurons with nutrients, clearing neuronal waste, especially neurotransmitters such as L-glu, which remained from synaptic neurotransmission. Also, they maintain ion levels and pH homeostasis in the brain [16]. In the 1990s, many studies proved that neurotransmitters change intracellular calcium levels in astrocytes due to the activation of astrocytic receptors. For example, L-glu, ATP, and acetylcholine (Ach) are able to evoke astrocytic calcium release from internal stores through inositol trisphosphate (IP3)-mediated mechanism which causes calcium oscillations [13, 15].

Astrocytomas are gliomas that resemble astrocytes, the supportive cells that encircle and protect the nerve cells, or neurons, in the brain. Recently, researchers found

that a majority of brain tumors contains glioma cells to be the main reason for brain cancers. The extremely aggressive types of astrocytomas are glioblastomas [17]. Since gliomas arise from the brain tissue itself, they can cause a number of symptoms ranging from simple headache to seizures, movement disorders, confusion, sleepiness, speech disorders, and coordination difficulties. Over the past three decades, the rate of brain tumors dramatically increased to affect about 18,000 patients every year in the USA alone.

1.4.2.1 Physiology of L-glu dynamics after Stimulating Tumor Cells

The application of KCL to nerve terminals releases L-glu from the vesicles due to the depolarization of the plasma membrane by K^+ ions and subsequent activation of Ca^{2+} channels. The L-glu release is also caused by membrane potential difference driven by existing K^+ and Na^+ gradients [18].

The application of cystine to nerve terminals releases L-glu from the vesicles. Glioma cells are vulnerable to L-glu induction - cystine depletion. Glioma cells lack the functional sodium-dependent high affinity L-glu uptake, but they have a high cystine–glutamate exchange activity. Cystine is taken up into the cells by exchange with L-glu through the glutamate–cystine exchanger. This L-glu release is normally stopped by a rapid L-glu uptake via the Na+ and K+ coupled L-glu transporters. Several human glioma cell lines, however, do not express Na+ and K+ coupled L-glu transporters. Because the glioma cells have a high cystine–glutamate exchange activity and a defective sodium-dependent L-glu uptake, they release large amounts of L-glu. It is known that growing glioma tumors actively kill surrounding neurons by releasing L-glu [17, 19, 20].

Ionomycin is also used to raise the intracellular calcium level followed by the release of L-glu from the cells. Ionomycin is an ionophore. Ionomycin kills the cells by allowing too much calcium ion to enter the cell, called exitotoxicity. The enhancement of calcium influx is due to the direct stimulation of store-regulated cation entry. Ionomycin also induces apoptosis in various cell lines. Ionomycin releases calcium from its intracellular stores without the involvement of G proteins, resulting in activation of calcium activated chlorine channels. The slow component of the ionomycin response is the entry of calcium from outside the cell and the fast component is released calcium from the intracellular stores [21].

1.4.2.2   Brain Tumor Cell Metabolism

Two opposing streams of chemical reactions occur in cells that constitute the metabolism of the cell [22]: (1) the catabolic pathways break down foodstuffs into smaller molecules, thereby generating both useful form of energy for the cell and some of the small molecules that the cell needs as building blocks, and (2) the anabolic, or biosynthetic pathways use the energy harnessed by catabolism to drive the synthesis of many other molecules that form the cell.

The cells release heat energy as it synthesizes molecules and assembles them into cell structures. Once the food is converted into glucose, a chain of reactions called glycolysis converts each molecule of glucose into ATP. Approximately 10^9 molecules of ATP are in the solution in a typical cell at any instant, and in many cells, all this ATP is used up and replaced every 1-2 minutes [22]. In all, approximately only half of this energy (which derived from the oxidation of glucose or fatty acids to form H_2O and CO_2)

is used to drive the cell activity. The rest of the energy (free energy) is released by the cell as heat.

A major function of brain tumor cells is to maximize their ability to synthesize substrates for membranes, nucleic acids and proteins for the increased proliferative rate [23]. Hence, a large amount of energy in the form of adenosine triphosphate (ATP) is required for these cells. This ATP is obtained by increasing the use of glucose many times. Also, the requirement of oxygen is high for tumor cells activity.

1.5   Prior Studies

1.5.1   Biosensors

A biosensor is an analytical device for the detection of a bioanalyte with a physicochemical detector component. Biosensors can be classified according to the biological element or their transduction element. Table 1.1 shows the classification.

Table 1.1: Common Biological Elements and Transducers used in Biosensors [24]

Biological Elements	Transducers
Enzymes	Electrochemical
Antibodies	Amperometric
Receptors	Potentiometric
Cells	Conductimetric
Membranes	Optical
Tissues	Fiber Optic
Organisms	Surface Plasmon Resonance
Organelles	Calorimetric
Nucleic acids	Heat Conduction
Organic molecules	Isothermal
	Acoustic
	Surface Acoustic Wave
	Peizocrystal Microbalance

1.5.2   L-glutamate Biosensors

Biosensors are the most rapidly developing techniques for the detection of bioanalytes. Various types of amperometric biosensors [25, 26] and optical biosensors [27] are used for the detection of L-glu. Although all these biosensors are sensitive and selective, complex methods for the preparation of the electrodes [27] and complex detection systems for the detection of fluorescence are required. In amperometric biosensors, though the electrodes coated with enzyme are replaced with 'enzyme modified electrodes' for faster response [28], the problem due to the direct contact of the enzyme with the reactants causes difficulty in calibrating the electrodes during measurement as the sensor degrades [28] (due to adsorption of biological molecules on the electrode). In the thermoelectric method, the sensor is not in direct contact with the reaction dynamics and is simple to calibrate. Optical biosensors have complex detecting systems with the fluorescent probe immobilized on the substrate [27].

The amperometric L-glu sensors have been used to detect the extracellular L-glu in various pharmacological studies. Few studies demonstrated changes in L-glu concentration in the rat's brain after stimulating with kcl, L-glutamate and glutamate uptake blocker [29, 30]. Osamu Niwa et al. used a microdialysis probe with a glassy carbon electrode modified with an Os-polyvinylpyridine mediator bottom film containing L-GLOD to detect L-glu from cultured nerve cells [31]. Table 1.2 gives the chronological development in L-glu sensors in terms of sensor structure and its element.

Table 1.2: L-glutamate sensors based on L-glutamate oxidase applied to neuronal samples (modified and adapted from [32])

Sensor Structure	Sensory element	Detection	Sample	Stimulation	Ref
Dialysis electrode	L-GLOD in solution	Oxidation at Pt	In vivo, rat striatum	Tail pinch	[33]
Dialysis electrode	L-GLOD in solution	Oxidation at Pt	In vivo, rat hippocampus	Electrical	[34]
Dialysis electrode	L-GLOD in solution	Oxidation at Pt	In vivo, rat striatum	Ischemia	[35]
Dialysis electrode	L-GLOD in solution	Oxidation at Pt with mediator ferrocene	In vivo, rat striatum	Anoxia	[36]
Capillary electrode	L-GLOD in solution	Reduction at Os-gel-HRP-modified Pt	Acute hippocampal slices	200 mM K^+ ischemia	[37]
Microdialysis	L-GLOD immobilized by crosslinking	Oxidation at Pt	In vivo, rat striatum and cortex	100-160 mM K^+	[38]
Microdialysis	L-GLOD immobilized by crosslinking	Reduction at Os-gel-HRP-modified GC	Cultured nerve cells	100 mM K^+	[39]
Electrode array	L-GLOD immobilized	Reduction	Cultured nerve cells	100 mM K^+	[40]
Electrode array	L-GLOD immobilized	Reduction	Hippocampal slice cultures	Muscimol (1 mM) electrical	[41]
Microsensor	L-GLOD immobilized by crosslinking on Pt-Ir	Oxidation	In vivo, rat hippocampus	100 mM K^+ electrical	[18]
Microsensor	L-GLOD immobilized by crosslinking	reduction	In vivo, rat striatum	100 μM tetrodotoxin	[42]

In vivo time dependent studies of L-glu uptake and release in the entire biological systems offer obvious advantages over *in vitro* studies, but these *in vivo* studies are difficult if not impossible to control.

1.5.3   Cell Metabolism Sensors

Cell metabolism sensors offer several advantages such as analyzing drug action on cells. The state of art in measuring cell metabolism is mostly based on the direct parameters like cell count, DNA synthesis, clonogenic activity, and cell viability. Some other tests are based on indirect parameters like the staining of global cell components (DNA, protein), the determination of ATP level, and the formazon formation after staining DNA. These parameters are measured by various assay tests which are simplified for routine tests. The assay tests certainly provide useful information such as concentration of ions. However, these different assays ultimately lead to cell death and the scope for kinetic analysis of the drug effect is very less. Therefore, assay based multiparametric sensor chips integrated with cell culture has been developed to detect cell metabolism and morphology of cells in real time [43]. Angela M. Otto, et al. used basic parameters like extrusion of acids into the extracellular microenvironment and oxygen consumption to detect cell metabolism [44]. They used sensors for detecting pH (ion-sensitive field effects transistors for monitoring extracellular pH) and pO_2 (amperometric oxygen electrode measuring oxygen consumption in medium) in their cell metabolism sensor. An alternative to detect the metabolism would be the detection of heat produced due to the metabolism of the cells.

Thermoelectric sensors have been used in macro scale to study the heat generations from muscle cells and nerve cells [45, 46]. Miniaturized calorimetric sensors

[47, 48] have also been developed to detect the real time measurements of changes in order to access the metabolic activity of individual cells in a noninvasive manner. These sensors use a low volume micro array which helps in using only a low number of cells. We developed a novel approach of thermoelectric detection of the cell metabolism in a microfluidic device that gives the real time dynamic metabolic activity of the cells.

1.6   Thermoelectricity and Thermopile

Thermopiles are made by connecting one or more thermocouples in the series. Thermocouples are created by joining two different metals together such that two junctions are formed, each of which can be exposed to different temperatures. One of these junctions is usually designated as the measuring (or active) junction and the other is designated as the reference junction. If the measuring junction is maintained at a temperature that is different from the reference junction, an electrical potential called the Seebeck Voltage, V_{12}, can be measured between the two junctions. The magnitude of the Seebeck voltage is proportional to the temperature difference between the junctions and the Seebeck coefficient (thermoelectric power) of the selected metal pair, S_{12}, as shown by Eq. 1.1

$$V_{12} = S_{12} (T_1 - T_2).$$ Eq. 1.1

If bulk antimony and bismuth are selected as the two metals, the Seebeck coefficient is 119 μV $°K^{-1}$. The magnitude of the Seebeck voltage of thin-film thermopiles also depends upon the number of thermocouple junction pairs that are connected in series, N, as shown by Eq. 1.2

$$V_T = N S_{12} (T_1 - T_2).$$ Eq. 1.2

Extremely small amounts of heat can be measured by positioning the measuring junctions in close proximity to the heat source. The reference junctions should be located away from the heat source, although close enough to possess the same baseline thermal signature as the measuring junctions.

1.7 Bio-chemical Detection Using Micro-Calorimeters

Microfluidic calorimeters are promising tools for the analysis of biochemical processes [49-51]. Thin-film thermopiles are desirable primary temperature sensing elements in these devices because they are durable, suitable for surface temperature measurement, highly sensitive to temperature changes, exhibit high common mode rejection, and provide non-varying temperature sensitivity [52]. Microfluidic calorimeters reduce the amount of biochemical samples, reduce cost, and increase portability [53]. These devices are often used to monitor the heat released from enzymatic reactions such as heat from the reaction of urea hydrolysis by urease [54], and the heat from the reaction of glucose oxidation by glucose oxidase [53, 55, 56]. They are also used to measure the heat released following nucleotide incorporation into DNA by klenow polymerase for the purpose of sequencing the DNA [57].

1.8 Layer-By-Layer Self-assembly

In many sensor applications, enzymes are immobilized on the sensor surfaces to prevent them from dissolving into the solution. Broadly, enzyme immobilization methods are classified into five types. They are:

1. Covalent Bonding

2. Gel Entrapment

3. Membrane Entrapment

4. Cross-Linking

5. Adsorption

Covalent attachment of enzymes is the most reliable method of enzyme immobilization since the enzymes are immobilized with strong chemical bonds [58]. However, enzyme loading is often not appreciable and depends on the surface area and the availability of attachment sites. Gel entrapment techniques work for loading massive enzyme immobilization by using a gel matrix, generally polyacrylamide, in which the enzyme is entrapped [59]. However, the technique is not perfect and the enzyme is eluted over time. In membrane entrapment, the enzymes are entrapped behind the membranes such as cellophane, nylon, etc. [60]. Cross-linking is a method in which the enzyme is bound to itself through the use of a bifunctional agent such as glutaraldehyde and inert protein such as albumin [61]. This process must be controlled properly as the excessive cross-linking may lead to enzyme deactivation. Adsorption is the simplest method, wherein the enzyme is physically attached to a support of opposite charge following solvent evaporation [62]. However, in this method the bond between the enzyme and support is weak and may be easily reversed compared to other methods.

Layer-By-Layer (LBL) electrostatic adsorption is an effective procedure for protein and enzyme immobilization. LBL assembly is based on the alternate adsorption of oppositely charged ions on the substrate. The technique is based on charge neutralization and charge re-saturation upon the adsorption of oppositely charged ions on the substrates (Figure 1.3) [63, 64]. Strong ionic bonds hold the oppositely charged species to form uniform and stable films. Charge re-saturation occurs during polyion

adsorption resulting in the terminal charge for each polyion layer adsorbed. There is no restriction for the choice of polyelectrolytes. Films in the range of 5-1000 nm can be obtained by knowing the composition of polyelectrolytes. Lvov et al. [64] described the standard procedure for layer-by-layer self-assembly and the effects of the sample preparation and polyion concentration. For the assembly of protein or enzyme multilayers, alternate adsorption with polyions is necessary. These polyions act as "electrostatic glue" to hold the proteins or enzymes [62, 65].
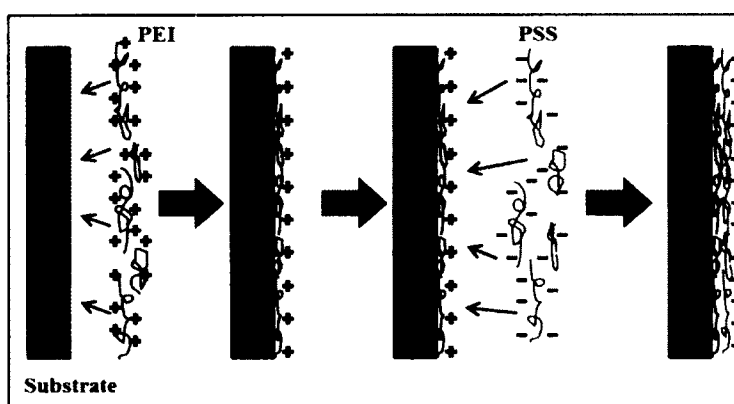
Figure 1.3: General Layer-By-Layer adsorption procedure

1.9 Cell Patterning

In vivo time dependent studies of L-glu uptake and release, and cell metabolism in entire biological systems offers obvious advantages over *in vitro* studies, but as discussed above, these *in vivo* studies are difficult if not impossible to control. A useful alternative method of studying the dynamics of L-glu release and uptake, and cell metabolism from cells is to study the dynamics of cultured cells integrated into a microfluidic biosensor system. This is now possible with advances in microfluidics, microfabrication, and cellular micro-patterning techniques [66].

Numerous techniques are now widely used for the immobilization of cells in microfluidic channels including: photolithography [67-69], micro-contact printing [70, 71], laminar flow patterning [72-74], and stencil patterning [75-77]. All these techniques modify the surface properties of the microfluidic channel surface followed by the selective adhesion of cells to the modified substrate. In photolithography, coated photoresist is exposed to ultraviolet light through a mask and developed to obtain the desired photoresist pattern. A cell adhesion polymer or protein is applied to the patterned surface and then the photoresist is lifted off to form the adhesive pattern onto which cells are bound [67]. Photolithography produces accurate patterns but requires access to clean-room facilities and expensive equipment. The chemicals used in photolithography can be toxic to cells [66]. In laminar flow patterning, the parallel flow of combined streams in the micro channels is used to pattern the cells along the flow path [78]. In micro contact printing, a PDMS stamp that has the self-assembled monolayers (SAMs) pattern of adhesive material is used. This pattern is transferred to the substrate surface when the PDMS stamp is brought into contact with the substrate. The patterning of SAMs gives control over the adsorption of adhesive proteins which facilitates the patterning of cells over substrates [71]. In stencil patterning, a thin piece of material (generally PDMS) that has holes (stencil) is used as a mask for selective patterning of cells [77]. The PDMS stencil is applied to the substrate and the cells are loaded into the holes. After the cells are attached, the stencil mask is peeled off, leaving the cellular islands on the substrate.

1.10   Microfluidics

Microfluidics deals with the manipulation of fluids that are geometrically constrained to a small scale. With this micro scale, low energy consumption and low

volumes can be obtained. Microfluidics has a large number of biomedical applications. The applications of microfluidics can be extended to biology, chemistry, medicine, energy generation, heat management, control systems, and display technologies. Microfluidic devices are the devices that have one or more features with micrometer length scale. In microfluidic devices, viscous forces dominate the inertial forces and the flow of the fluid is generally laminar at micro scale, i.e. the physics of the fluid flow differs from the macro scale. Microfluidic physics draws attention from different classical physics and chemistry such as thermodynamics, electrostatics, statistical mechanics, fluid mechanics, fluid dynamics, polymer physics, and elasticity [79]. The ratio of inertial to viscous forces is known as the Reynolds number (Re). Re is defined by Eq. 1.3

$$Re = \frac{\rho U_0 L_0}{\eta}.$$ Eq. 1.3

Where ρ is the density of the fluid, U_0 is the velocity, L_0 is the generic length, and η is the dynamic viscosity. The Reynolds number ranges between in the order of 10^{-6} to 10^1 in a typical microfluidic device with water as the working fluid, with velocities in the range of 1 $\mu m(s)^{-1}$- 1 $cm(s)^{-1}$ and channel radii in the range of 1-100 μm. These values confirm the domination of viscous forces over inertial forces in the micro scale region and results in a laminar flow.

The different fabrication methods used to make microfluidic devices include soft-lithography [80], hot embossing [81], dry and wet etching [82], laser ablation and xurography [83]. The most suitable method for device fabrication is chosen depending on the specific application.

Soft-lithography uses poly dimethylsiloxane (PDMS), a soft polymer with inorganic siloxane and organic methyl group attached to the silicon. The PDMS mixed

with a curing agent, when baked at high temperatures, turns into a transparent solid. The mixture of PDMS and the curing agent is poured over the mold containing micron scale patterns and heated at high temperatures. After cooling, patterned PDMS is removed from the mold. Then the patterned PDMS is covered with a flat surface like another PDMS layer or glass to form a microfluidic device.

Hot Embossing is a technique of imprinting microstructures on a substrate (polymer) at the substrate's glass transition temperature using a master mold (silicon tool). Depending on the design, master material and polymer material, the master structure is pressed into the polymer with a certain force. Later, the master and polymer substrate are cooled below the transition temperature.

Etching is a technique of pattern transfer by chemical or physical removal of a material from the substrate. Wet etching is done by using the chemicals such as hydrofluoric acid, phosphoric acid, nitric acid and others depending on the material to be etched. Dry etching uses small amounts of reactant gases such as O_2, CCl_4, and Cl_2.

Xurography is a rapid prototyping micro fabrication technique for creating micro structures in various films made of different materials. In this method, a cutting plotter with an addressable resolution of 10 μm is used to cut films of thickness ranging from 25 μm to 1000 μm. This prototyping is less precise than other fabrication methods but is a useful and inexpensive research tool. The time and prototyping cost saved allows researchers to focus on the device development before moving on to more expensive fabrication techniques.

1.11   Reaction Enthalpies

1.11.1   L-Glutamate Deamination

The L-glu biosensor system is based upon the thermoelectric measurement of the temperature change that results from the heat that is released when L-glu undergoes deamination in the presence of L-GLOD as shown in the following reaction (Eq. 1.4). L-GLOD is the enzyme that catalyzes the reaction of L-glu, oxygen and water giving rise to α-ketoglutarate, ammonia and hydrogen peroxide. The enthalpy change in a reaction is calculated from the heats of formation of the reactants and the products. The change in enthalpy is −30 kJ per mole. Since the change is negative, heat is released from the reaction

$$L - glutamate + O_2 + H_2O \xrightarrow{\text{glutamate oxidase}} \alpha - ketoglutarate$$

$$+ NH_3 + H_2O_2 \quad + 30 \, kJ/mole \, .$$

Eq. 1.4
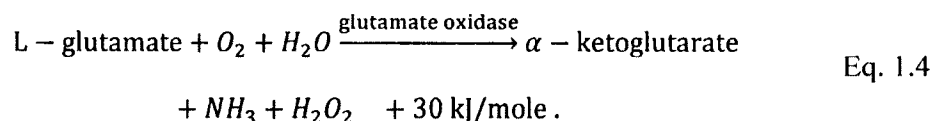
1.11.2   Cell Metabolism

The cell metabolism biosensor system is based upon the thermoelectric measurement of the temperature change that results from the heat released due to the metabolism of the cells. A large amount of energy in the form of ATP is required for these cells. This ATP is obtained by increasing the use of glucose and oxygen many times. During the usage of this ATP, approximately 50% of the energy is converted to heat energy [22].

Table 1.3 shows the cell metabolism enthalpies of various cell types. The glial tumor cells (glioblastoma) used in this project are assumed to have enthalpy similar to that of neuroblastoma cells.

Table 1.3: Heat production enthalpies of various cell lines.

Cell Type	Heat Production	Reference
Neuroblastoma	60-120 pW/cell	[84]
Reuber H35 cells	20-40 pW/cell	[84]
Leukemia cells	21.4 ±3.1 pW/cell	[85]
H35 cells	15 pW/cell	[86]
HTC cells	40 pW/cell	[86]
LS cells	34 ± 3 pW/cell	[87]

CHAPTER 2

METHODS AND MATERIALS

2.1   Thermopile Fabrication

The fabrication of thermopiles is possible using either a lift-off procedure or via the vacuum deposition of metal layers through shadow masks. Thin-film thermopiles are fabricated on glass coverslip supports (lower channel wall of microfluidic device) with a geometry that is suitable for integration with a microfluidic device using a high-vacuum, metal evaporation system (Model No. DV-502B, Denton Vacuum, Moorestown, NJ). A typical thermopile fabricated on the glass coverslip and Kapton® sheet is shown in Figure 2.1. These thermopiles have 60 bismuth-antimony thermocouple junction pairs and exhibit a Seebeck coefficient of 6.3 μV $(mK)^{-1}$.
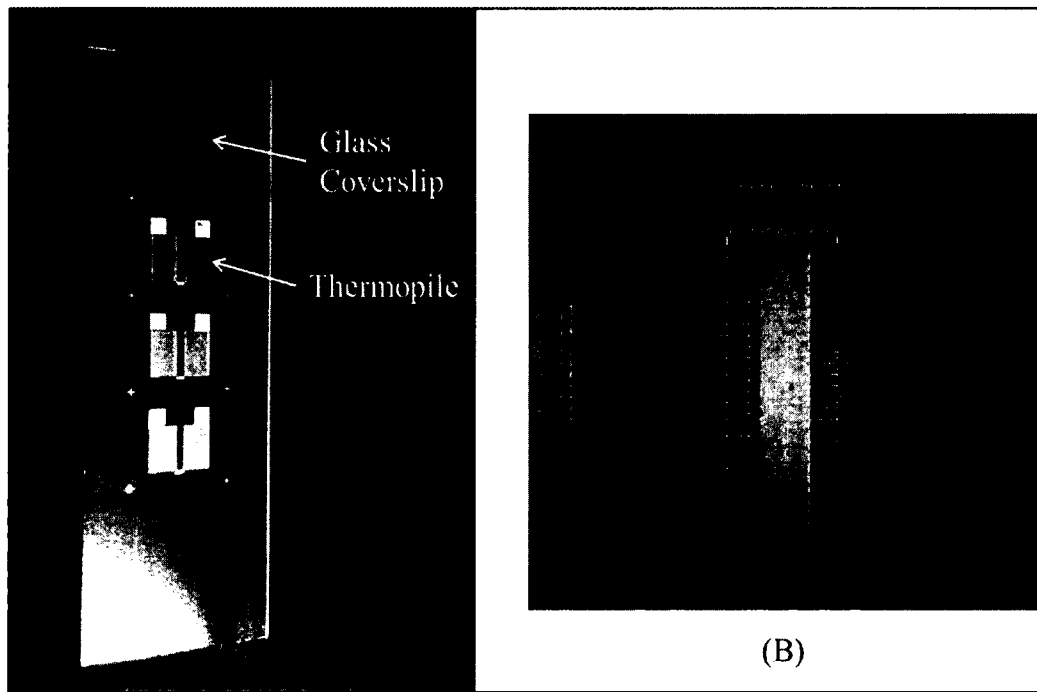
Figure 2.1: Typical thin-film thermopile fabricated on (A) Glass coverslip (B) Kapton® sheet

2.1.1   Thermopile Fabrication Using the
           Lift-off Procedure

The lift-off process is a simple method for making metallic patterns on a substrate, especially for noble metal thin films such as platinum, tantalum, nickel or iron which are difficult to etch by conventional methods. A general lift-off procedure is shown in Figure 2.2. First, a pattern is defined on a substrate using photoresist and exposure to ultraviolet light using the chrome mask. Figure 2.3 shows the chrome mask design with 25 thermopiles. A metallic film is then deposited over the substrate, covering the photoresist and the areas where the photoresist has been removed to form the pattern. Then, the photoresist is developed (removed) to leave only the desired metal pattern on the substrate. The process is then repeated to form the second metal film needed to form

the thermopile. Appendix A.1 provides a detailed protocol of how to make thermopiles using lift-off procedure.
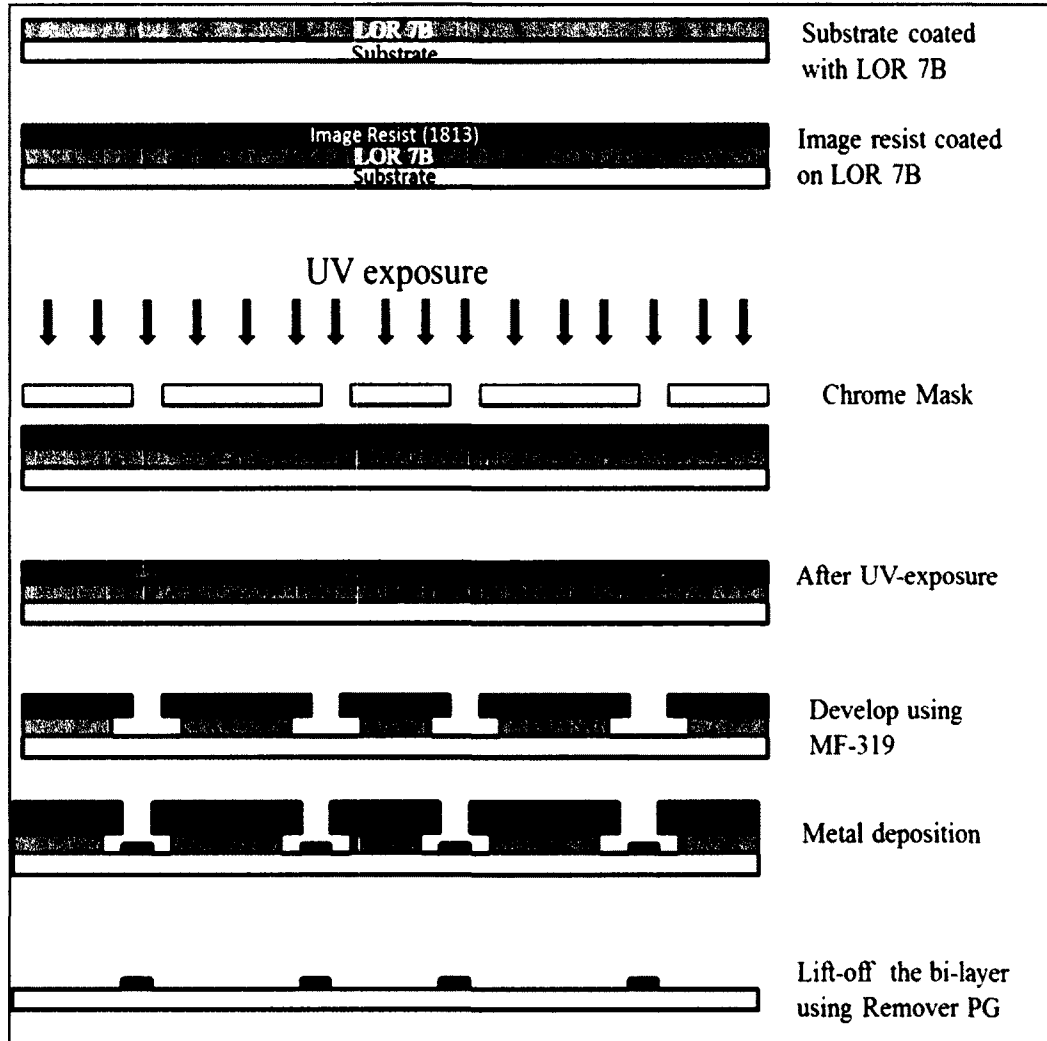
Figure 2.2: Block diagram showing the patterned deposition of metal lines on a substrate by the lift-off process
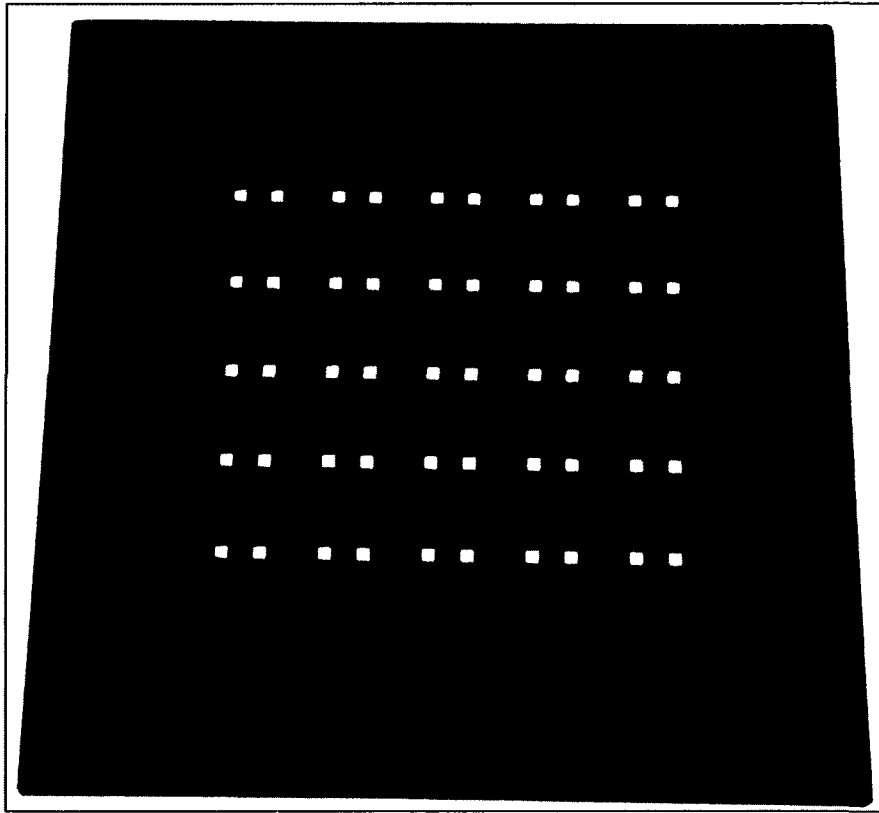
Figure 2.3: Chrome mask to expose UV light for fabricating thermopiles using lift-off photo-lithography procedure

A Scanning Electron Microscope (SEM) was used to image the overlapping Antimony/Bismuth junction pads of a thermopile fabricated using the lift-off procedure. SEM images of the top view and a zoom view of the thermopile at the overlapping Antimony/Bismuth junction are shown in Figure 2.4.
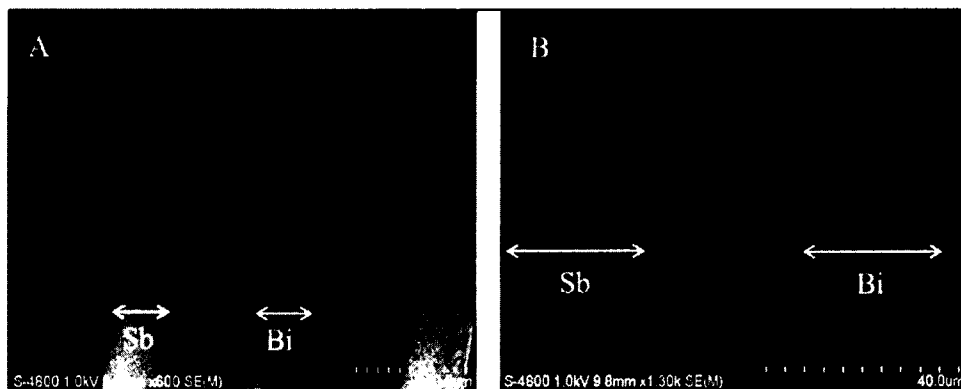
Figure 2.4: (A) SEM image of the Antimony/Bismuth overlapping junction of the thermopile. (B) Zoom view of the junction of the thermopile

2.1.2   Thermopile Fabrication Using Metal
Deposition through Shadow Masks

Bismuth-antimony thermopiles with 60 pairs of junctions were manufactured using shadow masks [88]. The thermopiles were made using custom designed shadow masks designed with AutoCAD software that were manufactured by Town Technologies, Inc. (Town Technologies, Inc., Somerville, NJ). Two shadow masks were designed for the deposition of bismuth and antimony thin films, respectively, on a microscopic glass coverslip of thickness 0.16 mm, thermal conductivity - 0.96 W $(m^\circ C)^{-1}$, and heat capacity- 0.84 J $(gm.^\circ C)^{-1}$, (Electron Microscopy Sciences, Hatfield, A).

A glass coverslip was placed behind the shadow mask designed to create the bismuth line pattern and suspended above the evaporator heat source. Bismuth metal (Bismuth shot, tear-shaped, -4+30 mesh, 99.9%, Sigma-Aldrich Chemicals, WWW.sigmaaldrich.com) was then heated until vaporized, and the vapors were allowed to travel through the shadow mask and condense on the support to form the bismuth pattern on the support. The shadow mask containing the antimony line pattern was carefully aligned to overlap with the bismuth lines at the thermocouple junctions. The

metal evaporation process was repeated using the second shadow mask and Antimony

metal (Antimony shot, 102 mm, 99.999% Sigma-Aldrich Chemicals,

WWW.sigmaaldrich.com). Following the deposition of the Antimony, the support

containing the thermopiles was removed from the metal evaporation chamber, tested for

electrical continuity and protected from physical damage using thin polyimide tape.

Typical thermopiles have an electrical resistance of about 30 kΩ. Figure 2.5 shows the

shadow mask to deposit antimony metal.
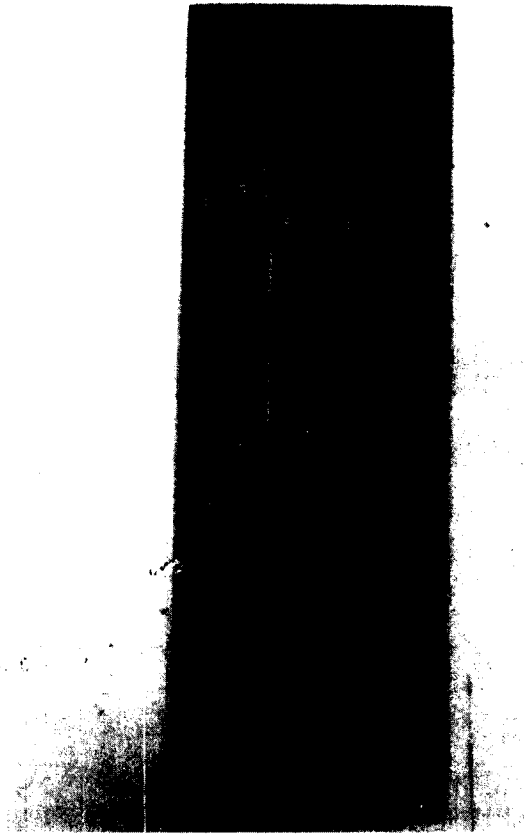
Figure 2.5: Mask to fabricate thermopiles using shadow mask procedure

2.1.3 Thermopile Testing

The fabricated thermopiles were tested for electrical continuity, electrical resistance and calibrated to determine its Seebeck coefficient. Testing of thermopiles for continuity and resistance was done under a microscope with a digital multi-meter. A schematic diagram of the measuring system used to measure the Seebeck coefficient is shown in Figure 2.6.
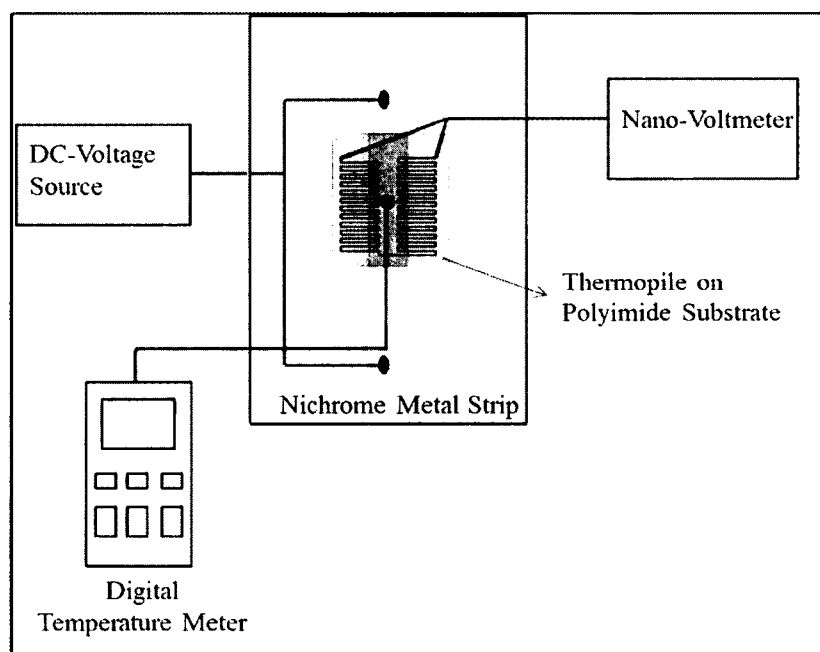
Figure 2.6: Measurement system used to measure the Seebeck coefficient of the fabricated thermopiles

An Agilent, Model E3630A DC power supply (Agilent, Inc., Loveland, CO) was used to apply voltage across the nichrome (80% NI/20% CR) metal strip (Scientific Instrument Services, Inc., NJ). The temperature of the nichrome metal strip increased due to heating associated with the conversion of electrical energy into heat and the temperature on the surface of the strip was measured using a digital temperature meter

(OMEGA® HH500RA High Accuracy Data logger/Thermometer, OMEGA Engineering, INC., Stanford, Connecticut). The thermopile output was measured using a nano-voltmeter (Agilent, Model 34420A nano-voltmeter (Agilent, Inc., Loveland, CO)). The entire measurement system with the exception of the DC power supply, nano-voltmeter and digital thermometer was contained in an insulated enclosure to reduce ambient temperature fluctuations. The nichrome metal strip was heated to a certain temperature which was measured using the digital thermometer and the corresponding thermopile output voltage was measured. Each thermopile output voltage corresponding to a given nichrome wire temperature was recorded. This procedure was repeated for various levels of heating by increasing the voltage across the nichrome metal strip. A calibration curve was obtained by plotting the thermopile output voltage as a function of nichrome wire temperature. The Seebeck coefficient of the thermopile was calculated from the slope of the calibration curve.

2.2   Enzyme Immobilization

2.2.1   Layer-By-Layer Self-Assembly

Layer-By-layer (LBL) self-assembly was used to immobilize the L-GLOD. LBL self-assembly is an adsorption technique used for immobilizing enzymes onto any substrate. Reagents needed for the immobilization are L-GLOD (Sigma-Aldrich, St. Louis, MO), polyethyleneamine (PEI) (Sigma-Aldrich, St. Louis, MO), Polystyrenesulfonate (PSS) (Sigma-Aldrich, St. Louis, MO), and reaction buffer (0.5 M Tris-HCL, pH 7.5) (Invitrogen Corporation, Carlsbad, CA). L-GLOD was mixed with reaction buffer to obtain 5 U ml^{-1} of solution. One hundred μl of PEI (50% W/V) was mixed with 10 ml of DI water to obtain a concentration of 5 mg ml^{-1}. PSS (25 mg) was

dissolved in 5 ml of DI water to obtain a concentration of 5 mg ml^{-1}. PEI is positively charged with a pKa 11.5 and L-GLOD is negatively charged with an isoelectric point of 6.2. A schematic of the enzyme immobilization process using LbL is shown in Figure 2.7. The adsorption of L-GLOD on the substrate was alternated with PEI to obtain multiple layers of L-GLOD. To accomplish this, the glass coverslip was first immersed in a PEI solution for 15 minutes, to form a polycation layer by electrostatic adsorption. Charge neutralization and resaturation takes place on the opposite end of the polyion layer. After rinsing in water, the glass substrate was immersed in a PSS solution for 15 minutes. The significance of intermediate water washing between adsorption cycles is that it removes 10% of weakly attached material from a resaturated polyion layer [64, 89]. By repeating this procedure, an evenly charged surface was obtained on the glass coverslip. Then, the L-GLOD solution (5 µl) was coated on the measuring junctions of the thermopile fabricated on the coverslip. After each immersion the coverslip was thoroughly dried under nitrogen gas. The procedure was repeated with PEI and L-GLOD to form multiple layers of L-GLOD. Please refer to Appendix A.2 for the detailed protocol of layer-by-layer immobilization.
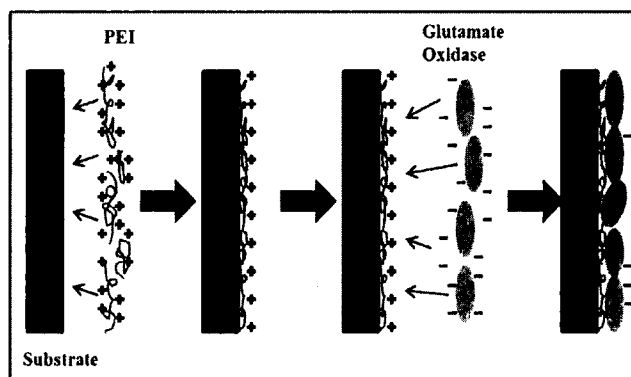
Figure 2.7: Layer-by-layer electrostatic adsorption of glutamate oxidase on glass coverslip

2.2.2 Quantitative Analysis of Immobilized Enzyme Mass and Thickness

A Quartz crystal microbalance was used to estimate the mass and thickness of the immobilized enzyme layer(s). An Amplex Red assay test based on fluorescence was performed to estimate the activity of the immobilized enzyme.

2.2.2.1 Quartz Crystal Microbalance (QCM) Monitoring

Quartz crystal microbalance (QCM) monitoring was performed for the evaluation of the effectiveness of the LBL assembly procedure. QCM has been used to study the multilayer film growth characteristics of LBL nano-structures, such as the mass of the films, thickness of the films, and interpenetration between layers [90]. A 9-MHz QCM gold electrode of 0.16 cm^2 diameter was used to estimate the adsorbed mass of the immobilized GOD and PEI. Under similar LBL conditions, the QCM electrode was immersed into the polyelectrolytes and the L-GOD along with the glass coverslip used for fabricating the microfluidic calorimeter. The QCM electrode was then dried and the change in its resonant frequency was recorded. This procedure was repeated for every layer to obtain the mass of the adsorbed L-GOD and PEI/PSS layers on the QCM

electrode. The mass and thickness of the adsorbed film was calculated using the Sauerbrey equation which relates the absorbed mass with change in resonant frequency of the crystal. The layer thickness is also calculated from the frequency change [91].

The frequency shift and the resonant frequency for a QCM are given by Eq. 2.1 and Eq. 2.2

$$\frac{\Delta F}{F} = -\frac{2\Delta M}{A\sqrt{\mu\rho}}.$$

Eq. 2.1

Where

ΔF = Frequency Shift in Hz

F = Resonace Frequency of the QCM

M = Total Mass of Protein

A = Surface Area of Slide $(0.16\ cm^2)$

$$\Delta F = -1.83 \times 10^8 \frac{M}{A}.$$

Eq. 2.2

So the mass of the immobilized film (Eq. 2.3) can be calculated as

$$\Delta M\ (ng) = -0.87\ \Delta F(Hz).$$

Eq. 2.3

The thickness of the immobilized film (Eq. 2.4) can be calculated using the formula

$$\Delta L\ (mm) = -0.017\ \Delta F(Hz).$$

Eq. 2.4

2.2.2.2   Amplex Red Assay of Immobilized L-GLOD Activity

The Amplex Red assay test (Invitrogen Corporation, Carlsbad, CA) was used to measure the activity of the immobilized L-GLOD. To perform the assay test, round glass coverslips of diameter 5 mm (Electron Microscope Sciences, Hatfield, PA) were used as the substrate to which L-GLOD was immobilized. These glass coverslips were small

enough to fit into 96 well plates. A fluorescence micro plate reader (BioTek, Winooski, VT) was used to detect the fluorescence emitted by the Amplex Red reaction(s) in the well plate. The procedure to perform the assay is published by the Invitrogen Corporation, Carlsbad, CA. The intensity of the fluorescence was detected using a fluorescence meter with excitation wavelength set at 530 ±12.5 nm and fluorescence detection set at a wavelength of 590 ±17.5 nm. The fluorescence reading is related to the production of hydrogen peroxide by the immobilized L-GLOD, which is a function of the activity of the L-GLOD. Please refer to Appendix A.3 for detailed protocol of the assay tests performed.

2.3 Cell Culture and Microscopic Techniques

2.3.1 Cell Culture

Brain tumor glioma cells (CRL 2303, purchased from ATCC, Manassas, VA) were cultured and grown according to vendor recommendations in Dulbecco's Modified Eagle Medium supplemented with 5% fetal bovine serum and 5% penicillin/streptomycin. These cells were plated in a Petri dish and maintained at 37° C in a humidified incubator containing 5% CO_2. Appendices B.1, B.2 and B.3 describe the detailed protocol of culturing, growing and re-plating the brain tumor cells.

2.3.2 Cell Counting Methodologies

Staining of cells using trypan blue is the standard procedure used to count the number of viable cells in a cell culture. Trypan blue from the vendor (sigma aldrich) contains 0.4% of trypan blue in 0.81% sodium chloride and 0.06% potassium dibasic. Trypan blue (blue acid dye) containing two azo chromophores has been used to stain collagen and amyloid of various tissues to estimate the proportion of viable cells in a

population [92]. The chromophore of this dye is negatively charged and does not react with the cells unless the cell membrane is damaged. Thus the viable (live) cells do not absorb the dye while non-viable (dead) cells do, allowing one to visualize the dead cells.

A Bright-Line Hemacytometer (product no. 15170-079, VWR) was used to count the number of viable cells in the population suspended on it. The Hemacytometer has two chambers with the coverslip placed on its top. A mixture of 50 μl of cell media and 50 μl of trypan blue was loaded into both chambers of the Hemacytometer using a pipette. The mixture had to be loaded immediately or in less than 15 minutes because the viable cells also begin to stain when trypan blue exposure is too long. A light microscope with a 10x objective lens was used to count the viable cells (which are not blue stained) and mathematical calculations were performed to calculate the density of the cells as described in the protocol designed by the vendor (Appendix B.4).

2.3.3   Analysis of Cell Viability in Cell Culture Preparation

Calcein AM (Calcein acetoxymethyl ester) is a vital fluorescent dye used to determine the viable cell count and helps to visually confirm that the cells are located in the desired region over the measuring junctions of the thermopile using the protocols mentioned in Appendix B.8. Calcein AM stain provides a simple, rapid, and accurate fluorometric method to measure cell viability, apoptosis, and cytotoxicity. Calcein AM is a non-fluorescent substance that permeates the cell wall of live cells. When added to live cells, it is hydrolyzed by intracellular esterases, converts to the strongly green fluorescent substance calcein, and is retained in the cell's cytoplasm. Calcein AM is a photostable reagent. It is not influenced by intracellular pH and is well retained in the cytoplasm of

live cells. Calcein AM is the most suitable indicator for staining viable cells. Due to its low cytotoxicity, it does not affect cell proliferation or viability.

Five microliters of pluronic acid at a concentration of 20% (weight/volume) in DMSO and 10 μl of a stock solution of calcein AM at a concentration of 1 mM were added into 5 ml of pre-warmed Locke's solution which had been equilibrated to 37° C. This Calcein AM and Locke's solution mixture was added to cells which are then incubated for approximately 30 minutes. The live cells produced fluorescence when exposed to ultraviolet light using an excitatory filter at 494 nm and an emission filter at 520 nm. The fluorescence intensity (proportional to number of live cells) was measured using the software IMAGE-PRO or IMAGE-J. A standard protocol for imaging cells using Calcein AM was published by Mark DeCoster et al. in the book chapter of *Microscopy: Science, Technology, Application and Education* [93].

2.3.4   DAPI Staining of Cells

To determine the cell count, 4, 6-diamidino-2-phenyindole (DAPI) was used. Staining with DAPI is very simple and requires no hydrolysis. The DAPI molecule intercalates between the DNA double helix molecules and emits fluorescence when bound to DNA [94]. A key aspect of this technique is that cells remain alive during this procedure.

DAPI solution was prepared by adding 0.1% dye to Locke's solution and vortexing. This loading solution was added to the cells for one hour in a CO_2 incubator, after which the cells were imaged with a Nikon inverted fluorescence microscope using a 450 nm excitation filter and a monochrome camera. The images were then analyzed using Image Pro®/Image-J software to determine the fluorescing or the cell area. The

fluorescence intensity of cell pixel area is proportional to the non-viable cell count. Refer to Appendix B.9 for the detailed protocol of DAPI staining of cells.

2.3.5 MTT Assay to Determine Metabolism

The MTT (3-(4, 5-dimethythiazol-2-yl)-2, 5-diphenyl tetrazolium bromide) Assay, a colorimetric method, was also used to test the viability of the cells.. MTT detects the live cells via the activity of the mitochondrial enzyme, succinate dehydrogenase that reduces MTT to a colored formazon dye [95]. The MTT (yellow colored dye) enters the cells and passes into the mitochondria where it is reduced a by succinate dehydrogenase to an insoluble, dark purple colored formazan product. The cells are then solubilized with an organic solvent (e.g. isopropanol) and the released solubilized formazan reagent is measured spectrophotometrically. Because the reduction of MTT can only occur in metabolically active cells, the level of succinate dehydrogenase activity is a measure of the viability of the cells.

Cells were plated in a 24-wellplate and MTT was added. The cells were incubated for an hour, and the MTT solution was then removed from each well. Isoproponal was added to the cells, and a portion of the solution from each well was transferred to a corresponding well of a second 94-wellplate. Absorbance of the converted dye was measured at a wavelength of 595 nm. The absorbance was quantified, and in relation to the number of cells in the culture, it gave a qualitative measure of culture health. A complete description of the assay can be found in Appendix B.10.

2.3.6 Calcium Imaging to Determine L-glutamate Release

Calcium imaging was performed by using calcium indicators that respond to calcium ions by changing their spectral properties. These are chemical indicators that are

highly selective for calcium ions. Some of the indicators are Fluo3, and Fluo8. Physiological astrocytic calcium levels stimulate L-glu release [96]. Appendix B.11 provides the detailed protocol of calcium imaging using FLUO 3.

Fluo3 calcium indicator is a highly sensitive dye for rapid measurement of calcium influx in the cells [97]. The fluorescence released from the cells can be monitored by an excitatory filter at 485 nm and an emission filter at 535 nm when the cells are placed under the fluorescent light.

Potassium chloride (kcl) elicits a calcium response when added to cells that are loaded with Fluo3. KCL increases the fluorescence instantaneously with an increase of calcium in the cells. Calcium ion uptake through voltage-dependent calcium ion channels is induced by depolarizing the cells in 50 mM kcl [98]. Cells can be maintained in a state of depolarization by raising the extracellular potassium ion concentration. Calcium uptake increases the release of neurotransmitter.

Ionomycin is an ionophore. Ionomycin is also used to raise the intracellular calcium level as a means of understanding calcium transport across the cell membranes. Ionomycin kills the cells by allowing too much calcium ion to enter the cell. The process is called exitotoxicity. The enhancement of calcium influx is due to the direct stimulation of store-regulated cation entry. Ionomycin also induces apoptosis in various cells lines like CRL 2303 and CRL 2199. Ionomycin releases calcium from its intracellular stores without the involvement of G proteins, resulting in activation of calcium activated chlorine channels. The slow component of the ionomycin response is the entry of calcium from outside the cell and the fast component is released of calcium from the intracellular stores [21].

2.3.7   Fluorescence Testing of L-Glutamate
         After Stimulation

The Amplex red assay test (Invitrogen Corporation, Carlsbad, CA) was used to measure the concentration of L-glu released by the glioma cells. L-glu determination is based on multi-enzymatic reactions detectable using fluorescence measurement. The principle of the method involving multi-enzymatic reactions has two steps: 1) L-glu is converted to α-ketoglutrate, NH_3, and H_2O_2 via L-GLOD. Then L-glu-pyruvate transaminase and L-alanine amplifies the H_2O_2 amount due to L-glu regeneration by tranamination of α-ketoglutrate. 2) Hydrogen peroxide reacts with 10-acetyl-3, 7-dihydroxyphenoxazine (Amplex red reagent) with horseradish peroxidase to produce resorufin. Resorufin has absorption and emission at 571 nm and 585 nm, respectively. Thus, fluorescent resorufin magnification monitors L-glu levels in the samples.

Using this assay, the amount of L-glu released was measured in the samples of cell media that were collected from the petri dish after the brain tumor cells were stimulated with 50 mM KCL. The samples were collected in regular intervals of time over a period of five minutes.

2.4   Cell Immobilization in Patterns

Cellular micro-patterning techniques have been developed to study fundamental cell biology, especially interactions of cells with other cells, cells with the surface, and cells with the medium [66]. The cells were immobilized over the opposite side of the coverslip than that which contained the thermopile. The cells were patterned on the surface of the coverslip such that they were immobilized only on the thermopile. This selective patterning of cells on the thermopile was selected because it might allow the thermopile to detect the maximum heat released by the cells during stimulation. The

following sections include the procedure for pretreatment of the coverslip and immobilization of cells on the coverslip.

2.4.1   Surface Sterilization

The glass coverslips were sterilized by wiping the surface of the coverslip with 70% ethanol to remove debris followed by exposure of the surface to ultraviolet light for at least 15 minutes to kill the bacteria.

2.4.2   Poly-L-lysine (PLL) Treatment

PLL adhesion technique of patterning cells is a commonly accepted method of immobilizing cells [99] on glass substrates. PLL is the polymeric version of the amino acid Lysine [100]. The coating of PLL over the surface of the glass changes the surface charge of the glass coverslip from negative to positive. This allows the cells to adhere to the surface when immobilized on the PLL coated area.

The PLL (0.005% in deionized water) was pipetted on the surface of the microscopic glass coverslip in a selective rectangular area marked underneath the surface of the coverslip with fine tip marker. This rectangular area covers the whole area of the thermopile. The glass coverslip was then left undisturbed for one hour at room temperature after which it was washed with Phosphate Buffered Saline (PBS) to remove any unbounded PLL from the surface. The coated PLL monolayer changed the surface charge of the coverslip to an evenly distributed positively charged surface. The glass coverslip was then placed in a petri dish, and the brain tumor cells (500 k cells per ml media) that were in the media solution were placed only on the PLL coated area. Placing cells only on the PLL coated area eliminated the chance of binding the cells in areas of the coverslip other than the thermopile area. Immobilization occurred when the

negatively charged cells came in contact with the positively charged PLL coated surface. The petri dish with cells over the thermopile region of the coverslip was then left undisturbed for two-three days in an incubator at 37° C. This time was sufficient for the cells to adhere to the PLL coated area and to increase the cell count to an acceptable level on the coverslip. The acceptable level of the cell count is the number of cells required to a detectable amount. This cell count could be as many as two-three million cells immobilized on the measuring junction of the thermopile. A small quantity of fresh media was added to the cells after every eight hours to prevent the complete evaporation of media when stored in the incubator. Cells can be immobilized either only on the measuring junction of thermopile or on the whole thermopile depending upon the experiment performed.

2.4.3   Viability Test for Immobilized Cells

Immobilized cells were stained with Trypan Blue to determine the cell viability. Whereas living cells exclude the dye, dead cells turn blue when Trypan Blue is absorbed by the cells. Trypan Blue (20X diluted) was applied to the immobilized cells that had been incubated for one day.

2.5   Microfluidic Calorimeter

A microfluidic device of single, straight, laminar flow channel with dimensions 60 mm × 12 mm × 0.1 mm was fabricated. The device had two inlets and one outlet arranged in a straight line along the center of the channel [88]. The components required to fabricate the microfluidic thermoelectric sensor were a glass microscope slide of dimensions 75 mm × 25 mm × 1.2 mm (Electron Microscopy Sciences, Hatfield, PA) and a glass coverslip of dimensions 75 mm × 25 mm × 0.16 mm (Electron Microscopy

Sciences, Hatfield, PA) with immobilized L-GLOD and brain tumor cells on the thermopile, and double sided polymer (Kapton®) tape with thickness of 100 μm. The following sections explain the preparation of the components of the microfluidic device and its assembly.

2.5.1   Preparation of Glass Microscopic
         Slide

The fabrication of the microfluidic device began by drilling the small holes through the microscopic slide along the center of the channel at the desired position of the inlets and the outlet. This drilling was done using a drilling press with a diamond tip drill bit of 1 mm diameter. Two ports with 1/16 inch inner diameter were then bonded to the inlet and outlet holes.

2.5.2   Preparation of Double Sided Kapton®
         Tape

2.5.2.1   Design of Microfluidic Channel

Using adobe illustrator software, a rectangular microfluidic channel with tapered ends was designed with the dimensions 60 mm x 12 mm as shown in Figure 2.8.

Double Sided Kapton Tape

60 mm

12 mm
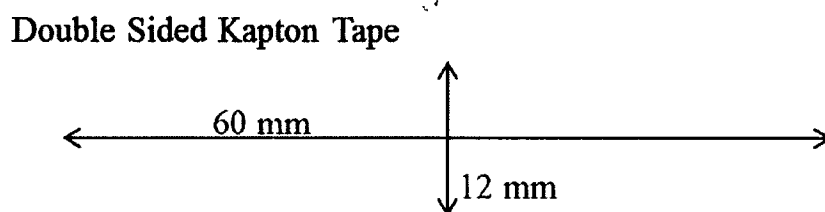
Figure 2.8: Design of the Kapton® tape cut in the form of the channel

2.5.2.2   Xurography

Xurography, a cutting method, was employed by using double sided Kapton® tape and a cutting plotter (Graphtec America, Inc., Santa Ana, CA) to form the 100 μm deep flow channel geometry [83]. The optimal plotter settings were chosen for the material so that the tape was cut at the desired depth and did not damage the plotter. The cut film was weeded using fine tweezers. Figure 2.8 shows the positive structures and negative structures after weeding is used for the flow channel in the device.

2.5.3   Preparation of Glass Microscope Coverslip

The thermopile on the coverslip has two measuring pads upon which two glued thin copper strips conducted leads (3M™ EMI Copper Foil Shielding Tape 1181, Conductive Acrylic Adhesive, 3M, St. Paul, MN) were attached. Silver print (Part No. 22-0023, GC Electronics) was coated at the junction of the copper strips and the thermopile pads to insure electrical continuity between the thermopile contact pads and the copper strips. Electrical continuity was tested by checking the resistance of the thermopile at the end of the copper strips after the applied silver print had dried. L-GLOD and brain tumor cells were then immobilized on the coverslip using the protocols explained in Section 2.4.

2.5.4   Fabrication of Microfluidic Calorimeter

The cut tape was sandwiched between the glass microscope slide and the thin coverslip (with fabricated thermopile), creating the microfluidic channel to form the microfluidic calorimeter as shown in Figure 2.9. The fluid from inlet 2 was hydro dynamically focused by the fluid from the inlet 1 so that the fluid from inlet 1 flowed only over the measuring junctions of the thermopile. The width of the hydro dynamically

focused stream was adjusted by changing the ratio of inlet 1 to inlet 2 volumetric flow rate. It was important that the focused fluid flow only over the measuring junctions of the thermopile to ensure that the reaction zone in the microfluidic device is limited to the measuring junctions of the thermopile.
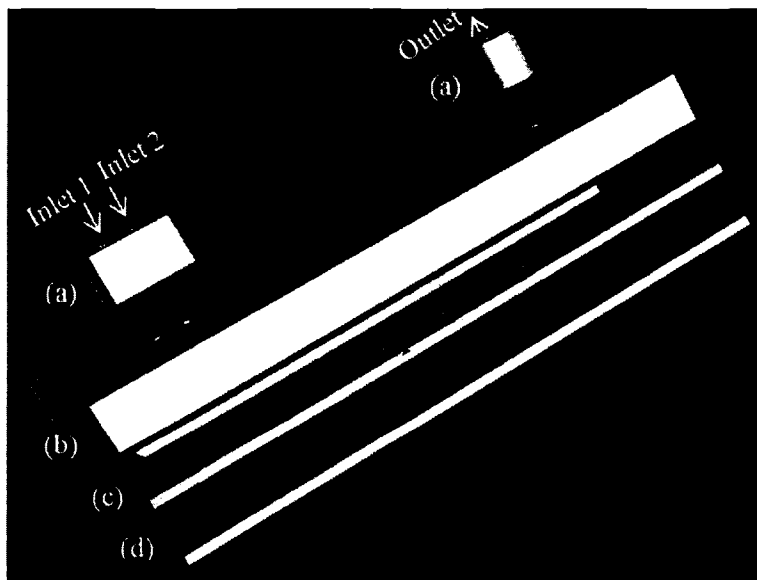
Figure 2.9: The exploded 3D view of the microfluidic calorimeter

2.5.5   Calibration of Microfluidic Calorimeter

Calibration of the microfluidic calorimeter was performed by incorporating a nichrome wire heating strip (1.52 mm wide and 0.025 mm thick, Scientific Instrument Services, Inc., Ringoes, NJ). The nichrome wire strip was incorporated on the center axis of the inside of the channel over its entire length including over the measuring junctions of the thermopile. The heated nichrome wire mimicked the exothermic reaction in the microfluidic calorimeter. The electric current was applied to the nichrome wire to generate the power required to heat the measuring junctions of the thermopile. Reverse

osmosis (RO) water was introduced into the microfluidic device from inlet 1 and 2 with flow rates of 100 and 25 μl min^{-1}, respectively. The microfluidic calorimeter response and temperature change at the heater with respect to the surrounding temperature was measured as a function of applied power. Figure 2.10 shows the integration of the nichrome heater inside the channel of the microfluidic calorimeter.
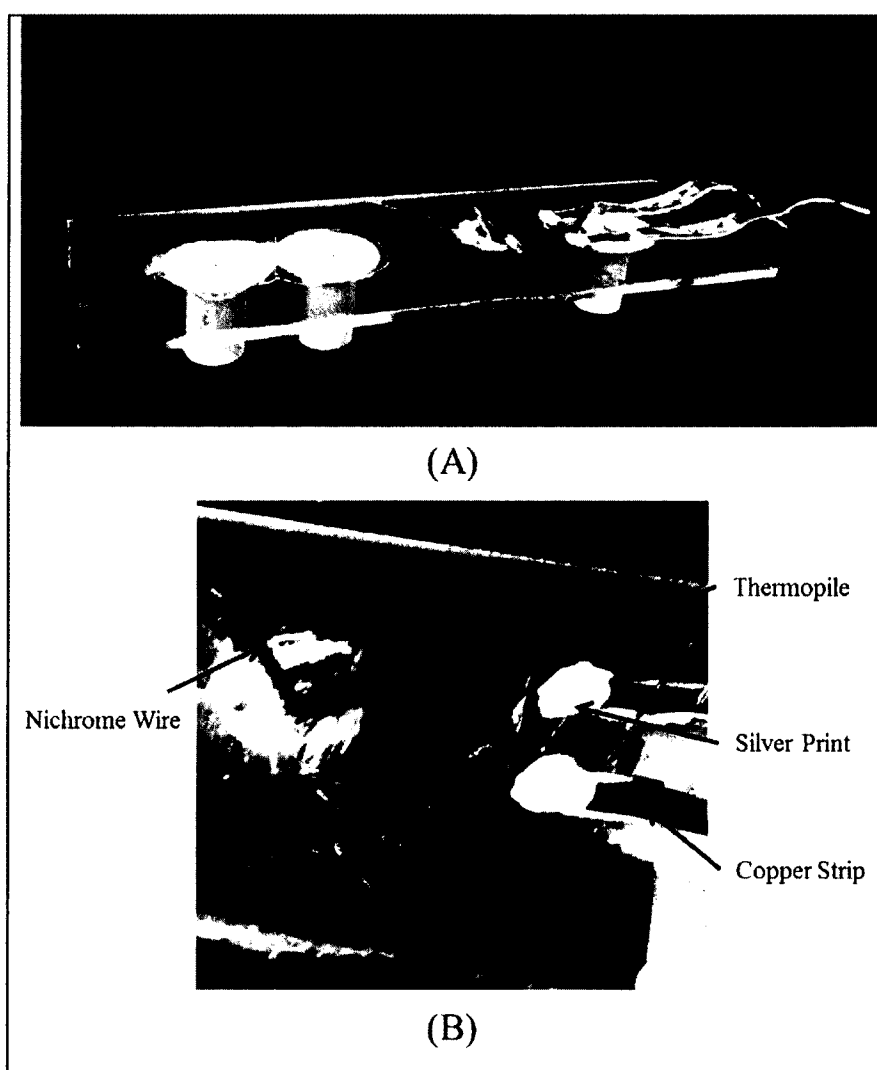
Figure 2.10: (A) Nichrome heater incorporation into the microfluidic device to calibrate the thermoelectric sensor. (B) Zoom view of the nichrome heater wire underneath the thermopile

2.5.6   Mathematical Model of Heat Transfer
          in Microfluidic Device

By a thermal model (Figure 2.11), the heat transfer from the channel to the

thermopile and substrate can be analyzed. At steady-state, the total heat generated (Q) is

given by Eq. 2.5

$$Q = q_1 + q_2 .$$ Eq. 2.5

Where,

Q is equal to the total heat produced at the coverslip surface.

q_1 is the heat transfer towards the glass slide and formulated as in Eq. 2.6

q_2 is the heat transfer towards the thermopile and formulated as in Eq. 2.7

$$q_1 = \frac{T_1 - T_\infty}{R_{conv,2} + R_f + R_{conv,1} + R_{gs} + R_{conv,3}} .$$ Eq. 2.6

$$q_2 = \frac{T_1 - T_\infty}{R_{cs} + R_k + R_{conv,4}} .$$ Eq. 2.7

Where T_1, T_∞ are the temperatures of the coverslip surface at the reaction zone

and air, respectively.

$R_{conv,1}$, $R_{conv,2}$ are the convection thermal resistances associated with the fluid and

glass slide, and fluid and glass coverslip, respectively.

$R_{conv,3}$, $R_{conv,4}$ are the convection thermal resistances associated with the glass

slide and air, and Kapton® and air, respectively.

R_{gs}, R_f, R_{cs} and R_k are the thermal resistances of the glass slide, the fluid, the

coverslip and Kapton, respectively.

The thermal resistance of a material (R) can be calculated by the following Eq. 2.8 [101]:

$$R = \frac{L}{k \cdot A}.$$

Eq. 2.8

Where:

L- thickness of the layer (m),

k- thermal conductivity (W m^{-1} K^{-1}), and

A- area of the layer (m^{2}).

Heat transfer rates q_1 and q_2 can be alternatively expressed in terms of the heat transfer coefficient (U) [101], which is analogous to Newton's law of cooling (Eq. 2.9 and Eq. 2.10) such as

$$q_1 = U_1 A\, \Delta T.$$

Eq. 2.9

$$q_2 = U_2 A\, \Delta T.$$

Eq. 2.10

Where U_1, U_2 are the overall heat transfer coefficients, A is the area of the layer and ΔT is the overall temperature difference.

From Eq. 2.7 and Eq. 2.10, the overall heat transfer coefficient is related to the total thermal resistance.

$$U_1 A = \frac{1}{R_{conv,2} + R_{conv,1} + R_f + R_{gs} + R_{conv,3}}.$$

Eq. 2.11

Similarly, from Eq. 2.8 and Eq. 2.11

$$U_2 A = \frac{1}{R_{cs} + R_k + R_{conv,4}}.$$

Eq. 2.12
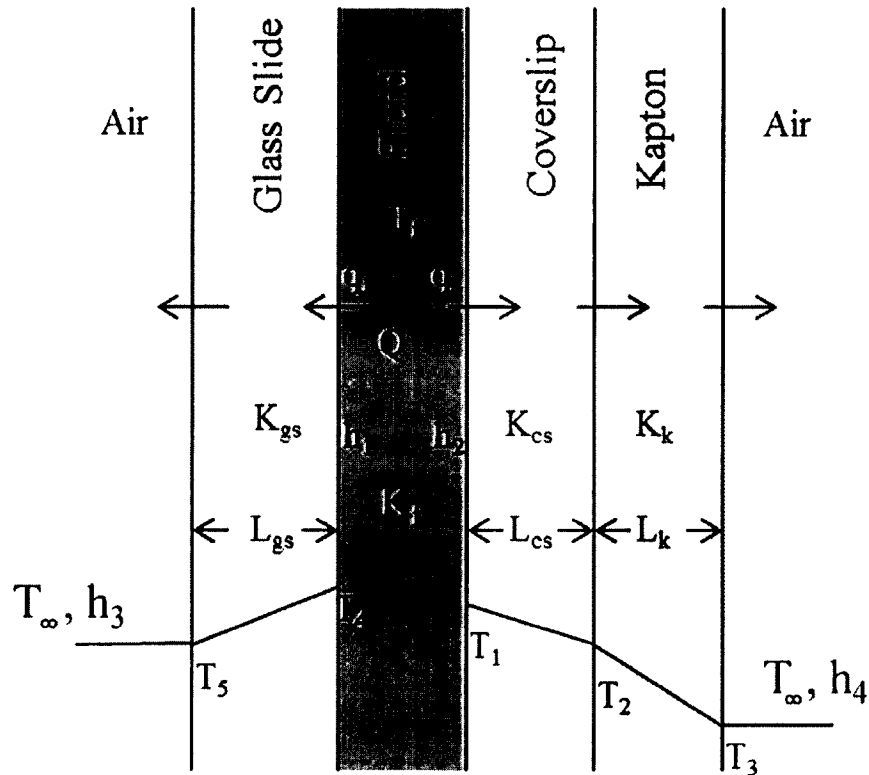
Figure 2.11: Thermal model of the proposed thermoelectric sensor. The surface temperatures of the coverslip, Kapton®, air, fluid, and glass slide are indicated by T_1, T_2, T_3, T_4, and T_5 respectively. The convective heat transfer coefficients at the fluid-glass slide and fluid-glass coverslip interfaces are indicated by h_1 and h_2. The convective heat transfer coefficients at the glass slide-air and Kapton®-air interfaces are indicated by h_3 and h_4. The thermal conductivities of glass slide, fluid, coverslip and Kapton are indicated by K_{gs}, K_f, K_{cs}, and K_k respectively

The area for each component is considered to be the same as the reaction zone area, which is approximately 24 mm² (the width of the hydro dynamically focused sample is approximately 4 mm and the length of the measuring junctions region is 6 mm). By Eq. 2., the thermal resistance of the glass slide is 48 K W⁻¹, the fluid (water) is 8.88 K W⁻¹, the glass coverslip is 6.07 K W⁻¹ and the Kapton is 34.48 K W⁻¹. Thermal resistance of the substrate towards the top channel wall is the cumulative thermal resistance of the fluid and the glass slide ($R_f + R_{gs}$) and the thermal resistance towards the thermopile is

the cumulative thermal resistances of the glass coverslip and Kapton $(R_{cs}+R_k)$. The thermal resistance towards the thermopile is R_{cs} when the thermopile is fabricated directly on the coverslip by eliminating the Kapton tape $(R_k$ is 0). By Eq. 2.11 , the heat transfer to the glass slide per temperature change is 0.017 W K^{-1} and by Eq. , to the thermopile via the coverslip and Kapton, it is 0.025 W K^{-1} and via the coverslip, it is 0.165 W K^{-1}.

2.6   Experimental Measurement System

The experimental measurement system consisted of the microfluidic thermoelectric sensor, two syringe pumps (Model '11' Plus syringe pumps, Harvard Apparatus, Holliston, MA) or two pressure pumps (Mitos P-Pump, Dolomite Microfluidics) and a nano voltmeter (Model 34420A, Agilent, Inc., Loveland, CO) enclosed in separate faraday cages to shield from electrical noise as shown in Figure 2.12. Extreme measures to control the ambient temperature were not unnecessary other than a simple enclosure for the microfluidic thermoelectric sensor. In the absence of large air convection currents, the enclosure was not needed. A pump was operated continuously to inject water/media/Locke's solution through the inlets using a 0.01 inch internal diameter Teflon (ETFE) tubing (Upchurch Scientific, Oak Harbor, WA). A six-Port Injection valve, Model V-451 (Upchurch Scientific, Oak Harbor, WA) with Teflon tubing for holding the sample was integrated between pump two and the microfluidic thermoelectric sensor. A sample loop of the variable length changed the sample volume according to experimental requirements. The experimental requirements would be either the single inlet device or the two inlet device. The larger the sample loop, the more time it takes for the sample to flow over the thermopile. When a single inlet was used, the sample fluid width in the device is the width of the device itself. So, the sample loop

length was increased to increase the sample volume and hence the sample time of travel over the thermopile is compensated. Also, changing the sample volume changed the transient time of the sample flowing over the thermopile.
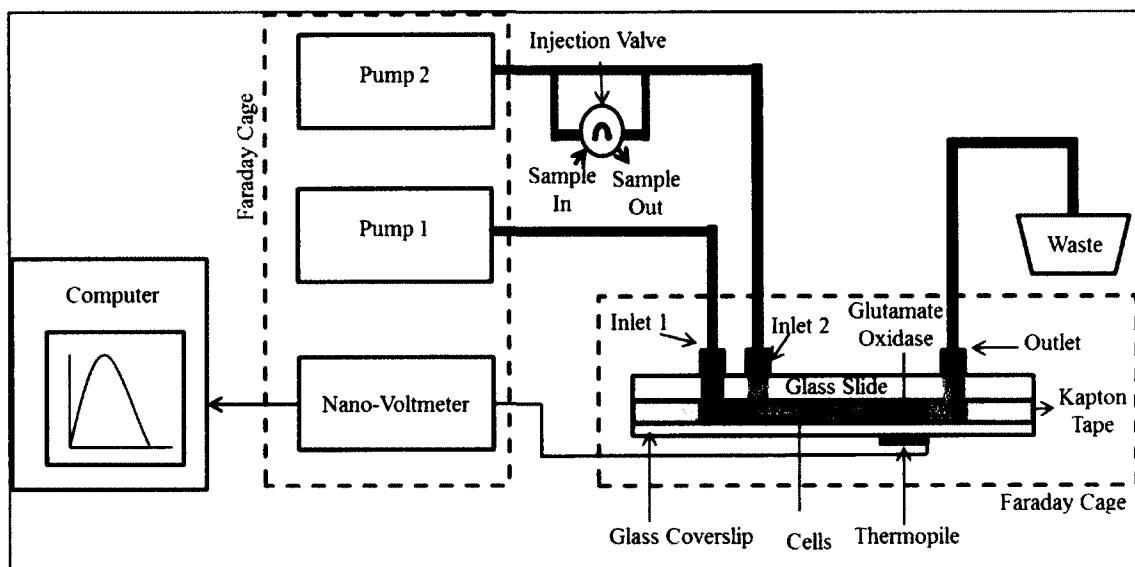
Figure 2.12: Block diagram of the experiment measuring system with two inlets

A sample was injected into the media/Locke's solution stream being supplied to the inlet using a 6-Port Injection valve, Model V-451 (Upchurch Scientific, Oak Harbor, WA). This impulse injection mode minimizes the sample's volume. When the leading tip of the sample bolus reached the first pair of measuring junctions of the thermopile, the reaction began to occur over the measuring junctions of the thermopile where the L-GLOD/brain tumor cells were immobilized. The heat of the reaction increased the temperature of the measuring junctions relative to the reference junctions. The response of the thermopile as voltage was measured using a nano-voltmeter. The output of the nano-voltmeter was recorded and processed using National Instruments Lab View Signal Express (National Instruments Corporation, Austin, TX).

2.7 Calibration of the Thermoelectric L-glutamate Sensor

To calibrate the L-glu sensor, two flow configurations were used. First a microfluidic device with two inlets, one outlet and a rectangular flow channel with L-GLOD immobilized to the inner surface of the glass coverslip over the entire thermopile (measuring and reference junctions) was used. An antimony/bismuth, thin-film thermopile fabricated on a Kapton® support sheet was attached to the external surface of the coverslip. The block diagram of this experimental system is shown in Figure 2.13. The flow rates at inlets 1 and 2 were adjusted to 100 and 25 µl min^{-1}, respectively. The water introduced through the inlets flowed in the channel and over the thermopile. The water from inlet 2 was hydro dynamically focused by the inlet 1 flow. Hence, the fluid from inlet 2 flowed along the center of the channel and only over the measuring junctions of the thermopile. A 6-Port injection valve (Model V-451, Upchurch Scientific, Oak Harbor, WA) with a sample loop that holds 5 µl sample was placed between the pump supplying the flow to inlet 2 and inlet 2. The sample was injected into the buffer stream being supplied to inlet 2 using the 6-Port Injection valve. Under these conditions, the L-glu sample flowed into the inlet 2 flow path. The reaction took place at the measuring junctions of the thermopile when the sample carried by inlet 2 flow path reached the thermopile.
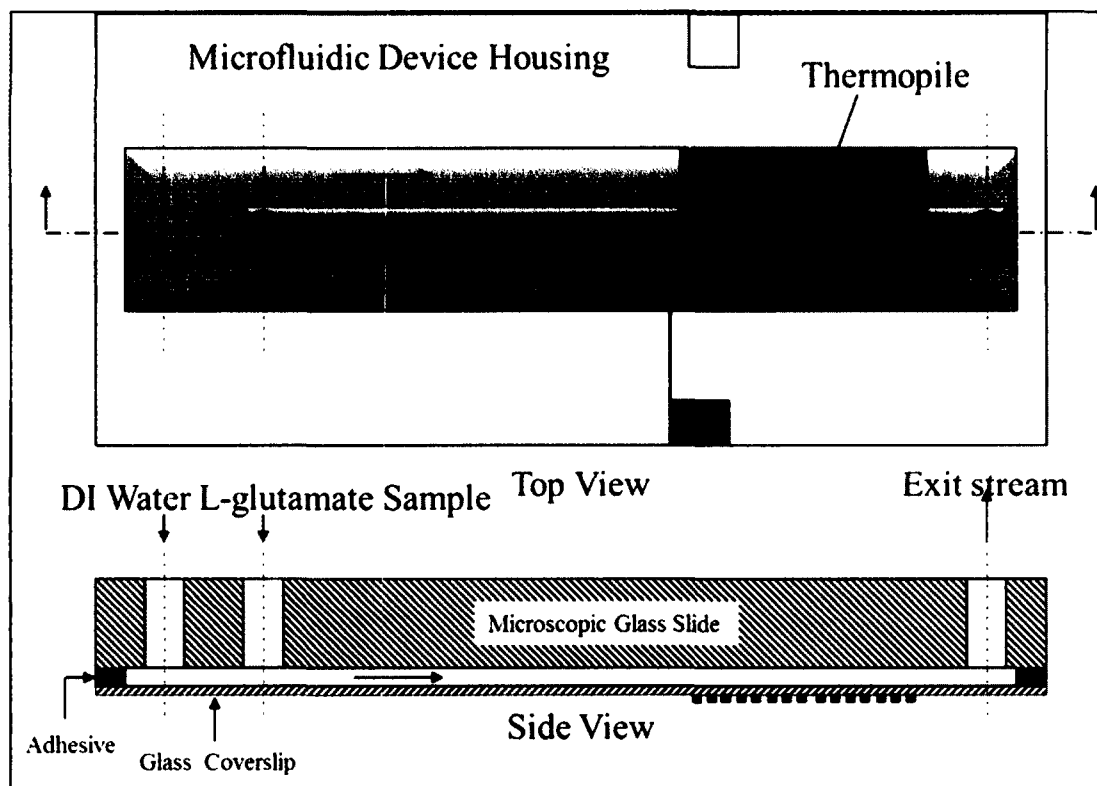
Figure 2.13: Top view and cross sectional side view of thermoelectric L-glu sensor with two inlets

Secondly, to increase the lowest detection limit, the microfluidic device with a thermoelectric sensor was modified to have only one inlet and the L-GLOD was immobilized only over the measuring junctions of the thermopile instead of immobilizing it on the entire thermopile area. Also, to reduce thermal resistance between the reaction zone and the thermopile, the thermopile was fabricated directly on the outer channel wall of the coverslip. The L-GLOD was immobilized to the inner surface of the glass coverslip using LbL self-assembly. The block diagram of this experimental system is shown in Figure 2.14 and the block diagram of the microfluidic sensor is shown in Figure 2.15. The flow rate operated at the inlet was 50 µl min^{-1}. The reaction took place at the measuring junctions of the thermopile when the sample reached the thermopile upon

which the L-GLOD was immobilized. A 40 µl sample loop was connected to the injection valve. Because the L-GLOD was only immobilized over the measuring junctions of the thermopile, the heat generated during the deamination reaction was conducted to the measuring junctions of the thermopile but not to the thermopile reference junctions causing the measuring junction temperature to increase relative to the temperature of the reference junction.
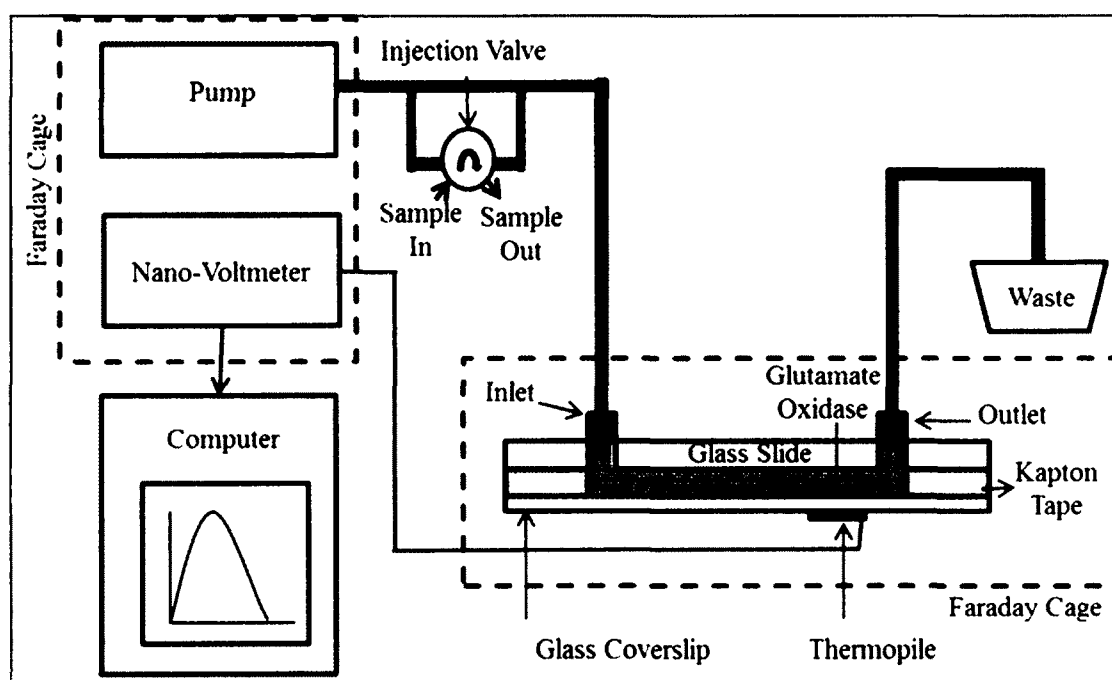
Figure 2.14: Block diagram of the experiment measuring system with one inlet
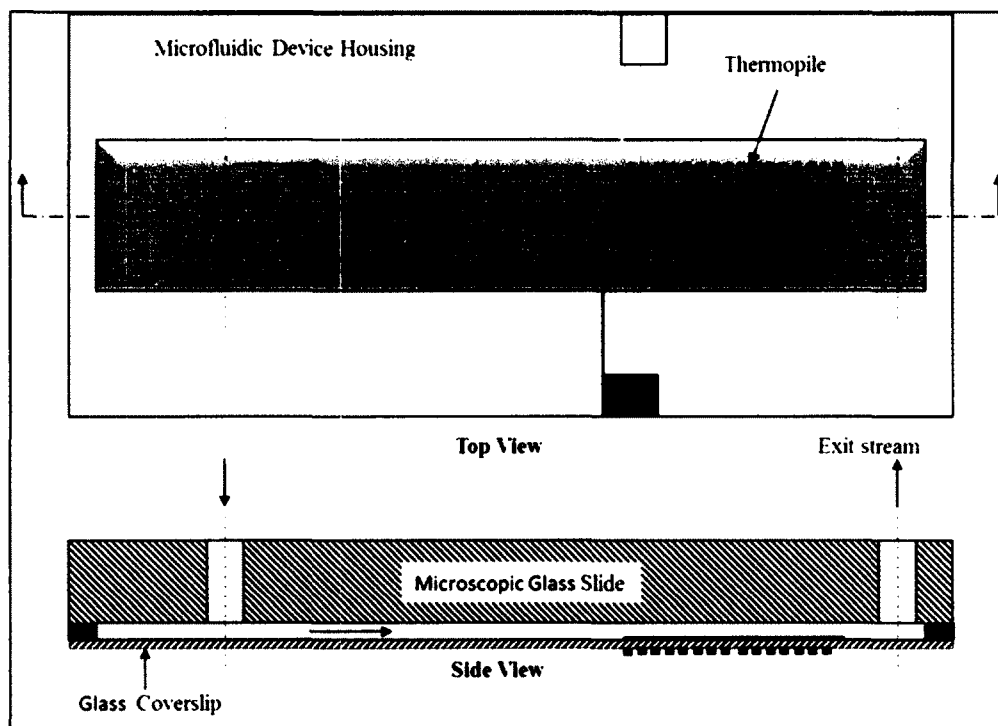
Figure 2.15: Top view and cross sectional side view of thermoelectric L-glu sensor with one inlet

L-glu (Sigma Aldrich.com) in powder form was used to make solutions containing various concentrations of L-glu. A solution containing 100 mg dL^{-1} of L-glu was first prepared using RO water in a large volumetric flask and diluted to lower concentrations. To calibrate the L-glu sensor, a series of experiments in which L-glu solutions with concentrations ranging from zero to 100 mg dL^{-1} were introduced into the microfluidic device. Each solution was introduced a minimum of three times. Following each injection, the change in the thermopile EMF was continuously recorded and was used to calculate the area-under-the-curve (AUC) which was equivalent to the total heat generated. AUCs were plotted as a function of L-glu concentration as a means of determining the minimal detection limit and linearity of the system.

2.8 Detection of L-glutamate from
Immobilized Brain Cells

To detect the L-glu from brain cells, L-glu was immobilized only on the

measuring junctions of the thermopile and the brain tumor cells were immobilized over

the whole thermopile. Stimulation solutions were introduced into the buffer flowing

within the microfluidic device using the six port injection valve located upstream from

the inlets to the microfluidic device. The block diagram of this experimental system is

shown in Figure 2.16. The stimuli that were used to stimulate L-glu release from the

brain tumor cells were 50 mM kcl and 2 μM ionomycin.
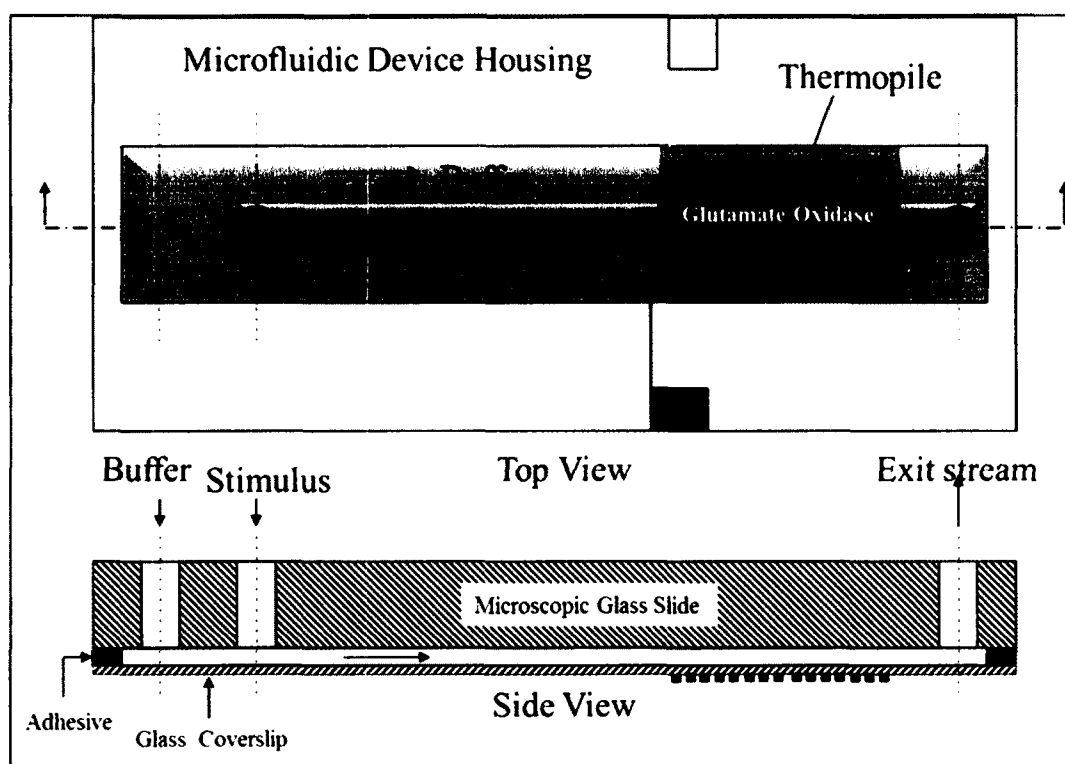
Figure 2.16: Top view and cross sectional side view of thermoelectric L-glu sensor with immobilized brain tumor cells

2.9   Detection of Brain Tumor Cell
Metabolism

Control experiments were done to detect the metabolism of the brain tumor cells

when immobilized on both the measuring and reference junctions of the thermopile. A 52

µl volume sample loop was connected to the injection valve to inject stimulation

solutions. The block diagram of this experimental system is shown in Figure 2.17. The

stimuli that were used to stimulate the brain tumor cells were 50 mM kcl and 2 µM

ionomycin.
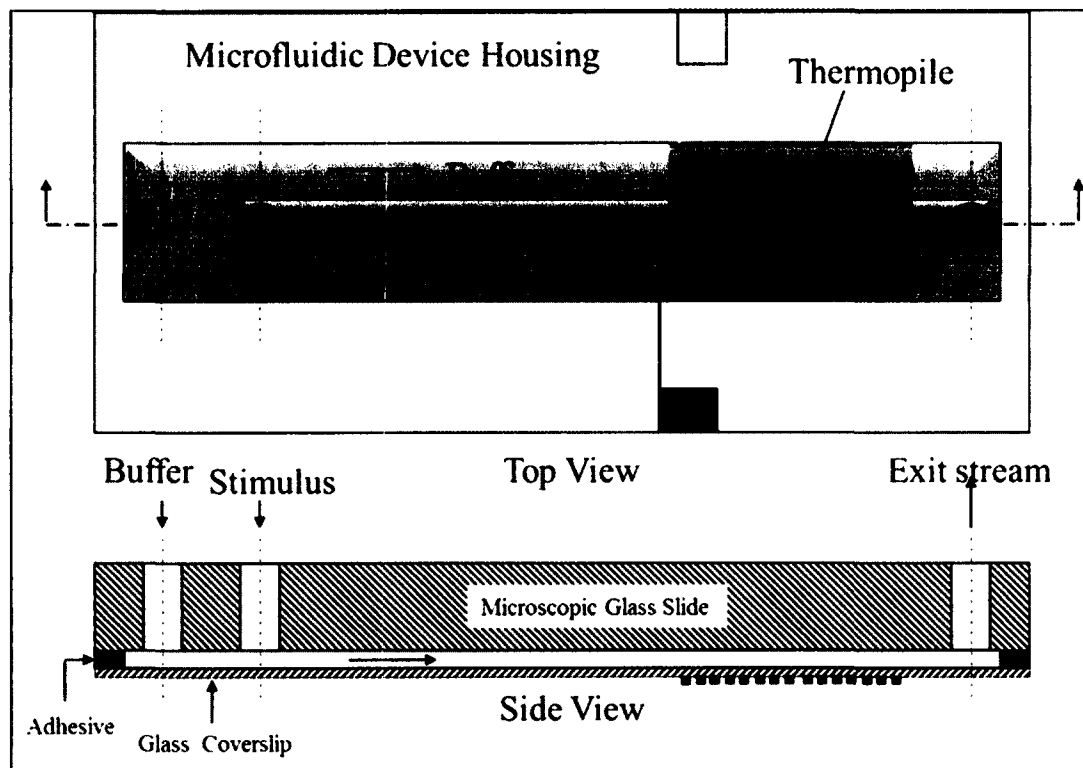
Figure 2.17: Top view and cross sectional side view of thermoelectric metabolism
sensor

In another set of experiments, the heat generation change from the cells was

measured by terminating the supply of glucose to the cells over the measuring junctions.

The termination of glucose supply decreased the metabolism of the cells and eventually

led to cell death. A decrease in the baseline signal was expected which implied reduced metabolic activity of the cells on the measuring junctions. To terminate the glucose supply to the cells, the Locke's solution, without glucose, was injected for a period of time at inlet 2 while Locke's solution, with glucose, was continuously injected at both inlets.

CHAPTER 3

RESULTS

3.1   Thermopile Testing

The thermopiles fabricated on the polyimide supports were tested to measure their Seebeck coefficients. The thermopile was placed in the measurement system shown in Figure 2.6, and the response was measured for applied temperature changes. These experiments were performed with two different nichrome wires of widths 3.18 mm and 1.52 mm. Figure 3.1 shows the response of the thermopile for known quantities of heat when the nichrome wire width used was 3.18 mm. Figure 3.2 shows the response from three thermopiles for temperatures associated with different applied energy levels when the nichrome width used was 1.52 mm. When the width of the nichrome wire used was 3.18 mm, the Seebeck coefficient measured for the thermopile was very low ~3.4 LV (m° C)$^{-1}$. Thermopiles showed a Seebeck coefficient of ~6.3 LV (m° C)$^{-1}$, however, when the width of the nichrome wire used was 1.52 mm. The measured thermopile response for known quantities of power was also measured and is shown in Figure 3.3. Thermopile heat power sensitivity of the thermopile was ~0.8 V W^{-1}.
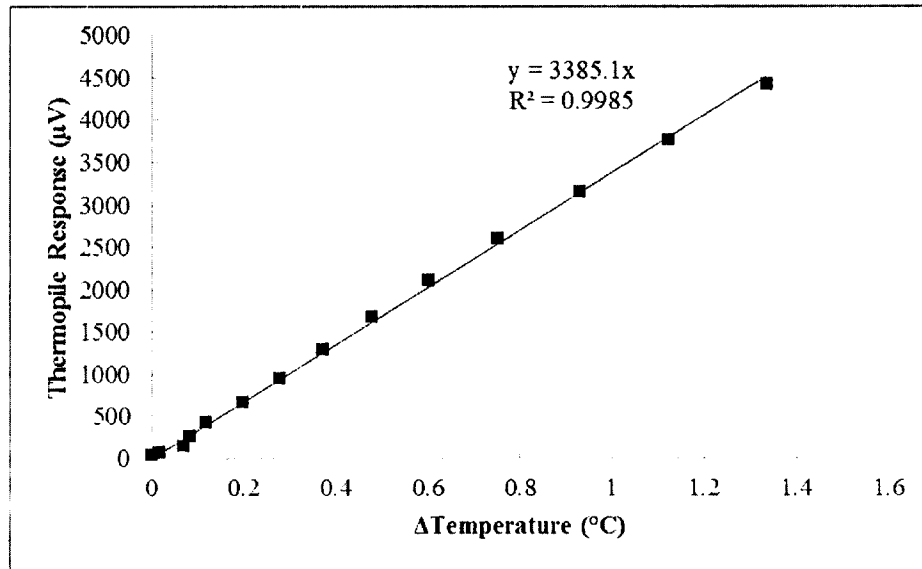
Figure 3.1: Thermopile (20 KΩ) response for known quantities of temperature (Nichrome wire width = 3.18 mm)
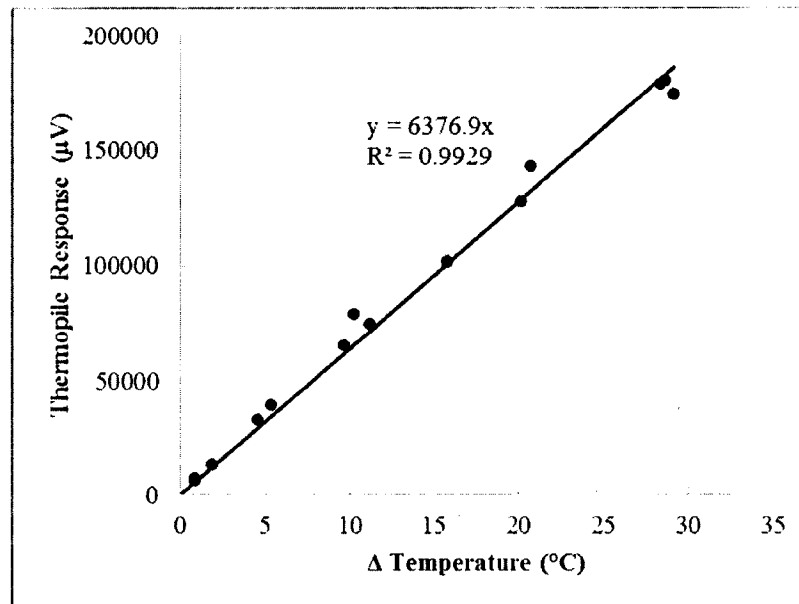
Figure 3.2: Thermopile responses for known quantities of temperature measured for three different thermopiles of resistances 18 kΩ, 19 kΩ and 28 kΩ (Nichrome wire width = 1.52 mm)
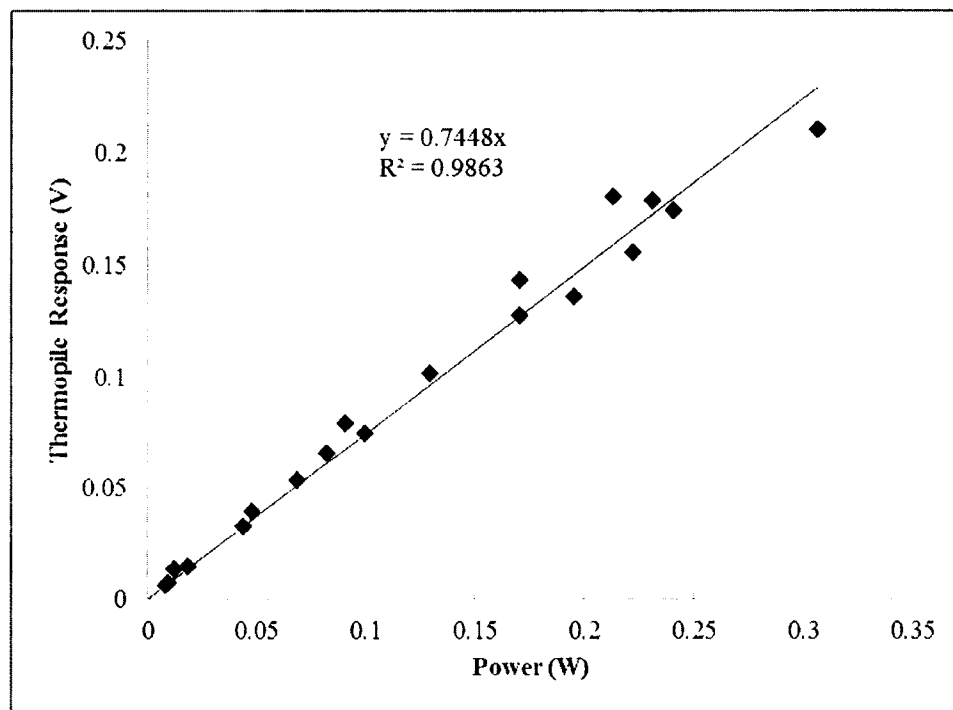
Figure 3.3: Measured thermopile response for known quantities of heat

3.2   Thermoelectric Sensor Calibration

The microfluidic thermoelectric sensor was also calibrated by applying known amounts of heat in the microfluidic device. This was done by incorporating the nichrome heater wire either on the measuring junctions of the thermopile (reaction zone) or on the center of the entire channel length. Calibration of the thermoelectric sensor was investigated and studied using both configurations.   To mimic the glucose measurement experiments, fluid was also flowing in the microfluidic device. The response of the thermoelectric sensor was recorded after applying a constant current (low and high currents) for ~30 seconds to the nichrome wire. The width of the nichrome wire used was 1.52 mm. The power (P) applied to the nichrome wire was calculated by Eq. 3.1

$$P = I^2 R$$ Eq. 3.1

Where I is the current applied to the nichrome wire, amps, R is the resistance of the nichrome wire, ohms, and the resistance (R) of the wire depends on the length of the nichrome wire used.

The typical response of the sensor is shown in Figure 3.4. A constant current of 433 mA was applied to the nichrome wire for ~30 seconds. When the heater was turned on, the voltage (response) of the thermopile increased and then approached a constant level after some time. When the heater was turned off, the thermopile voltage decreased back to the baseline value. The response of the sensor was quantified by the area under the curve (AUC), which represents the total heat detected by the sensor, and by the peak height, which represents the temperature increase caused by the current. The integration time for the AUC is the red line in Figure 3.4, which begins when the heater is turned on and ends when the curve returns to the baseline.
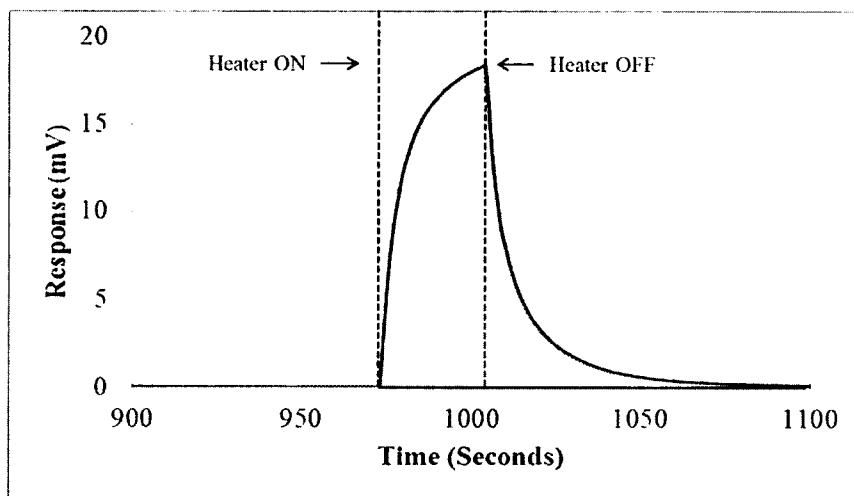
Figure 3.4: The typical response of the thermoelectric sensor when constant current for ~ 30 seconds is applied to the integrated nichrome heater wire. The nichrome wire is integrated only the measuring junctions of the thermopile

The response of the sensor increased linearly with the applied power. The areas under the curves of the responses were plotted against the power applied, and the slope of the graph was the sensitivity of the thermoelectric sensor. When the nichrome heater was integrated at the center of the whole channel length, the thermoelectric sensor had a sensitivity of 1.62 V-s W^{-1} with an R^2 value of 0.9967 (Figure 3.5) for applied low currents and a sensitivity of 1.59 V-s W^{-1} with an R^2 value of 0.9992 (Figure 3.6) for applied high currents. The slight decrease in the sensitivity from 1.62 V-s W^{-1} to 1.59 V-s W^{-1} was caused by conduction of heat from the measuring junctions to the reference junctions, even though the fluid was flowing in the channel.
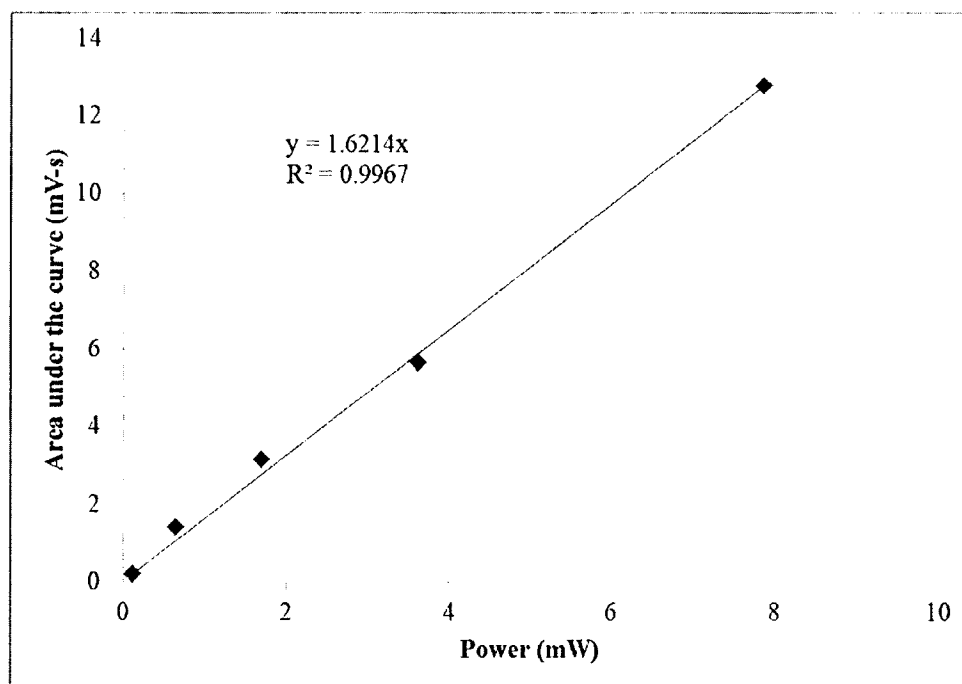
Figure 3.5: Area under the curve plotted as a function of applied power (low currents) by heating the nichrome wire incorporated on the inner side of the microfluidic device bottom channel wall all along the channel length. Water was continuously injected through inlet 1 and inlet 2 at flow rates of 100 µl min^{-1} and 25 µl min^{-1}, respectively
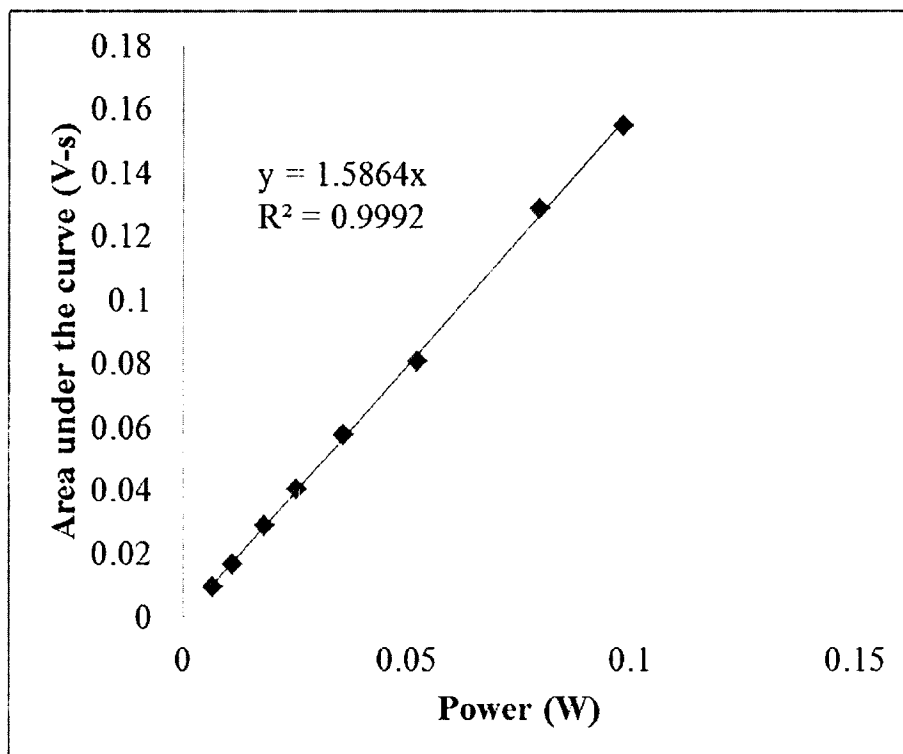
Figure 3.6: Area under the curve plotted as a function of applied power (high currents) by heating the nichrome wire incorporated on the inner side of the microfluidic device bottom channel wall all along the channel length. Water was continuously injected through inlet 1 and inlet 2 at a flow rate of 100 µl min^{-1} and 25 µl min^{-1}, respectively

The thermoelectric sensor had a sensitivity of 1.3393 V-s W^{-1} with an R^2 value of 0.9998 (Figure 3.7) when the nichrome heater was integrated only on the measuring junctions of the thermopile. The sensitivity of the thermoelectric sensor was higher when the nichrome wire was incorporated in the center and along the entire channel length. This increased sensitivity might be caused by the increase in the temperature of the fluid while it flowed from the inlet to the thermopile.
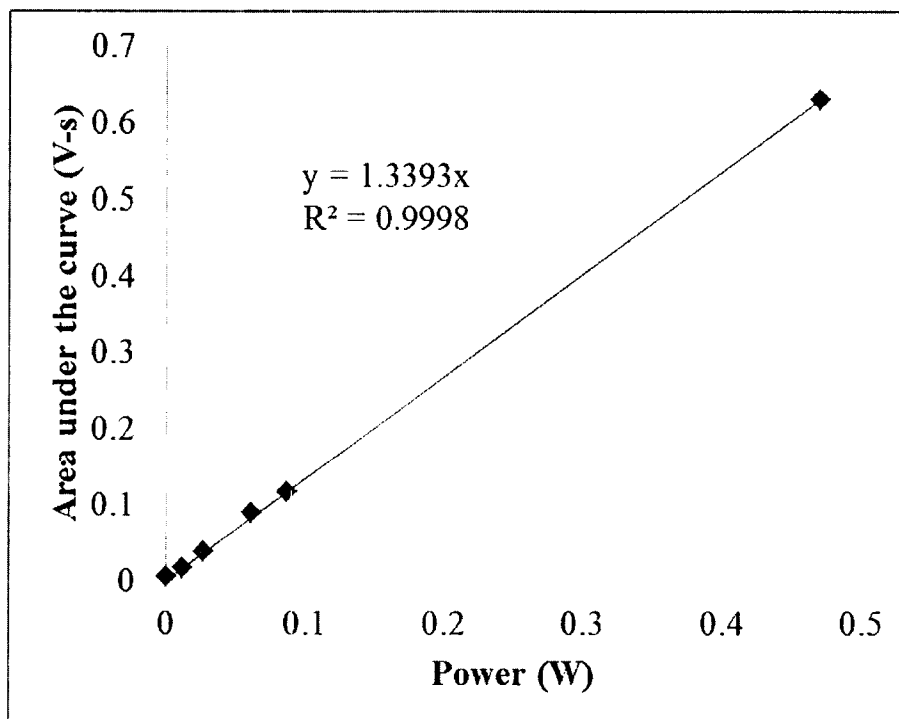
Figure 3.7: Area under the curve plotted as a function of applied power by heating the nichrome wire incorporated on the inner side of the microfluidic device bottom channel wall on the measuring junctions of the thermopile. Water was continuously injected through inlet 1 and inlet 2 at flow rates of 100 μl min^{-1} and 25 μl min^{-1}, respectively

3.3   Quartz Crystal Microbalance (QCM)
Analysis of Immobilized Enzyme

In this study, the multilayers on the coverslip were the precursor layers (PEI/PSS) and (PEI/GOD)$_n$, where n represents the number of L-GLOD layers on the coverslip. Figure 3.8, Figure 3.9, and Figure 3.10 show the QCM monitoring of the frequency shift for the polyelectrolytes and L-GLOD multilayer construction at various experimental conditions.
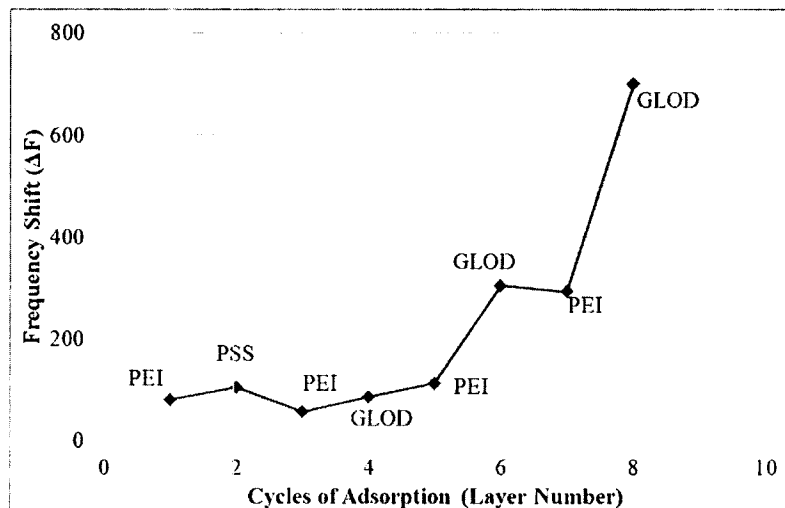
Figure 3.8: The L-GLOD assembly process showing frequency shift (Hz) versus cycles of adsorption. Three precursor layers were immobilized before L-GLOD immobilization. The concentration of PEI and PSS used was 0.1 mg ml^{-1} and the concentration of L-GLOD used was 0.1 U mL^{-1}. The electrode was dipped in PEI and PSS for 15 minutes and was dipped in L-GLOD for 30 minutes
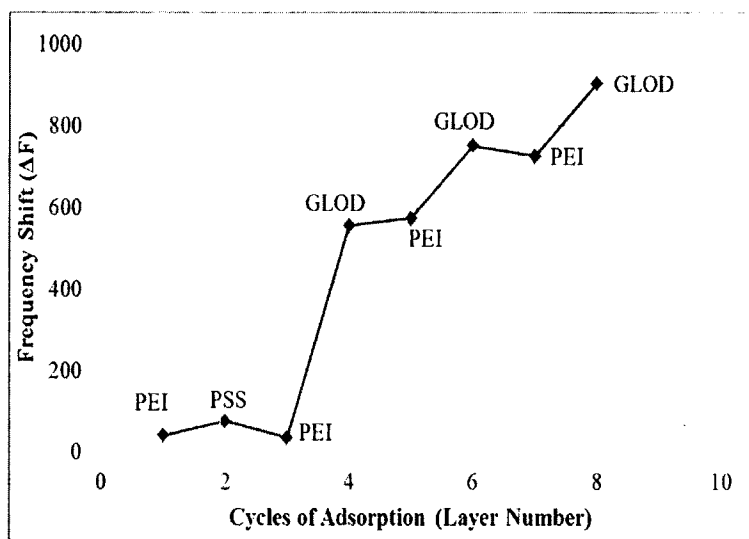
Figure 3.9: The L-GLOD assembly process showing frequency shift (Hz) versus cycles of adsorption. Three precursor layers were immobilized before L-GLOD immobilization. The concentration of PEI and PSS used was 0.1 mg ml-1 and the concentration of L-GLOD used was 0.1 U mL^{-1}. The electrode was dipped in PEI and PSS for 15 minutes and was dipped in L-GLOD for 2 hours
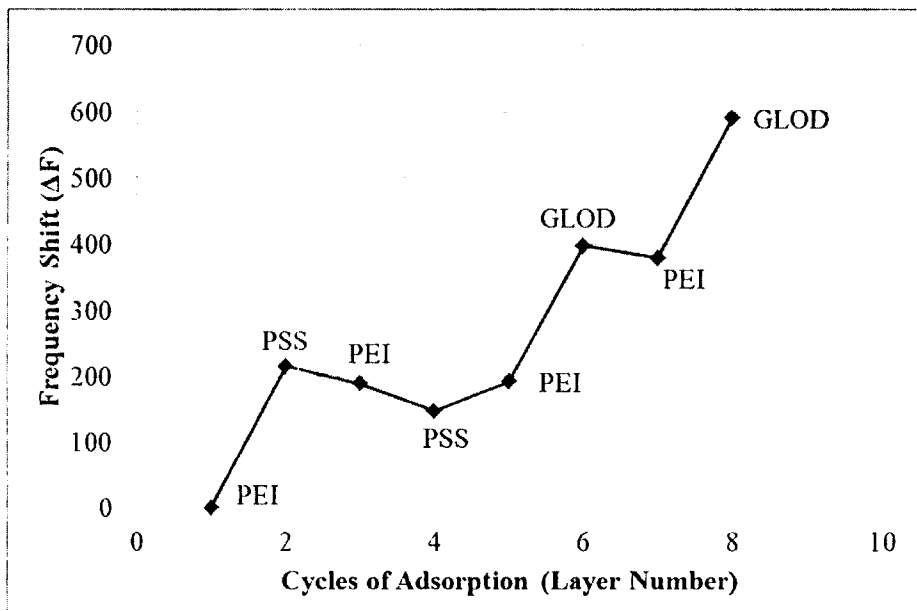
Figure 3.10: The L-GLOD assembly process showing frequency shift (Hz) versus cycles of adsorption. Five precursor layers were immobilized before L-GLOD immobilization. The concentration of PEI and PSS used was 0.1 mg ml^{-1} and the concentration of L-GLOD used was 0.1 U mL^{-1}. The electrode was dipped in PEI and PSS for 15 minutes and was dipped in L-GLOD for 2 hours

The Sauerbrey relation of mass and thickness estimation from frequency shift predicts that a 1 Hz change in ΔF corresponds to a change in the crystal mass of 0.87 ng (Eq. 2.) and a thickness of 0.017 nm (Eq. 2.). From Figure 3.8, the mass of immobilized L-GLOD in each consecutive layer is 25 ng, 167 ng, and 355 ng. From Figure 3.9, the mass of immobilized L-GLOD in each consecutive layer is 455 ng, 154 ng and 155 ng. From Figure 3.10, the mass of immobilized L-GLOD in each consecutive layer is 179 ng and 183 ng. QCM mass distribution of L-GLOD layers for various protocols of LBL is shown in Figure 3.11.
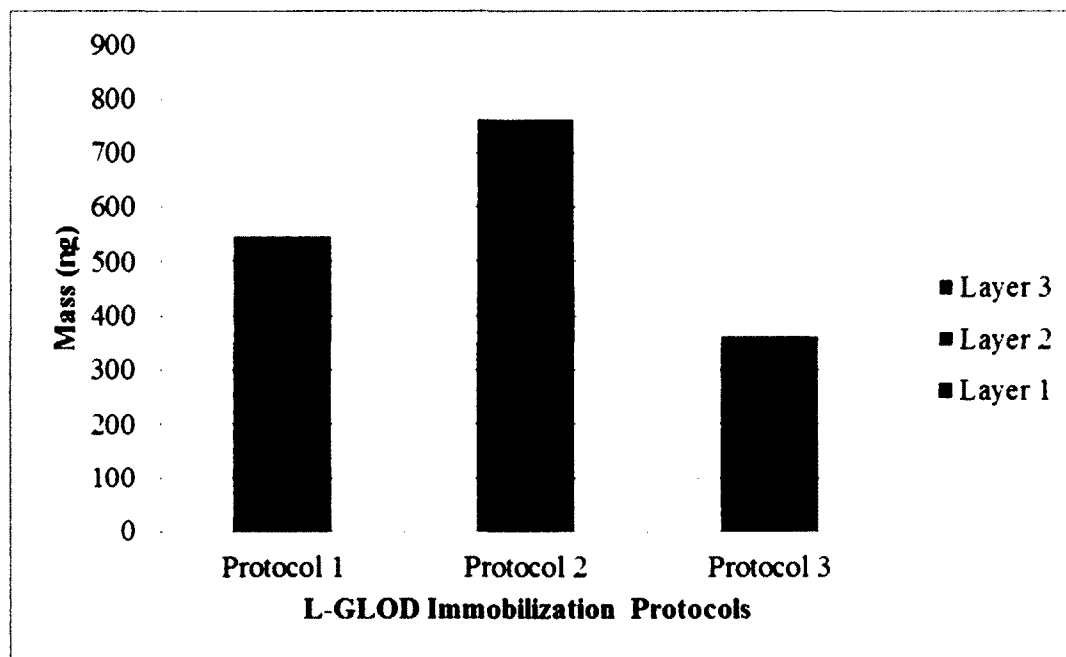
Figure 3.11: QCM mass distribution of L-GLOD layers for various protocols of LBL

3.4   Fluorescence Analysis of Immobilized Enzyme

L-GLOD was also immobilized on round glass coverslips of 5 mm diameter under conditions identical to the LBL conditions stated in Section 2.2.1. Multiple layers of immobilized L-GLOD on the coverslips was used to determine the activity of the L-GLOD using the Amplex red assay and a fluorescence meter. The Amplex red assay test (Invitrogen Corporation, Carlsbad, CA) was performed to measure the activity of the L-GLOD layers. Fifty μl of reactant solution (100 μM Amplex® reagent, 0.25 U ml^{-1} Horseradish peroxidase, 0.5 U ml^{-1} L-glutamate-pyruvate transaminase, 40 μM L-glu, and 200 μM L-alanine) and 50 μl of the reaction buffer were used for the activity test. Four layers of L-GLOD took less time to reach its maximum fluorescence value when compared to the two layers of L-GLOD (Figure 3.12). The maximum value is the same in both cases since the L-glu concentration is the same in all wells.
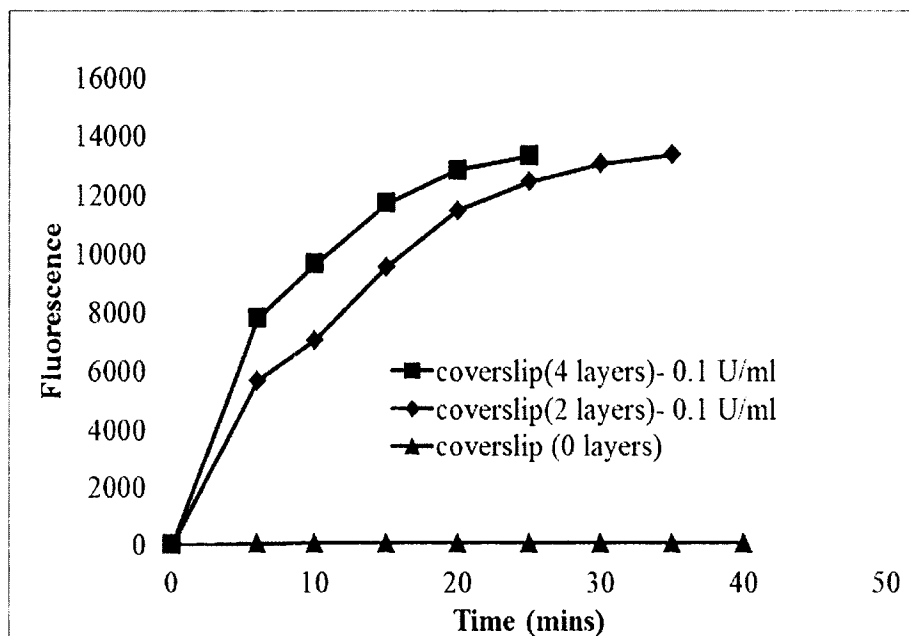
Figure 3.12: Monitoring of L-glu deamination kinetics to quantify immobilized L-GLOD activity on round glass coverslips. The concentration of L-GLOD used for immobilization was 0.1U ml^{-1}. Two and four layers of immobilized L-GLOD were investigated. Fresh coverslip without L-GLOD were used for negative control

The kinetics of L-glutamate deamination was also studied when the L-GLOD was in immobilized form and in bulk form. Figure 3.13 shows that the amount of L-GLOD adsorbed in one, two, and three layers of immobilized L-GLOD is between 0.1 and 0.04 units.
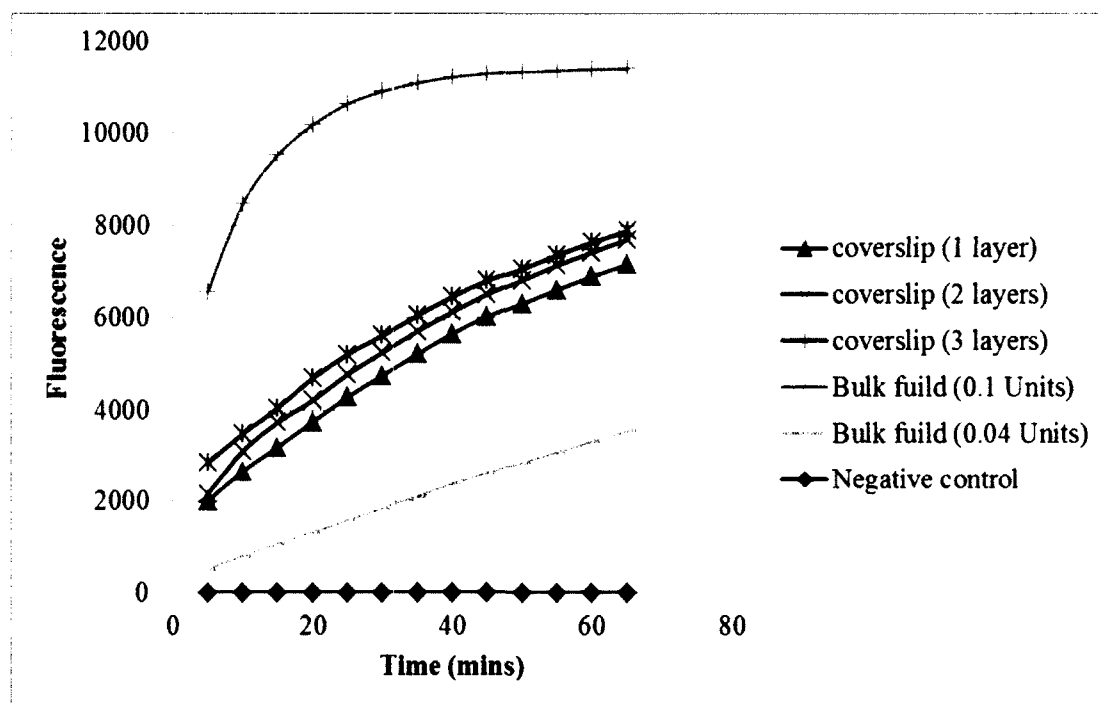
Figure 3.13: L-glu deamination kinetics with L-GLOD in immobilized form and bulk form. The concentration of L-GLOD used for immobilization was 0.1U ml^{-1}. One, two and three layers of immobilized L-GLOD, and 0.1 U and 0.04 U of bulk L-GLOD were investigated. A coverslip without L-GLOD was used for negative control

The fluorescence response for multilayers of L-GLOD immobilized on the coverslip was reported in Figure 3.14 after incubation for sixty minutes at room temperature. The activity of the enzyme increased with an increase in the number of immobilized glutamate oxidase layers. The increase in the activity was not significantly higher for multiple layers of L-GLOD.
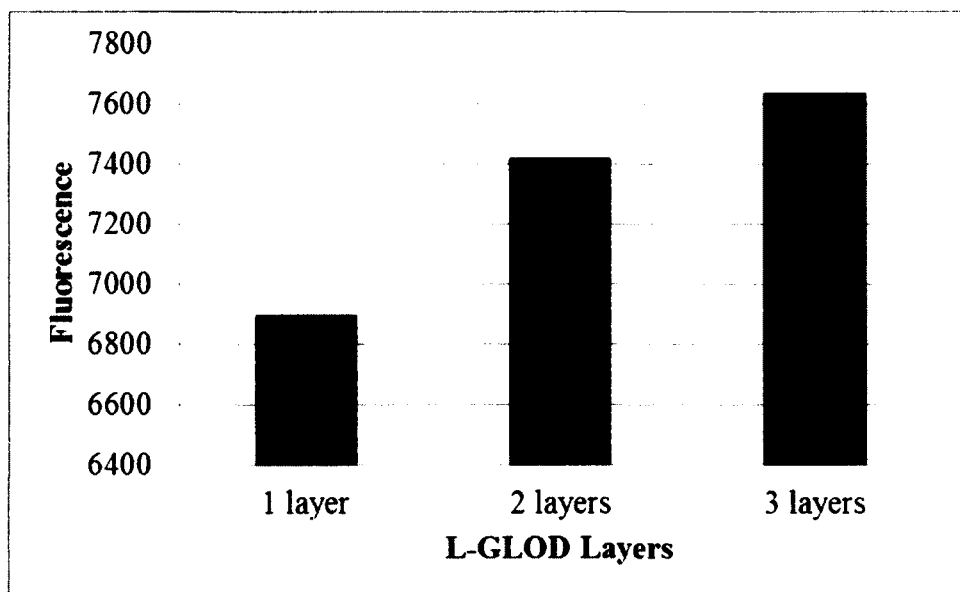
Figure 3.14: Fluorescence of immobilized multilayers of L-GLOD. Data was collected after sixty minutes of incubation at room temperature. One, two and three layers of immobilized L-GLOD were investigated

The stability of the immobilized L-GLOD films for a period of eight days was studied. L-GLOD activity decreased ~40% over a period of 8 days when stored in de-ionized (DI) water at room temperature. The activity decreased ~49% over a period of eight days when stored in Tris-Buffer (pH 7.5) at room temperature, and ~73% over a period of eight days when stored in air at room temperature. Figure 3.15 shows the storage stability of immobilized L-GLOD in air, water, and buffer.
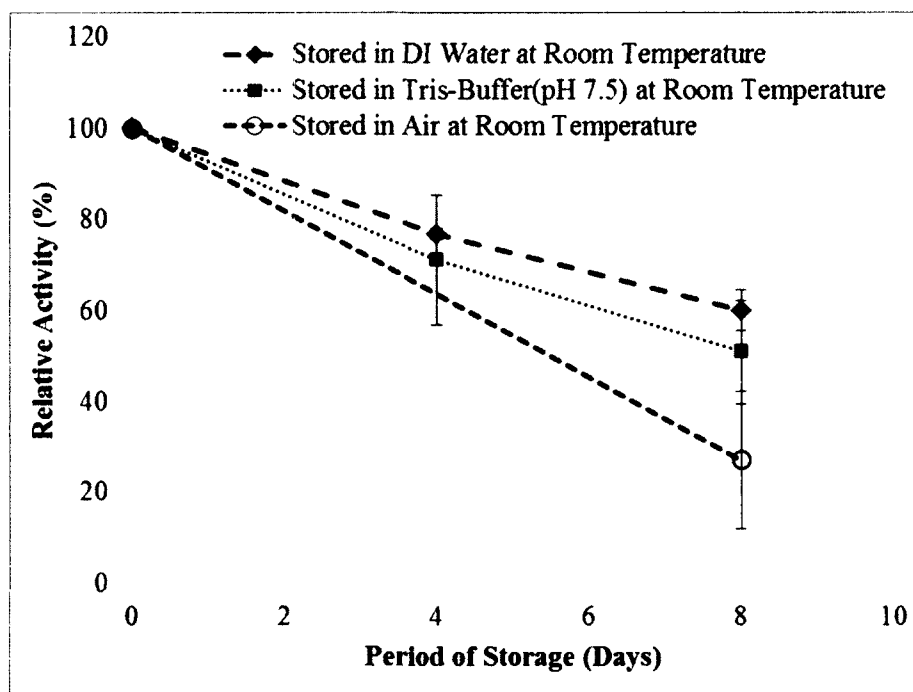
Figure 3.15: Storage stability of immobilized L-glutamate oxidase films

3.5 Cell Imaging

3.5.1 Selective Adhesion of Cells Using PLL

The selective adhesion of the cells obtained in the PLL-coated area (towards left of the marked line) is shown in Figure 3.16.

Figure 3.16: Selective adhesion of brain tumor cell line CRL 2303 on PLL coated substrate imaged with a 100X objective lens. The image was taken four hours after plating the cells on the glass coverslip

3.5.2   Cell Imaging Using Calcein AM to
         Determine Viability

To quantify the differences between the live (healthy) or apoptosing cell cultures,

the cells were fluorescently stained with Calcein AM®. Figure 3.17 shows the live cells

that were loaded with calcein AM. As shown in the figure, calcein AM permeated into

the cell wall of the live cells was hydrolyzed by intracellular esterases, converted to the

strongly green fluorescent substance calcein, and retained in the cell's cytoplasm.
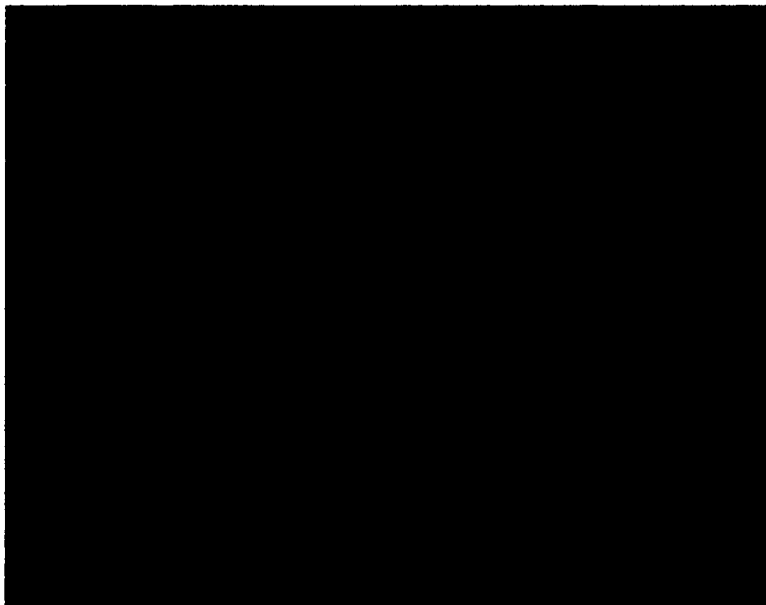
Figure 3.17: Testing of viability in brain tumor cell line CRL 2303 loaded with Calcein AM imaged with an 200X objective lens

3.5.3 DAPI Staining of Cells to Determine Dead Cells

The cells in the Petri dish were loaded with DAPI stain and incubated for 20 minutes at 37° C and 5% CO_2. Figure 3.18 shows the imaging of dead cells loaded with DAPI. The image was taken after twenty minutes of incubation using a 450 nm excitation filter. The fluorescence intensity of cell pixel area is proportional to the non-viable cell count.
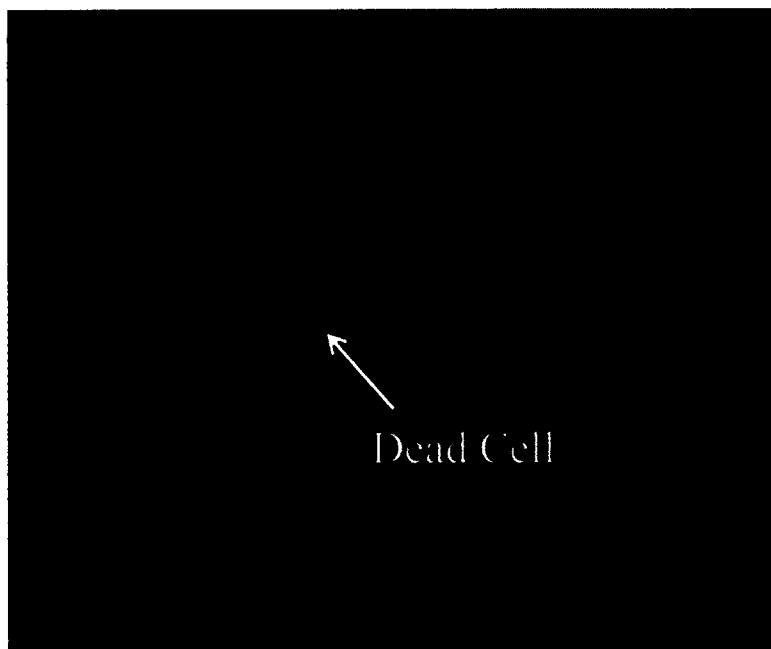
Figure 3.18: DAPI staining of dead cells nuclei at 200X magnification after 20 min of incubation

3.5.4   MTT Assay Test for Cells to
          Determine Metabolism

To measure metabolic activity by means of a calorimetric assay, 3-(4, 5-Dimethylthiazol-2-yl)-2, 5-diphenyltetrazolium bromide (MTT) was used. Reduction of MTT only occurs in metabolically active cells, and the level of activity is a measure of the viability and metabolic activity of the cells. Figure 3.19 shows the absorbance of MTT assay by the tumor cells signifying the metabolism of brain tumor cells.
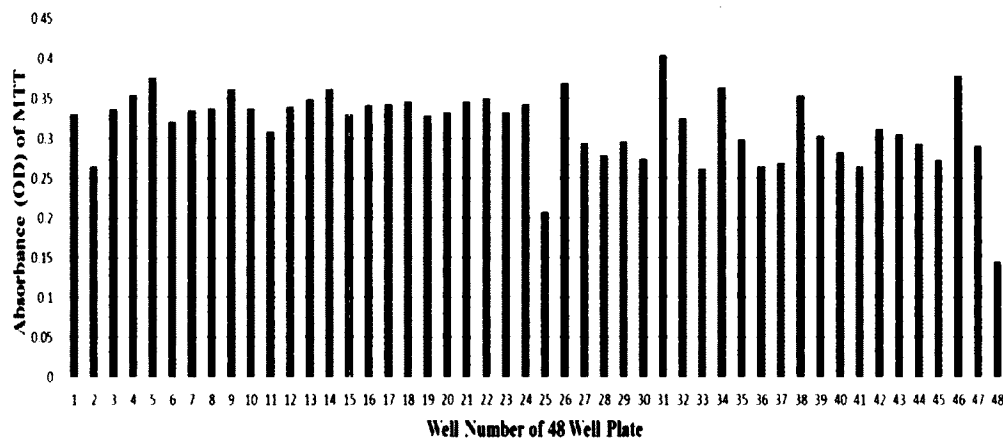
Figure 3.19: Absorbance of MTT Assay signifying the metabolism of brain tumor cells (CRL 2303). A Plate reader set to 575 nm wavelength was used to analyze the assay

3.5.5   Calcium Imaging Using Fluo3

Imaging of calcium is important in determining the L-glutamate levels in the cells. The increase in the intracellular calcium ion concentration stimulates L-glu release from the cells. Figure 3.20 shows the normalized fluorescence intensity of calcium response in the cells stimulated with kcl and ionomycin. The graph shows the dynamics of the intracellular calcium levels. Six regions of interest were selected in the video that was taken to study the calcium levels inside the cell following stimulation with kcl and ionomycin. These six regions of interest are represented in Figure 3.20 below as N-ROI 1, 2, 3, 4, 5, and 6.
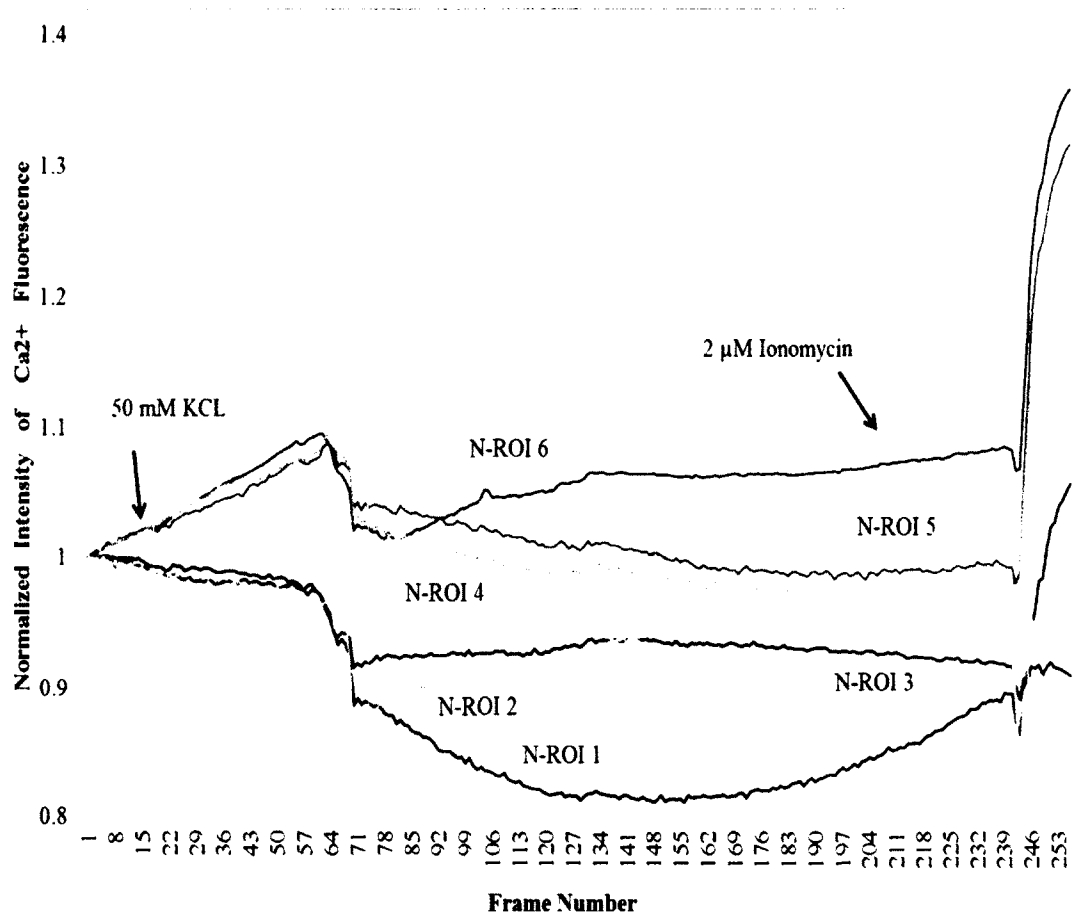
Figure 3.20: Normalized intensity of Ca^{2+} fluorescence of brain tumor cells (CRL-2303) in response to kcl and ionomycin. The data is recorded at two frames per second. N-ROI represents normalized region of interest

As shown in Figure 3.20, the calcium ions levels inside the cells increased for about 25 seconds when stimulated with 50 mM kcl and then immediately returned to the base level (N-ROI 4, 5, and 6). There was approximately an 8% increase in the concentration of calcium in the cells. There is a large immediate increase in the intracellular calcium levels of 40% when 2 μM ionomycin was added to the cells. Figure 3.20 shows the recording of three healthy cells and three unhealthy cell regions. The unhealthy cell regions did not respond to the KCL and ionomycin stimulation except N-ROI 1, which responded slightly (16 % increase in calcium level) to ionomycin.

3.6   Fluorescence Analysis of L-glutamate
Release from Cells

L-glu release from glioma cells was measured using the Amplex Red Assay

response from fluorescent spectrophotometer. To measure the L-glu released from glioma

cells, samples of cell media were collected after 0.5, 1, 2, 3, 4, and 5 minutes after the

stimulation of the cells with 50 mM KCL. The change in L-glu over a period of five

minutes following the stimulation of the cells with 50 mM KCL is shown in Figure 3.21.
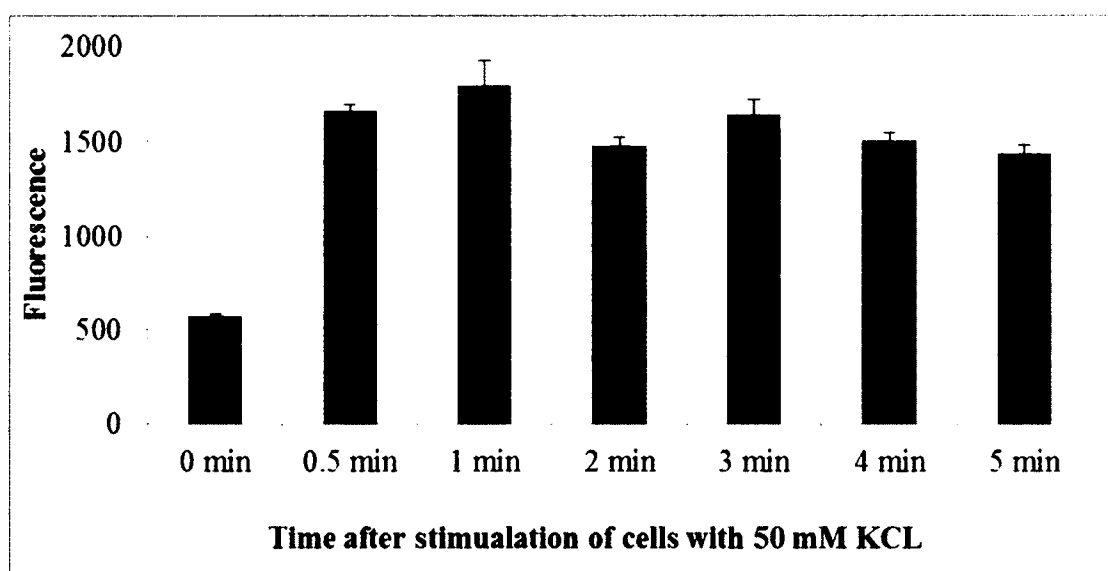
Figure 3.21: Fluorescence response of L-glutamate for brain tumor cell line CRL 2303
media samples following kcl stimulation. The cells were plated in a petri dish at a
density of 200,000 cells ml⁻1. After 24 hours, the cells were treated with stimulating
chemical (50 mM kcl). The samples of cell media were collected in regular time
intervals after treatment

3.7   Cell Immobilization in Microfluidic
Thermoelectric Sensor

Brain tumor cells of cell line CRL 2303 were immobilized over the coverslip

surface above the measuring and reference junctions of the thermopile fabricated on the

opposite side of the coverslip. This was accomplished by pipetting 150 - 200 μL of the

media with cells on the PLL coated area over the thermopile as shown in Figure 3.22. The concentration of cells used for immobilization of cells was 200,000 per ml. The surface tension of the droplet held the media on the surface of the thermopile.
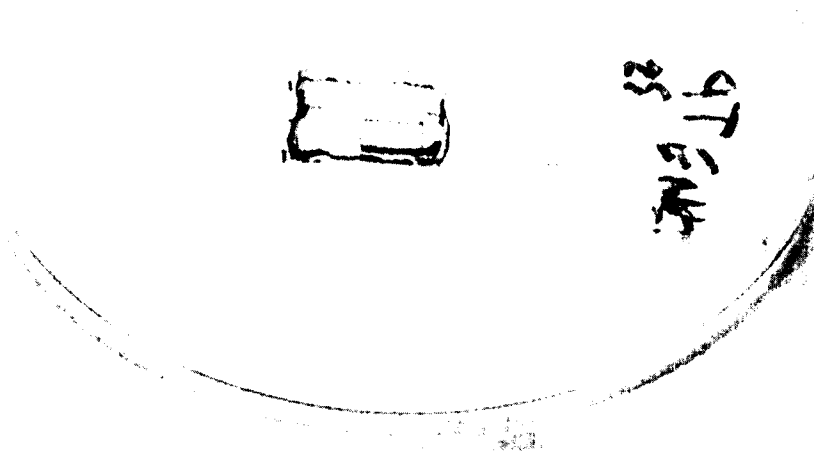
Figure 3.22: Brain tumor cells being immobilized over the thermopile on the coverslip

The immobilized cells on the coverslip were imaged after one day and two days as shown in Figure 3.23. The image shows the area between the two columns of the measuring junctions of the thermopile. The cell density of the immobilized cells was observed to increase from day one to day two.
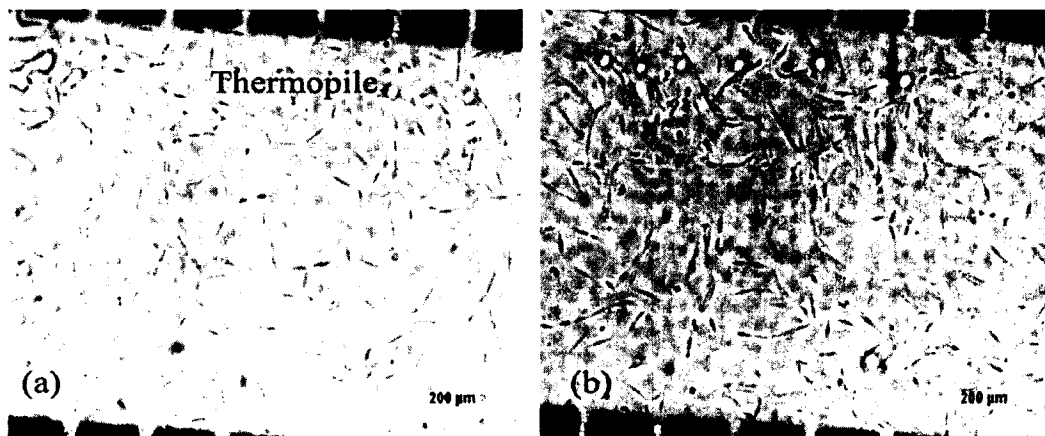
Figure 3.23: Immobilized cells on the coverslip after (a) Day 1 and (b) Day 2 before device fabrication. The concentration of cells used for immobilization was 200,000 cells per ml of media. Brain cancer cell line CRL 2303 immobilized on coverslip over the thermopile (reference and measuring junctions). Cells were incubated in 5% CO_2 at 37° C

The cells were immobilized only on the PLL coated area as shown in Figure 3.24.

The viability of the immobilized cells was also tested using trypan blue dye as shown in

Figure 3.24 (c). As trypan blue loads into the dead cells, the dead cells turn blue as

indicated with text on the image.
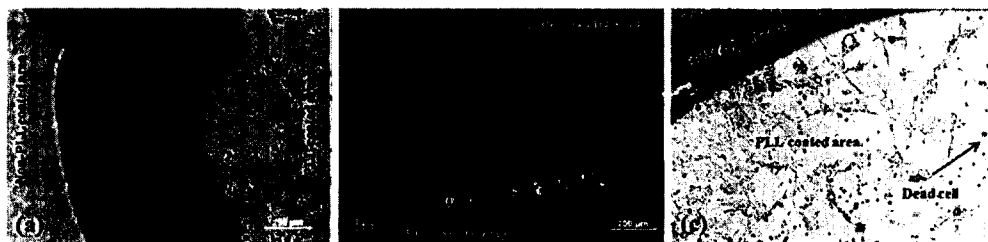
Figure 3.24: (A) Immobilized Cells on PLL coated and PLL uncoated surface before 1-day incubation. (B) Immobilized Cells on PLL coated and PLL uncoated surface following 1-day of incubation. (C) Cell viability

After two days, once the cells were completely attached and confluent, the

coverslip was used to fabricate the microfluidic thermoelectric sensor. Figure 3.25 shows

the microfluidic thermoelectric L-glu sensor with the brain tumor cells immobilized on the inner surface of the device's coverslip. Although Figure 3.25 shows three thermopiles fabricated on the coverslip, the cells are immobilized only on the thermopile which has copper straps connected to collect the data.

Figure 3.25: Fabricated microfluidic device with cells immobilized at a location upstream from the inlet

The fabricated L-glu sensor was used to detect the dynamics of L-glu released from immobilized brain cells using the flow injection system operated by syringe pumps. Figure 3.26 shows the images of immobilized cells in the microfluidic device imaged at various stages of the experiment.
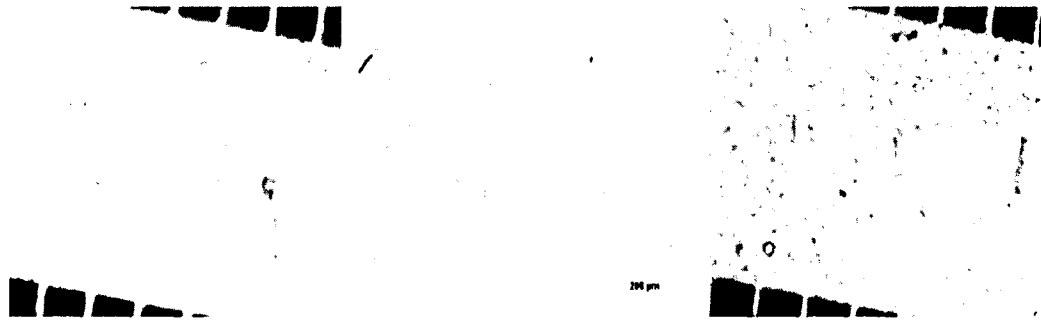
Figure 3.26: Immobilized cells on the coverslip after (a) 5 minutes, (b) 3 hours and (c) 7 hours after device fabrication and continuous flow of media at 50 μl min⁻¹. Brain cancer cell line CRL 2303 immobilized on coverslip over the thermopile (reference and measuring junctions). Cells were incubated in 5% CO_2 at 37° C. The length of the scale bar is 500 μm

The concentration cells in the media used to immobilize the cells was increased from 200,000 cells per ml of media to 500,000 cells per ml of media. Figure 3.27 shows the immobilized cells in the microfluidic device at different scale views. The cells were imaged after 48 hours of incubation in 5% CO_2 at 37° C. The population of the cells on the measuring junction of the thermopile (18 mm²) or reaction zone was approximately 2×10^6 cells.

Figure 3.27: Immobilized brain tumor cells in the microfluidic device on the surface of the coverslip over the thermopile on the opposite side of the coverslip. (a) 100X view. The length of the scale bar is 500 μm. (b) 400X view. The length of the scale bar is 200 μm. The concentration of cells used for immobilization was 500,000 cells per ml of media. The cells were imaged after 48 hours of incubation in 5% CO_2 at 37° C

The immobilized cells in the microfluidic device were imaged after three - four hours of experiment under continuous flow of media over the cells. Figure 3.28 shows the images of the immobilized cells that were confluent before and after the flow experiments. At the beginning of the experiment, approximately 2×10^6 cells were

present on the thermopile, and after the continuous flow experiment approximately 1.8 ×

10^6 cells were present.
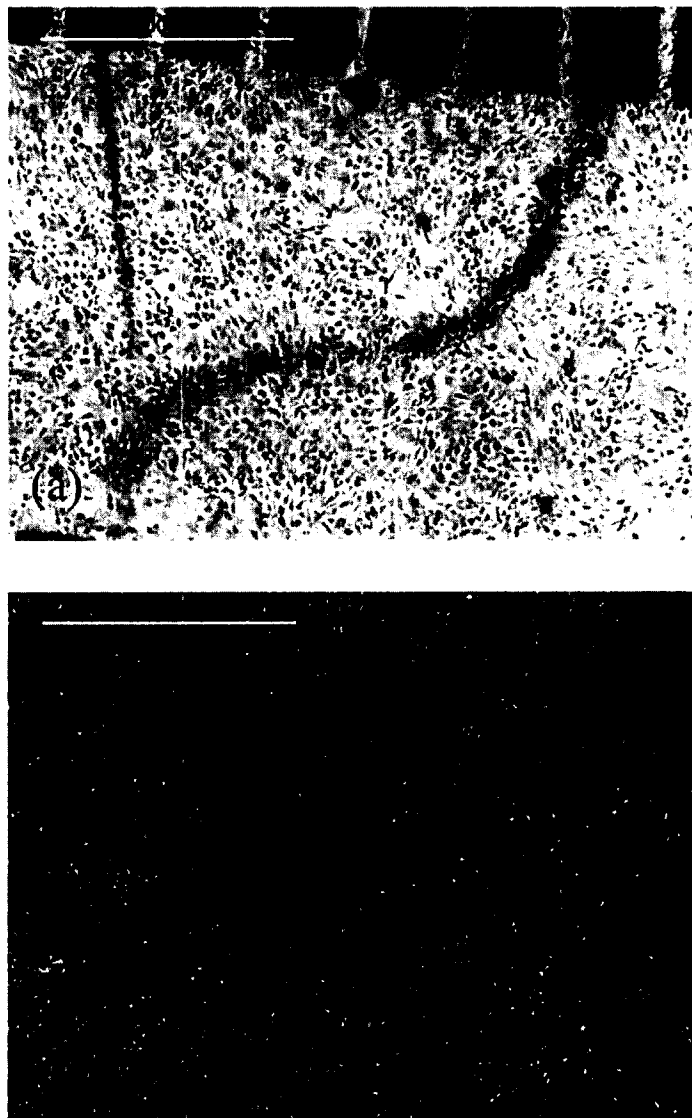
Figure 3.28: Immobilized cells in microfluidic device on coverslip over thermopile under continuous flow conditions (a) at the beginning of the experiment and (b) after the experiment. The Locke's solution flow rate was 50 μl min⁻¹ and 25 μl min⁻¹ at inlet one and two, respectively. The images were taken at 100X magnification. The length of the scale bar is 500 μm.

3.8   Thermoelectric L-glutamate Sensor

3.8.1   Calibration of Thermoelectric L-glu
Sensor

The L-glu sensor's output voltage is increased by the heat released on the

measuring junctions by the L-glu reaction in the presence of immobilized L-GLOD, and

it slowly returns to the baseline as the sample flows beyond the thermopile. Five μL L-

glu solutions of different concentrations were introduced into the microfluidic device,

using the sample loop. Responses of the sensor for various concentrations of L-glu were

recorded. A two inlet device with flow rates of 100 μl min^{-1} at inlet one and 25 μl min^{-1} at

inlet two was used. One layer (PEI/GLOD) of L-GLOD was immobilized on the bottom

channel wall of the microfluidic device. A thermopile fabricated on a Kapton® sheet was

attached to the external surface of the coverslip. Figure 3.29 shows the typical response

of the thermopile following the injection of an L-glu sample of concentration equal to

100 mg dL^{-1}. The area under the curve represents the total heat produced during the

reaction. Figure 3.30 summarizes the response of the thermopile for various L-glu

concentrations. The response was linear in the range of 0 - 100 mg dL^{-1} (0 - 54 mM) L-

glu concentration. The response of the L-glu sensor saturated when the concentration of

L-glu was greater than 100 mg dL^{-1} (54 mM). The lowest detection limit of the L-glu

sensor was 5 mg dL^{-1}. The sensitivity of the sensor was 1.02 LVs mg^{-1} dL^{-1} (18.5 nVs

mM^{-1}) in the linear range of 0 - 100 mg dL^{-1} (0 - 54 mM).
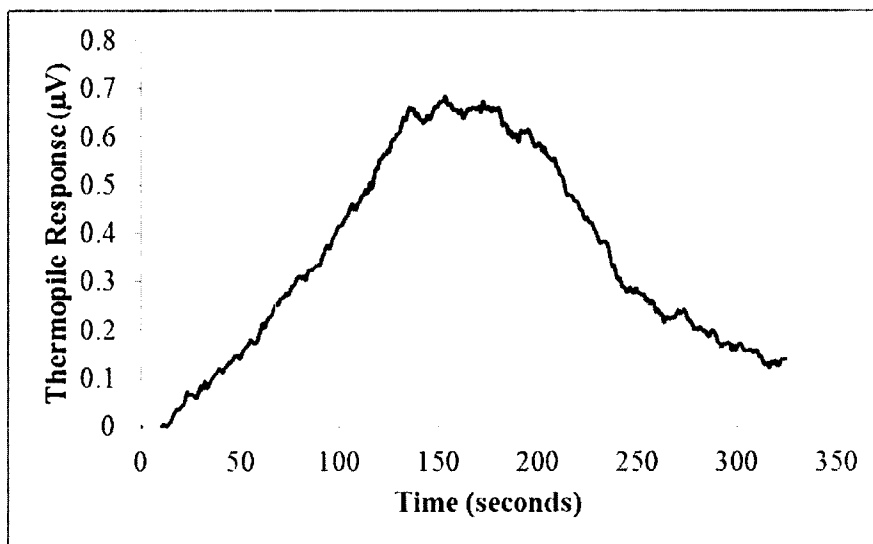
Figure 3.29: Typical thermopile response of the thermoelectric L-glu sensor for 100 mg/dl of L-glu concentration
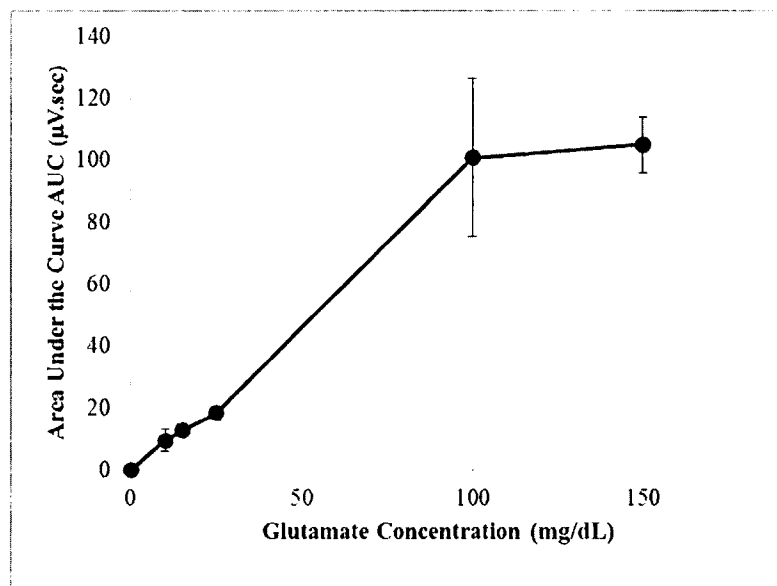
Figure 3.30: Response of thermoelectric L-glu sensor for various concentrations of L-glu samples. One layer of L-GLOD was immobilized. The concentration of L-GLOD used for immobilization was 0.1 U ml^{-1}. The microfluidic device with two inlets and one outlet was used. Flow rates imposed at inlet one and inlet two were 100 μl min^{-1} and 25 μl min^{-1}, respectively. A five μl sample of L-glu was introduced into the device. The thermopile was fabricated on a Kapton® sheet and attached to the external surface of the coverslip

A microfluidic device with one inlet and one outlet was used to perform similar experiments for the calibration of the L-glu sensor. In these experiments, a flow rate of 50 μl min^{-1} at the inlet was used. One and two layers of L-GLOD were immobilized on the bottom channel wall of the microfluidic device. Figure 3.31 shows the typical response of the thermopile following the injection of an L-glu sample of 100 mg dL^{-1} concentration. Under these conditions, the signal peak was observed to be larger (1.4 μV) in comparison to the experiments where the thermopile was fabricated on Kapton® and the device was used with two inlets (0.6 μV) (Figure 3.29). Figure 3.32 shows the response of the thermoelectric L-glu sensor in this series of experiments for various L-glu concentrations when one layer of L-GLOD was immobilized. The response was linear in the range of 0 - 50 mg dL^{-1} L-glu concentration. The response of the L-glu sensor started saturating and approached a constant voltage when the concentration of L-glu was greater than 50 mg dL^{-1}. The lowest detection limit of the L-glu sensor is 0.1 mg dL^{-1}. The sensitivity of the sensor was 0.6 μVs per mg dL^{-1} in the linear range of 0.1 - 50 mg dL^{-1} with an R^2 value of 0.9998.
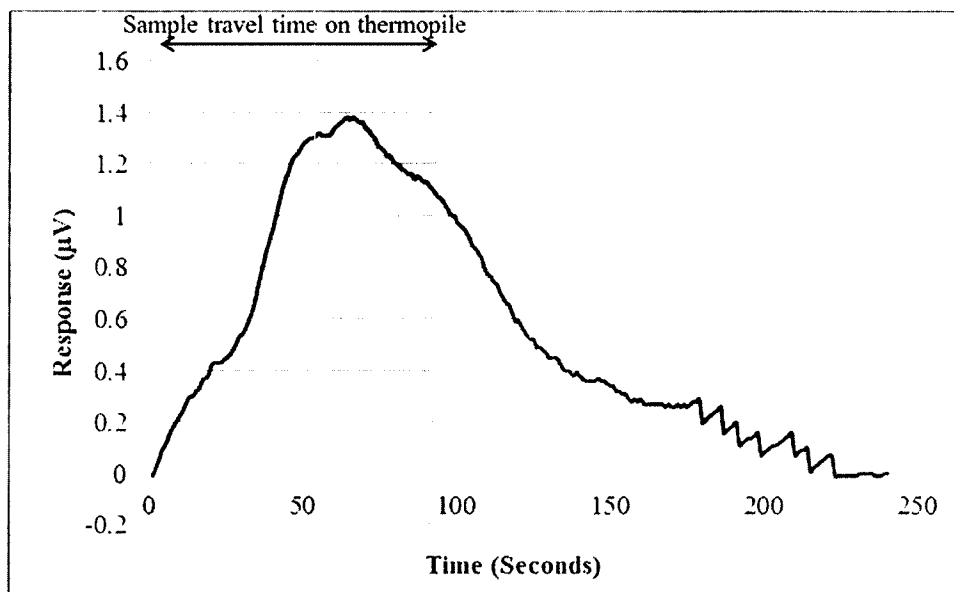
Figure 3.31: Typical response of the sensor for 100 mg/dl of glutamate concentration
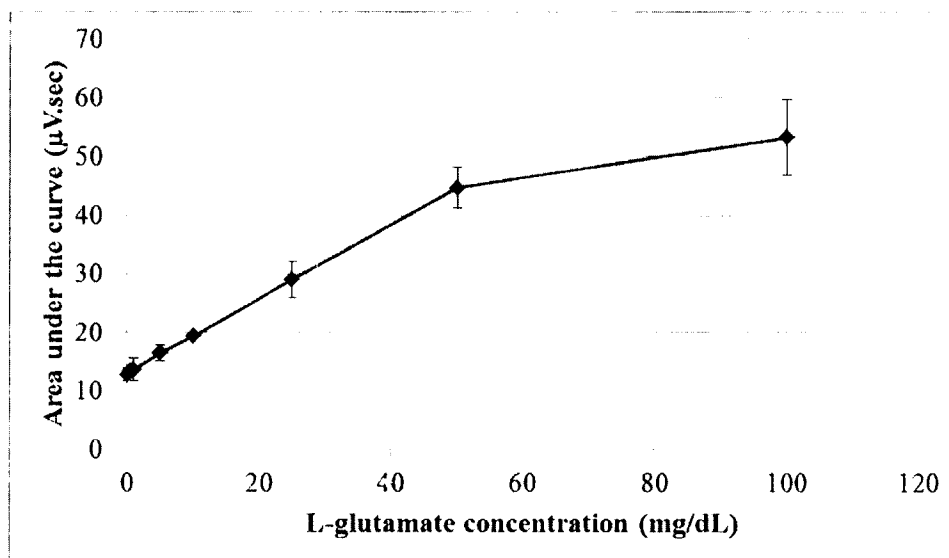
Figure 3.32: Response of thermoelectric L-glu sensor for various concentrations of L-glu samples. One layer of L-GLOD was immobilized. The concentration of L-GLOD used for immobilization was 5 U ml^{-1}. A microfluidic device with one inlet and one outlet is used. Flow rate operated at the inlet was 50 µl min^{-1}. A 40 µl sample of L-glu was introduced into the device. The thermopile was directly fabricated on the external surface of the coverslip

Figure 3.33 shows the response of the thermoelectric L-glu sensor for various L-glu concentrations when two layers of L-GLOD were immobilized. The response exponentially increased in the range of 0 - 25 mg dL^{-1} L-glutamate concentration. The response of the L-glu sensor started saturating when the concentration of L-glu was greater than 25 mg dL^{-1}.
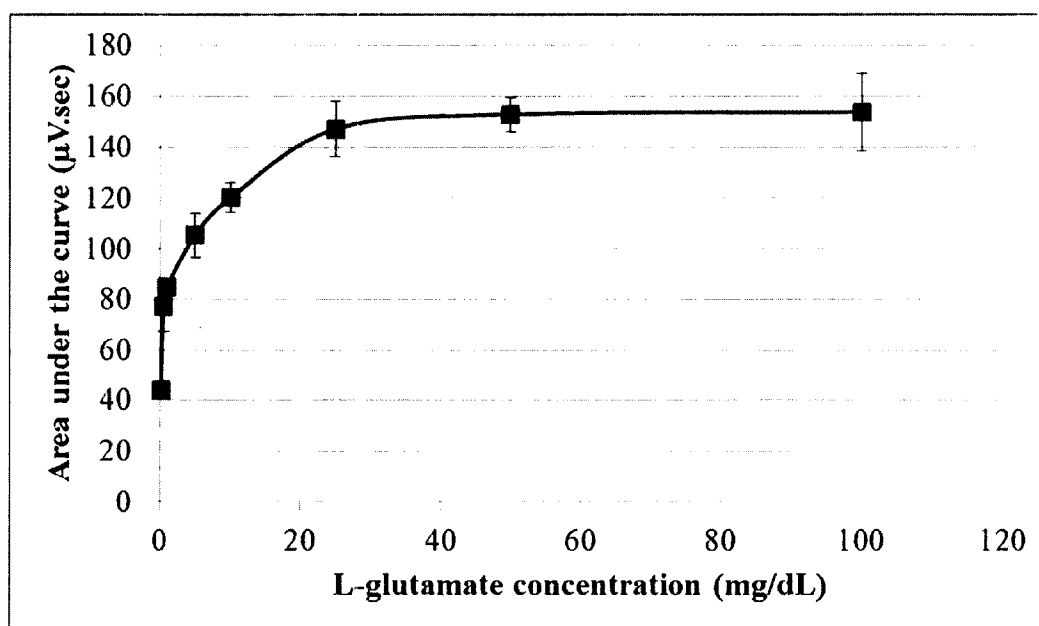
Figure 3.33: Response of thermoelectric L-glu sensor for various concentrations of L-glu samples. Two layers of L-GLOD were immobilized. The concentration of L-GLOD used for immobilization was 5 U ml^{-1}. A microfluidic device with one inlet and one outlet was used. Flow rate operated at inlet was 50 µl min^{-1}. A 40 µl sample of L-glu was introduced into the device. The thermopile was fabricated on the external surface of the coverslip

One layer and two layers of L-GLOD were immobilized on the glass coverslips. Experiments were conducted separately with each device with either one or two layers of L-GLOD. The effect of the number of layers on the response was analyzed by introducing samples containing varying concentrations of L-glu. Two layers of L-GLOD

shows the increased response compared to one layer of L-GLOD as shown in Figure

3.34. The lowest detection limit of the L-glu sensor was 0.1 mg dL^{-1}.
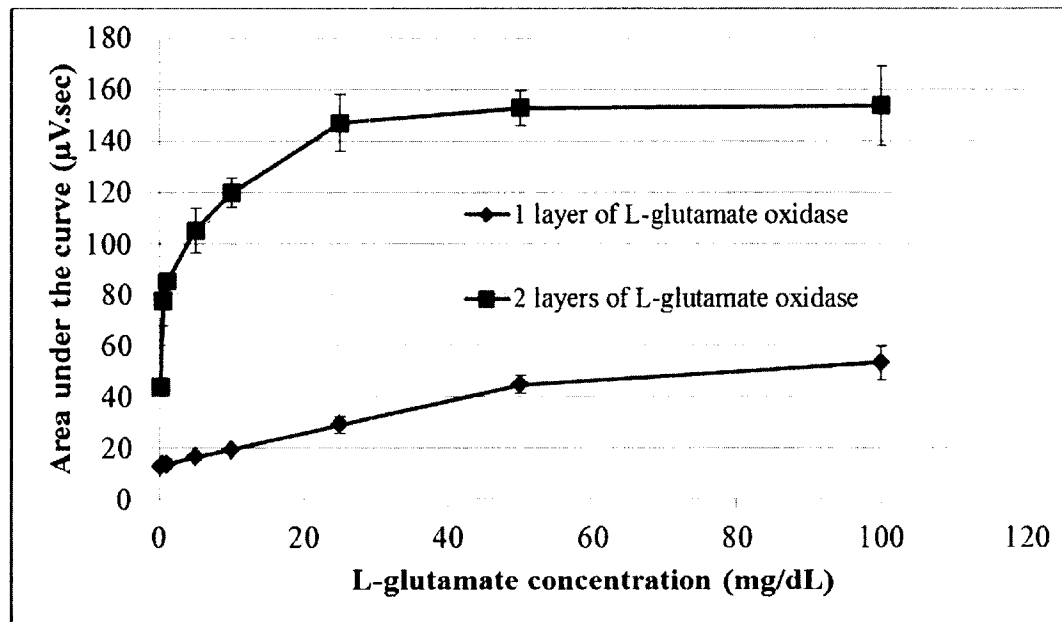
Figure 3.34: Thermoelectric response of L-glu samples (various concentrations) for one and two layers of immobilized L-GLOD. The concentration of enzyme used for immobilization is 5 U ml^{-1}

3.8.2   Thermoelectric Detection of L-glu
from Externally Cultured Cells

L-glu release from externally cultured glioma cells that were grown in a petri dish

was also measured using the thermoelectric sensor. In these experiments, media samples

were taken from the petri dish and injected into the microfluidic L-glu senor using the

six-port injection valve.   These results were compared with the fluorescent

spectrophotometer response as explained in Section 3.6.   In these experiments, samples

were collected from the petri dish after regular intervals of time for five minutes after the

stimulation with 50 mM kcl. The line under the curve shown in Figure 3.35 shows the

area used to compute the total heat generated from the L-glu reaction following injection

of the media from the petri dish taken 30 seconds following stimulation with 50 mM kcl.

The release and uptake of L-glu by the cells in the petri dish after the stimulation of the

cells with 50 mM kcl over a period of five minutes is shown in Figure 3.36.
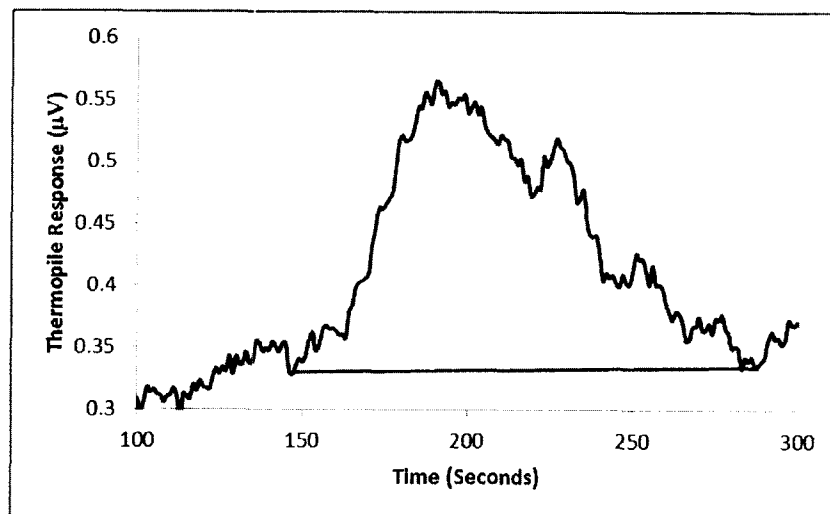
Figure 3.35: Typical L-glu response of the cell media collected after 30 seconds of stimulating with 50mM kcl
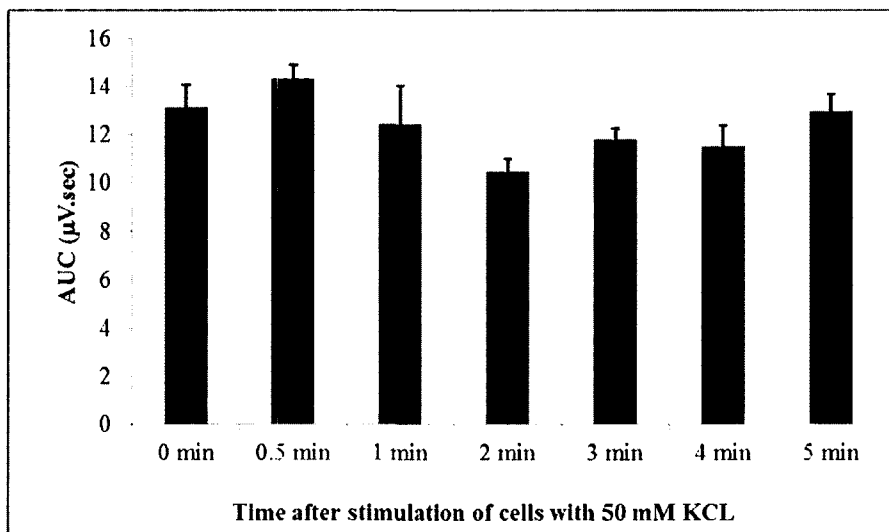
Figure 3.36: Thermoelectric L-glutamate sensor response of brain tumor cell line CRL 2303 media injections following KCL stimulation. The cells were plated in a Petri dish at a density of 200,000 cells per ml. After 24 hours, the cells were treated with stimulating chemical (50 mM KCL). The samples of the cell media were collected in regular time intervals after treatment and analyzed using the microfluidic thermoelectric L-glu sensor

3.8.3 Thermoelectric Detection of L-glu from Immobilized Cells

The dynamics of L-glu release from immobilized cells monitored is shown in Figure 3.37. The graph shows the parallel vertical blue lines indicating the transient time of the stimulus (KCL or Ionomycin) flowing over the thermopile. The red line shows the area under the curve due to the heat released by the L-glu reaction. The peak height increased 150 nV when stimulated with 50 mM KCL and the peak height increased 350 nV when stimulated with 2 µM Ionomycin (Figure 3.38).
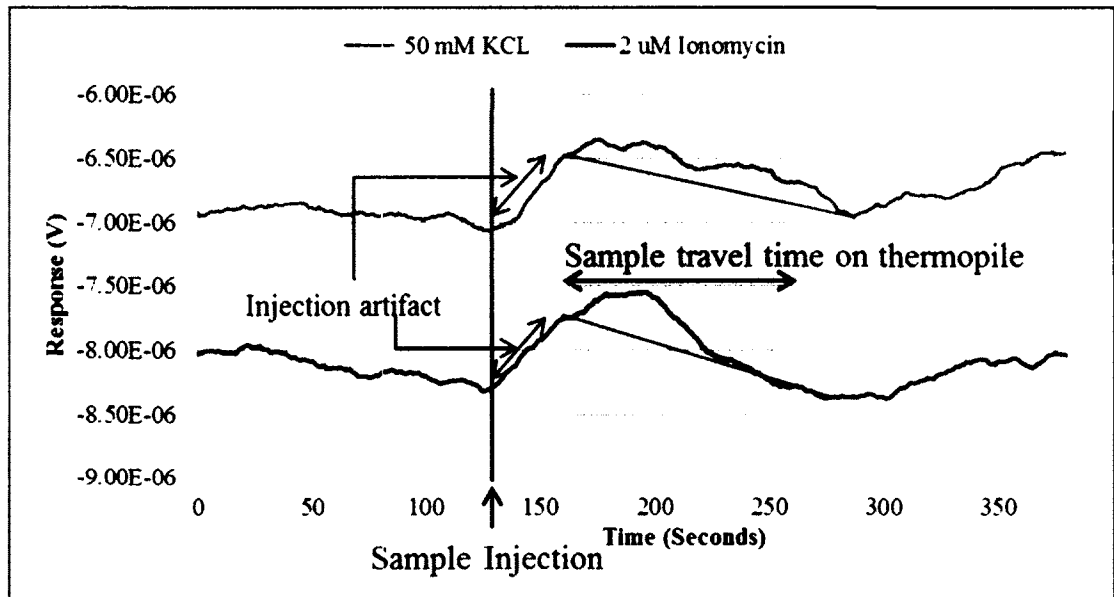
Figure 3.37: Thermoelectric L-glutamate sensor response of immobilized brain tumor cell line CRL 2303. The cells were stimulated with either 50 mM KCL or 2 μM Ionomycin
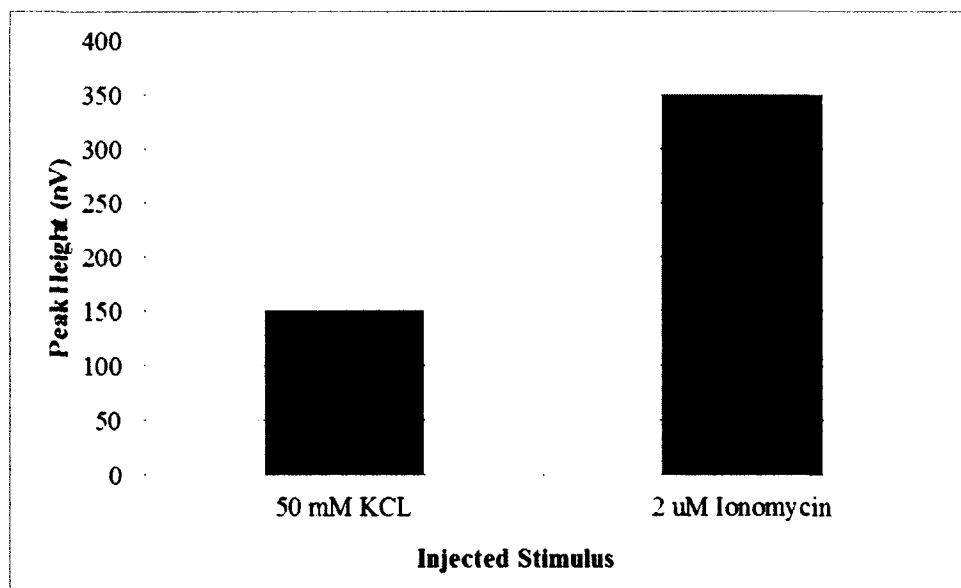
Figure 3.38: Thermoelectric L-glutamate sensor response of immobilized brain tumor cell line CRL 2303

3.9   Thermoelectric Detection of Brain
Tumor Cells Metabolism

Experiments were performed to detect the heat produced (response) from the

immobilized brain tumor when a stimulus was applied. In one set of experiments, the

brain tumor cells were immobilized on the thermopile without the immobilization of L-

GLOD on the thermopile. A stimulus of KCL or Ionomycin was used to stimulate the

immobilized cells. Locke's solution was used as the buffer to make 50 mM KCL and 2

µM Ionomycin. The thermopile signal increased sharply when the cells were stimulated

with Ionomycin, but it did not change when the cells were stimulated with KCL, as

shown in Figure 3.39. The peak height of the thermopile response to Ionomycin was 250

nV.
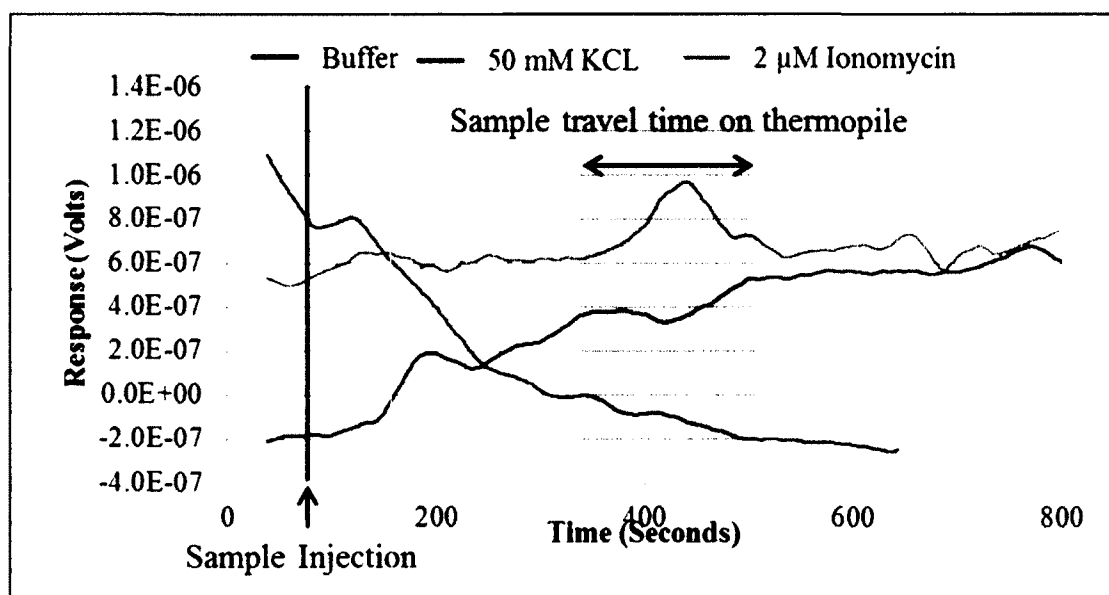
Figure 3.39: Thermoelectric response of brain tumor cells after stimulating with 50 mM KCL and 2 µM Ionomycin. The data shown is averaged at moving average of 38. The concentration of cells used to immobilize was 200,000 cells per ml media

Experiments were also performed to detect the glucose metabolism activity of the brain tumor cells. The metabolism decrease was detected by measuring the decreased baseline following elimination of the glucose supply to the cells located over the measuring junctions of the thermopile. The supply of glucose was stopped by injecting Locke's solution without glucose through inlet two. Pure Locke's solution was continuously injected at inlet 1. The flow rates maintained at inlet one and two were 100 and 25 μl $(min)^{-1}$. Experiments were done by injecting Locke's solution without glucose for a shorter time period of 3.5 minutes and a longer time period of 45 minutes.

The decrease in the metabolism after elimination of glucose for 3.5 minutes is shown in Figure 3.40. The figure shows two consecutive injections of Locke's solution without glucose. In the first injection (red line), the metabolism decrease was observed after three minutes following elimination of glucose and the decrease continued for one additional minute even after the supply of the glucose was restored. The cells recovered back to the initial metabolic level approximately three minutes after glucose was restored. In the second injection (blue line) after 12.5 minutes of the first injection, the metabolism decrease is observed almost immediately after glucose removal. The cells required 4 minutes to recover to their baseline metabolism after the supply of glucose was restored. In both of the injections, a small decrease in the baseline of 150 nV was recorded.
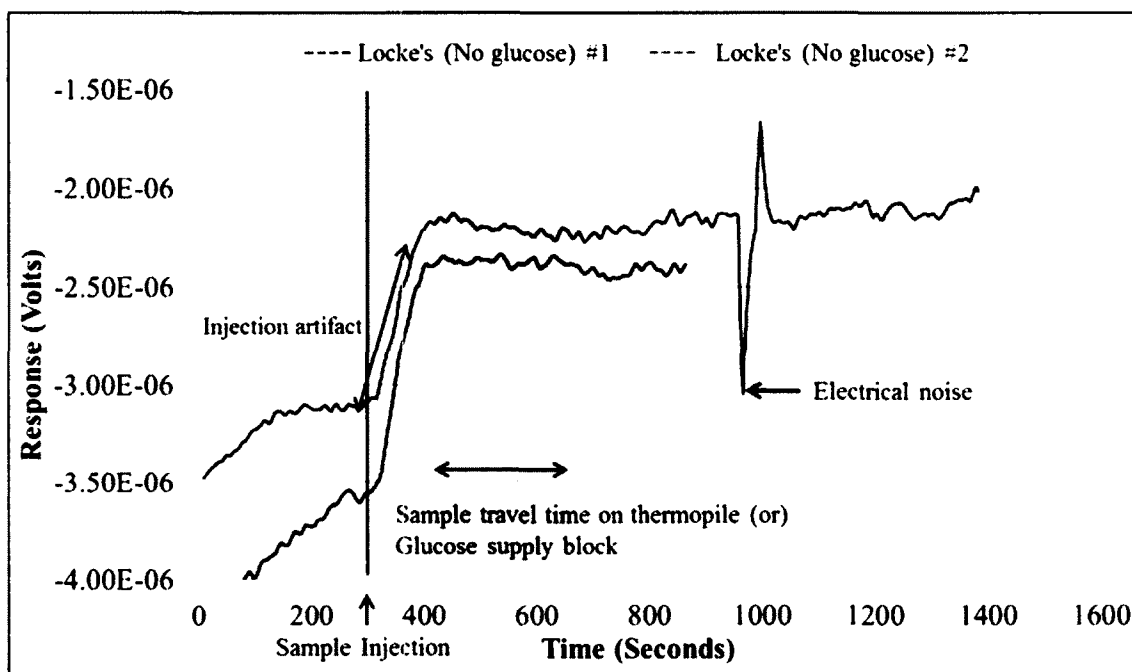
Figure 3.40: Thermoelectric detection of brain cell metabolism after stimulating with Locke's solution without glucose for shorter time periods

The decrease in the metabolism after the removal of the glucose supply for 45 minutes is shown in Figure 3.41. A significant decrease of 1.96 μV in the thermopile signal is observed 13 minutes following the removal of the glucose. The decrease in the thermopile signal continued for an additional 40 minutes after the supply of the glucose was restored. The total decrease in the thermopile signal was 4.6 μV.
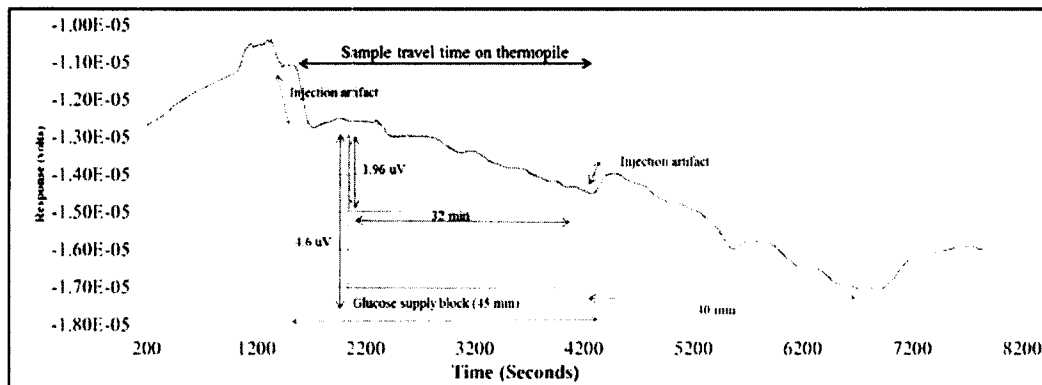
Figure 3.41: Thermoelectric detection of brain cell metabolism after stimulating with Locke's solution without glucose for longer time periods

CHAPTER 4

DISCUSSION

4.1 Pitfalls

Several issues were encountered during the process of fabricating the thermopiles using the lift-off procedure, fabricating the microfluidic device, and setting up the measurement system. These issues and solving strategies are discussed in the following sections.

4.1.1 Lift-off-Photolithography

The major advantage of fabricating the thermopiles using the lift-off procedure over the shadow masks procedure is a higher yield. The chrome mask designed for the lift-off procedure can produce a maximum of 25 thermopiles per production run and the shadow mask procedure can produce a maximum of nine thermopiles per run (Figure 2.3 and Figure 2.5). The lift-off procedure takes at least six hours and the shadow mask procedure takes at least three hours for each production run. Also, the risk of metal lines flaking is high with the manual positioning of the shadow masks directly over the metal lines. In the lift-off procedure, the chrome mask never comes in contact with the metal lines directly. Once the lift-off procedure is optimized with all the parameters, there is no risk of flaking of the metal lines during the lift-off stage using Remover PG.

For the clean lift-off processing, the Lift-Off Resist (LOR) film should be 1.33 to 1.5 times thicker than the thickness of the metal deposition. The maximum thickness that can be attained with the LOR 7B is 1.2 μm. The process of making the thermopiles requires two metal depositions. Therefore, the total thickness of the metal lines (bismuth and antimony) at the junctions should be less than 0.8 μm. Also, for better continuity of the metal lines at the junctions, the antimony deposition thickness (second metal line) should be larger than the bismuth deposition thickness (first metal line) to ensure continuous overlap of the metals at the junction. Figure 2.4 shows an image of the thermopile at the antimony-bismuth junction when both the metals lines are deposited at identical thickness. Under this condition, there is a high likelihood that there will not be electrical continuity at the junction. This thickness limitation necessitated that the thermopiles be constructed with a low total metal thickness (< 1.2 μm), which yielded high resistance thermopiles (resistance is inversely proportional to the thickness of the metal lines). The typical resistance of the thermopiles fabricated with lift-off procedure is ~180 kΩ.

The thermopiles fabricated using shadow masks has the measured Seebeck coefficient of ~6.3 μV (m °C)$^{-1}$ is comparable to the calculated theoretical Seebeck coefficient (7.14 μV (m °C)$^{-1}$) for antimony-bismuth thermopile with 60 junctions.

4.1.2 Fabrication of Microfluidic Thermoelectric Sensor

The probability of accumulating air bubbles in the dead space of microfluidic channel was high. Air bubbles trapped in the dead space of the channel tend to travel towards the center of the channel when the fluid is flowing in the channel. Air bubbles in the channel disturb the normal flow of the fluid. For this reason, the tapered end

geometry of the microfluidic device channel was used to eliminate corners that create dead space. Hence, this channel geometry aids in decreasing the air bubbles that interfere with the focused flow (Figure 2.8). The reactant solution can leak from the microfluidic device when the bond between the Kapton® tape and either the glass slide or the coverslip is inadequate, following the assembly of the microfluidic device. To avoid this leakage, proper care must be taken during the assembly of the microfluidic device to press the double sided Kapton® tape hard on to the glass slide and glass coverslip. Excessive force, however, will break the fragile glass coverslip and its integrated thermopile.

4.1.3   Noise Reduction

Sources of noise in the signal include thermal noise and electrical noise. The thermal noise is mainly caused by changes in the environmental temperature. Temperature changes can be reduced by insulating the microfluidic calorimeter with an external enclosure, such as a Styrofoam box. Thermal EMF error that comes from the thermocouple junction formed by the test lead wires (copper) with the measuring metal (bismuth) of the thermopile can be minimized by connecting a small copper wire between the measuring metal and the test lead wire.

Electric noise arises from various sources. Radio frequency (high frequency) interference that comes from cell phones and communication transmitters can be minimized by keeping the test leads far away from the rear panel cables of the experimental instruments. Power line noise (50 Hz or 60 Hz) present in dc signals can be minimized by integrating the input for a fixed period of time (three sec) using the integration capability of the nano voltmeter. Ground loop noise caused by common earth

ground for both the device undergoing testing and the voltmeter can be minimized by removing the ground referencing and connecting all meters to the same electrical outlet. Appendix C.2 lists all settings optimized for the nano voltmeter and Signal Express software.

4.2   Thermopile Calibration

Three thermopiles were fabricated on Kapton® supports using the metal masks and the thermal evaporation technique. The resistances of these thermopiles were 18 kΩ, 19 kΩ, and 28 kΩ, respectively. The thermopiles were protected from oxidation and physical damage by attaching a polyimide tape on the thermopile. Without the polyimide tape, the thermopile resistances changed over time. The width of the nichrome wire used in the testing setup (Figure 2.6) was chosen such that the heat generated was positioned exactly over the thermopile measuring junctions. If the nichrome wire was too wide, the measured Seebeck coefficient was lower than the theoretical value (Figure 3.1) because the heat generated was also conducted to the reference junctions of the thermopile. The average measured Seebeck coefficient for the three thermopiles (Figure 3.3) was ~7 μV (m° C)$^{-1}$. The measured Seebeck coefficient was similar to the Seebeck coefficient of thermopiles reported by Towe et al. [102]. It was also close to the theoretical Seebeck coefficient, which is 7.14 μV (m° C)$^{-1}$.

4.3   Analysis of Immobilized Enzyme

To increase the amount of L-GLOD immobilized, the amount of deposited material was measured with the QCM, the procedure was modified as needed. In all protocols, the concentration of PEI and PSS used was 0.1 mg mL^{-1} and the concentration

of L-GLOD used was 0.1 U mL^{-1}. Initially, (Protocol 1) the QCM electrode was dipped in PEI and PSS solutions for 15 minutes and was dipped in L-GLOD for 30 minutes as shown in Figure 3.8. Since the time of dipping the electrode in L-GLOD was just 30 minutes, only smaller amounts (25 ng) of L-GLOD were adsorbed in the initial layers. In later layers, the amount of immobilized L-GLOD was increased (167 ng and 355 ng) due to the increase in the precursor layers to form a more evenly charged surface. To increase the mass of L-GLOD in the initial layers, Protocol 1 was altered either by increasing the time of dipping the electrode in L-GLOD to two hours (Protocol 2) or by increasing the number of precursor layers from three to five (Protocol 3). In Protocol 2, the adsorption of L-GLOD in the initial layer was increased (455 ng), as shown in Figure 3.9. In Protocol 3 (Figure 3.10), the adsorption of L-GLOD in the first (179 ng) and second (183 ng) layers did not significantly increase compared to the adsorption in Protocol 2.

4.4 Fluorescence Analysis of L-glu Release from Externally Cultured Cells

The cells released L-glu after KCL stimulation. The CRL 2303 media was used in these experiments. The fluorescence reading at zero min (before KCL stimulation) was non-zero because the media contains 3.62 mM of L-glu. The L-glu levels increased in the media collected at 30 seconds after stimulation of KCL. There was no significant uptake of L-glu until five minutes (Figure 3.21). This means, the cells might require more than five minutes to uptake the released L-glu.

4.5 Thermoelectric L-glutamate Sensor

The response of the L-glu sensor increased linearly for the injection of L-glu concentrations ranging from 0 - 100 mgdL^{-1} (0 - 54 mM). The sensor response saturated

after 100 mg dL^{-1} (54 mM) because oxygen transport limits the reaction. Injection of oxygen-saturated L-glu samples might increase the linear range of the response over a broader range of L-glu concentrations. The variation in the standard error of the response was high, possibly due to flow fluctuations caused by the syringe pumps. Because the enzyme was immobilized over the entire area of the thermopile, the effect of flow fluctuations on the L-glu responses was caused by the change in the width of the hydrodynamic focusing causing variations in the reaction site area and the diffusion of L-glu.

Three modifications to the system were made to improve the L-glu sensor's sensitivity. First, the two-inlet device was modified to a single-inlet device. Secondly, the technique for immobilizing L_GLOD and the amount of L-GLOD immobilized on the channel was increased. Thirdly, the thermopile was fabricated directly on the coverslip instead of on a Kapton® support. When combined, these modifications decreased the lowest detection limit from 5 mg dL^{-1} to 0.1 mg dL^{-1}. (Figure 3.30 and Figure 3.32).

The change to a single-inlet device eliminated the hydrodynamic focusing of fluid. Eliminating the second inlet eliminated the lateral diffusion of the L-glu sample and decreased the dilution of the L-glu flowing down the stream. For this configuration the L-GLOD enzyme was immobilized only on the measuring junctions so that the reaction takes place only on the measuring junctions of the thermopile.

The method of L-GLOD immobilization was modified by pipetting the L-GLOD on the measuring junctions and storing the device in the refrigerator until the enzyme evaporated completely. The modified method increased the adsorption of L-GLOD on to

the surface. The concentration of L-GLOD was increased to 5 U mL^{-1} from 0.1 U mL^{-1} which improved L-GLOD adsorption.

Fabrication of the thermopile directly on the coverslip differed from the previous method in which the thermopile was fabricated on the Kapton® sheet and attached to the coverslip using super glue. This method eliminated the additional thermal resistance that the Kapton® support and super glue imposed between the heat source and thermopile, thus increasing the heat flow to the thermopile.

The base response (AUC) before stimulating the cells (at zero min) with KCL represented the normal L-glu levels in media (Figure 3.36). When the cells were stimulated with KCL at zero min, the L-glu level in the media collected at 30 sec. After 30 sec, an uptake of L-glu was observed from the cells. Again, after another 30 sec further uptake from the media by the cells was measured. Comparing Figure 3.32 and Figure 3.36, the concentration of L-glu measured at zero min (13 µVs) corresponds to the concentration of L-glu in prepared media, 3.96 mg (dL)$^{-1}$ of L-glu (ATCC, Vendor's formulation of DMEM). The response of the L-glu sensor varied from 10 to 14 µVs. The 4 µVs variation corresponded to 1.22 mg (dL)$^{-1}$ of L-glu in media. These results are comparable to the results measured with an electrochemical transistor developed by Senaka Kanakamedala et al. and used to detect L-glu from cultured brain tumor cells [103].

In Figure 3.37, the immobilized brain tumor cells were stimulated with 50 mM kcl and 2 µm ionomycin. A 52 µl sample (stimulus) has been injected into the microfluidic device using the sample loop of injection valve. The transient time of the stimulus to the reach the thermopile after injection is 50 seconds. The transient time was

calculated using flow rates of the stimulus and the dimensions of the tube and microfluidic device. When the stimulus was injected, a significant increase in the baseline was observed due to the pressure change in the tubing system followed by the change in the flow rate of the stimulus. After stimulating cells with 2 μm ionomycin, a response with peak height of 350 nV was observed with L-GLOD immobilized, and a response with peak height of 250 nV was observed without L-GLOD immobilized (Figure 3.37 and Figure 3.39). This means, response of 250 nV was due to the metabolism change and the additional response of 100 nV was due to the L-glu release from the immobilized cells.

4.6 Experiments to Detect Metabolism of Brain Tumor Cells

Stimulation of the immobilized cells with 50 mM KCL did not produce a measureable change in the thermoelectric L-glu sensor signal (significant decrease in metabolism). When stimulated with ionomycin, a significant change (250 nV) in the thermopile signal was detected over a period of 138 seconds (Figure 3.39). This change likely resulted from an increase in the cell metabolic rate following the resulting large L-glu release from the cells. These results are well supported by Figure 3.20, which shows a calcium influx recorded after stimulating the cells with 50 mM KCL and 2 μM ionomycin. The large influx of calcium ion into the cells might cause an imbalance in membrane potential resulting in metabolic changes. Ionomycin raises the intracellular calcium level followed by the release of L-glu from cells. The enhancement of calcium influx is caused by the direct stimulation of store-regulated cation entry. Ionomycin releases calcium from its intracellular stores without the involvement of G proteins, resulting in the activation of calcium activated chlorine channels. The slow component of

the ionomycin response is the entry of calcium from outside the cell and the fast component is released of calcium from the intracellular stores [21].

The cells begin to use glucose from internal glucose stores for the production of ATP when the supply of external glucose is stopped. In Figure 3.40, when Locke's solution without glucose was first injected for 3.5 minutes, the cells might have changed their major energy generation pathway to use the internal glucose stores immediately after the external glucose supply was stopped. This use of internal glucose could have allowed the cells to maintain their normal metabolism rate for few minutes (3 minutes) followed by a slight decrease in the baseline thereafter. Following the second injection of Locke's solution without glucose, the metabolism decrease was almost instantaneous (45 seconds) because most of the internal glucose was consumed in first injection. As shown in Figure 3.41, when the Locke's solution without glucose was injected for 45 minutes, a similar decrease (150 nV) in the thermopile signal was observed after four minutes and decrease continued for another nine minutes. This implies that during the first four minutes after injection, the cells might have changed their major energy generation pathways to use the internal glucose stores, immediately after the external glucose supply was stopped. For the next nine minutes, the cells might still have been using the internal glucose but with decreased metabolic rate as the internal glucose stores were slowly used up. Then, a significant drop in the voltage response (4.6 μV) for next 62 minutes was observed. During this 62 minutes period, the cells might be switching their energy generating pathways to various sources like lipids and proteins, and the cells were out of energy generation sources. Even though the glucose is supplied after 32 minutes, the cells could not change the momentum suddenly to switch the energy transport pathway.

The sensitivity of the thermopile calibrated was 7 μV/m° C, and the heat transfer towards the thermopile calculated was 0.165 W/° C. Based on this calibration and calculation, the sensitivity of the device was 23.57 μW/ μV. The –4.6 μV baseline drift observed in Figure 3.41 therefore corresponds to a total power production was 108.42 μW. If the population cells on the measuring junction of the thermopile (18 mm^2) was 2×10^6, then the total heat released would be 108.42 μW/2×10^6 cells or 54 pW/cell (anaerobic conditions). This is comparable to the results produced by C. Loesberg et al., in which the neuroblastoma cells release 60-120 pW/cell under aerobic conditions [84].

The baseline of the sensor response had very low frequency noise fluctuations that decreased the signal-to-noise ratio. These fluctuations were caused by flow fluctuations produced by the syringe pumps that were used to pump the fluid into the microfluidic device. The replacement of the syringe pumps with pressure driven pumps (dolomite® pumps) decreases these flow fluctuations and improve the signal-to-noise ratio.

4.7   Factors Affecting the Quality of the Results

The following parameters affect the results or the voltage output of the thermoelectric sensor:

1. The Seebeck coefficient of the thermopile.

2. The heat transfer towards the thermopile from reaction zone.

3. The concentration of the L-GLOD immobilized.

4. The population and the viability of the cells immobilized.

5. The concentration of the stimulus injected.

6. The time for which the cells are stimulated.

7. The supply of oxygen during the reaction.

8. The signal-to-noise ratio.

CHAPTER 5

CONCLUSIONS AND FUTURE WORK

5.1   Conclusions

A microfluidic thermoelectric biosensor was successfully fabricated for the real time detection of L-glu dynamics and glucose metabolism from immobilized brain tumor cells. The device fabrication methods were simple and inexpensive. The device design and its effect on the fluid flow (hydro dynamically focusing of one inlet flow by the other inlet flow) were successfully demonstrated. Layer-by-layer self-assembly methods were implemented to immobilize L-GLOD in selective areas. Fluorescence based assay tests and quartz crystal microbalance analysis were performed to quantify the immobilized enzyme. A successful protocol was developed to immobilize cells in selective areas on the coverslip inside the microfluidic device. Various staining methods were used on the cell cultures to determine cell count and viability. The advantages of the integration of cells and thermopile in a microfluidic device were demonstrated.

The primary sensing element, the thermopile, was tested to find the Seebeck coefficient. The measured Seebeck coefficient of ~6.3 μV (m °C)$^{-1}$ was comparable to the calculated theoretical Seebeck coefficient for an antimony-bismuth thermopile with 60 junctions. The thermoelectric sensor was calibrated by applying known amounts of heat under identical experimental conditions. The thermoelectric L-glu sensor was calibrated

with 50 mM kcl and 2 μm ionomycin. The results of L-glu release from cells were also compared with fluorescence based assay tests. Experiments were also performed to detect the reduced metabolism in cells after blocking glucose supply to the cells under anaerobic conditions. Low sample volume consumption and fast response time of device permits monitoring of real time biochemical processes.

5.2   Future Work

The sensitivity of the sensor can be increased by placing the thermopile inside the microfluidic device. This will eliminate the thermal resistance caused by the coverslip. Integration of the thermopile inside the microfluidic device can be achieved by coating the fabricated thermopile with the thin layer of resist to eliminate the direct contact of fluid. The resist material chosen should be an electrical insulator and should be biocompatible (cell friendly). The contact pads of the thermopile should be extended outside the device. Also, the sensitivity can be increased by increasing the number of junctions of thermopile to accommodate a larger number of cells during immobilization or connecting the multiple thermopiles in the series.

The normal levels of extracellular L-glu can be detected when cells are immobilized only on the measuring junctions of the thermopile, unlike immobilizing cells over both measuring and reference junctions. The effect of ATP and cystine stimulation on brain tumor cells L-glu release can also be investigated. Immobilizing normal astrocytes and neurons, and stimulating these cells with kcl, ionomycin, ATP and cystine will give a comparative study between tumor cells, astrocytes and neurons.

Because the fabricated thermoelectric sensor takes advantage of the universal nature of heat power production of chemical reactions, use of this sensor can be extended

to cell metabolism measurements when stimulated with various drugs. Stimulators that increase or decrease the cell metabolism can be used to stimulate the immobilized cells, and the sensor can detect the dynamics of cell metabolism in real time. The aerobic metabolism generates more heat than the anaerobic metabolism. Hence the oxygen supply to the immobilized cells helps increase the cell metabolism. Bubbling oxygen to the buffer before injecting might increase the supply of oxygen to the cells.

In prospect of broader aspects, this thermoelectric biosensor can be used to test the effect (metabolism) of various drugs on any kind of cells that are immobilized inside the device.

APPENDIX A

THERMOELECTRIC SENSOR FABRICATION

A.1.   Lift-off Procedure

1. Fastening of Polyimide tape to the silicon substrate.

2. Pre-dehydrating of substrate at 200° C for Five min to dehydrate all water molecules present on the substrate.

3. Spin coating of LOR7B is done with the below operating parameters.

   - **Level-1**

   Rotation speed- 300 rpm

   Rotation acceleration- 200 rpm/sec

   Time of rotation- eight sec

   - **Level-2**

   Rotation speed- 1000 rpm

   Rotation acceleration- 10,000 rpm/sec

   Time of rotation- 45 sec

   With the above parameters, the LOR7B is coated at 1.3 micrometer thickness.

4. Soft-Baking of LOR7B is done at 180^0C for five min.

5. Five min wait time for the substrate get it cool.

6. Spin coating of Photoresist 1813 is done with the below operating parameters.

   - **Level -1**

   Rotation speed- 1000 rpm

   Rotation acceleration- 100 rpm/sec

   Time of rotation- 10 sec

- Level-2

Rotation speed- 3000 rpm

Rotation acceleration- 500 rpm/sec

Time of rotation- 90 sec

With the above parameters, the photoresist is coated at one micrometer thickness.

7. Soft-Baking of photoresist 1813 is done at 115^0C for 90 sec.

8. Five min wait time for the substrate get it cool.

9. Exposing the substrate under UV light for eight sec using the mask which has pads. The exposure energy of UV light from the mask aligner we are using is 13 mJ/cm^2, which gives the total dose of 104 mJ/cm^2

10. Developing the substrate with MF-319 for 45 sec followed by the DI water for five sec.

11. Deposition of bismuth metal with thermal evaporator.

    One gram of bismuth metal is used for depositing on the substrate. It gives the total thickness of 8300A^0. The heating of the boat is done by increasing the power level at regular intervals. At 8% power level, the current generated is 70 amps which deposits the bismuth at 15-18 A^0/sec.

12. Developing the bismuth deposited substrate with Remover PG using ultrasonicator at 60^0C and with Iso-propyl Alcohol at ambient temperature, followed by rinsing with DI water leaves the required pattern on the substrate, removing the unwanted metal.

13. The process from above points (1-9) is repeated with substrate (Kapton sheet). Exposing the substrate under UV light is done by using the mask without pads in this process.

14. Deposition of bismuth and antimony metal.

    0.1gm of bismuth and 1gm of antimony are placed in separate boats in the thermal evaporator. First bismuth is deposited at 800A^0 thickness with the same power level mentioned in point 10. Secondly antimony is deposited at 11030 A^0. The heating of antimony boat is done at 7% power level which generates 60 amp to deposit the metal at three - five A^0/sec.

15. Continue the process as in the point 11.

A.2.   L-GLOD Immobilization

1. Prepare solutions of PEI, PSS and L-GLOD. The concentration of PEI and PSS is 5 mg ml^{-1} and L-GLOD is 5U ml^{-1} at pH 6. Prepare 15 ml solutions of PEI and PSS.

2. Take a glass coverslip with thermopile fabricated and dip it in PEI solution for 15 minutes.

3. Wash the glass coverslip with water for one min to remove the loosely bounded PEI and dry it with nitrogen.

4. Dip the glass coverslip in PSS solution for five min.

5. Wash the glass coverslip with water for one min to remove the loosely bounded PSS and dry with nitrogen.

6. Repeat steps two and three in the procedure again to form a precursor layer.

7. Using pipette, coat 10 µl of L-GLOD on glass coverslip over the measuring junctions of thermopile and place it in refrigerator at 4 °C until the enzyme evaporates.

8. Wash the glass coverslip for one min and dry it with nitrogen.

9. Repeat steps two and three in the procedure again to form a PEI layer.

10. Repeat seven and eight steps in the procedure for the desired number of layers.

11. Thus, alternate layers of PEI and L-GLOD are immobilized over the measuring junction of thermopile on the glass coverslip.

A.3. Assay Tests

Reagents used for assay

Table A.1: Template for inserting tables in Appendices.

Materials	Amount
Amplex® Red reagent (MW = 257)	2 vials, each containing 0.26 mg
Dimethylsulfoxide (DMSO), anhydrous	0.7 mL
Horseradish peroxidase	10 U†
Hydrogen peroxide (H_2O_2, a stabilized ~3% solution (the actual concentration is indicated on the component label) (MW = 34)	500 µL
5X Reaction buffer (0.5 M Tris-HCl, pH 7.5)	10 mL
L-Glutamate oxidase, recombinant from E. coli	1 U‡
L-Glutamate–pyruvate transaminase from pig heart	1 U§
L-Glutamic acid, monosodium salt, monohydrate (MW = 187.1)	20 mg
L-Alanine (MW = 89.1)	20 mg

† 1 unit is defined as the amount of enzyme that will form 1.0 mg purpurogallin from pyrogallol in 20 seconds at pH 6.0 at 20° C.

‡ 1 unit is defined as the amount of L-glutamate oxidase that will form 1.0 μmole of α-ketoglutaric acid from L-glutamic acid per minute at pH 7.4 at 30° C.

§ 1 unit is defined as the amount of L-glutamate–pyruvate transaminase that will convert 1 μmole of α-ketoglutarate to L-glutamate per minute at pH 7.6 at 37° C in the presence of L-alanine.

Stock solution preparation

1. Prepare a 10 mM stock solution of the Amplex® Red reagent: Allow one vial of Amplex® Red reagent and DMSO to warm to room temperature. Just prior to use, dissolve the contents of the vial of Amplex® Red reagent (0.26 mg) in 100 μL DMSO. Each vial of Amplex® Red reagent is more than sufficient for approximately 100 assays, with a final reaction volume of 100 μL per assay. Store this stock solution frozen at –20° C, protected from light.

2. Prepare a 1X working solution of reaction buffer by adding 4 mL of 5X reaction buffer stock solution (Component E) to 16 mL of deionized water (dH$_2$O). This 20 mL volume of 1X reaction buffer is sufficient for approximately 100 assays of 100 μL each, with a 10 mL excess for making stock solutions and dilutions.

3. Prepare a 100 U mL^{-1} stock solution of horseradish peroxidase (HRP) by dissolving the contents of the vial of HRP (Component C) in 100 μL of 1X reaction buffer. After use, divide the remaining solution into small aliquots and store frozen at –20° C.

4. Prepare a 20 mM H$_2$O$_2$ working solution by diluting the ~3% H$_2$O$_2$ stock solution (Component D) into the appropriate volume of dH$_2$O. The actual H$_2$O$_2$ concentration is indicated on the component label. For instance, a 20 mM H$_2$O$_2$ working solution can be prepared from a 3.0% H$_2$O$_2$ stock solution by diluting 23 μL of 3.0% H$_2$O$_2$ into 977 μL of dH$_2$O. Note that although the ~3% H$_2$O$_2$ stock

solution has been stabilized to slow degradation, the 20 mM H_2O_2 working
solution will be less stable and should be used promptly.

5. Prepare a 5 U mL^{-1} stock solution of l-glutamate oxidase by dissolving the
   contents of the vial of l-glutamate oxidase (Component F) in 200 µL of 1X
   reaction buffer. After use, divide the remaining solution into small aliquots and
   store frozen at –20° C.

6. Prepare a 100 U mL^{-1} solution of l-glutamate–pyruvate transaminase by
   dissolving the contents of the vial of l-glutamate–pyruvate transaminase
   (Component G) in 100 µL of 1X reaction buffer. After use, divide the remaining
   solution into small aliquots and store frozen at –20° C.

7. Prepare a 200 mM solution of l-glutamic acid by dissolving the contents of the
   vial of l-glutamic acid (Component H) in 534 µL of 1X reaction buffer. After use,
   store the remaining solution frozen at –20° C.

8. Prepare a 200 mM stock solution of l-alanine by dissolving the contents of the
   vial of l-alanine (Component I) in 1.12 mL of 1X reaction buffer. After use,
   freeze the remaining solution at –20° C.

Glutamic Acid Assay

Glutamic Acid Assay The following protocol describes the assay of l-glutamic
acid in a total volume of 100 µL per microplate well. The volumes recommended here are
sufficient for ~100 assays.

1. Prepare a l-glutamic acid standard curve: Dilute the appropriate amount of 200
   mM l-glutamic acid stock solution into 1X reaction buffer to produce l-glutamic
   acid concentrations of 0 to 20 µM. Use 1X reaction buffer without l-glutamic acid

as a negative control. A volume of 50 μL will be used for each reaction. Note that the l-glutamic acid concentrations will be two-fold lower in the final reaction volume.

2. Dilute the l-glutamic acid-containing samples in 1X reaction buffer. Use a volume of 50 μL for each reaction.

3. Prepare a positive control by diluting the 20 mM H_2O_2 working solution to 10 μM in 1X reaction buffer.

4. Pipet 50 μL of the diluted samples and controls into separate wells of a microplate.

5. Prepare a working solution of 100 μM Amplex® Red reagent containing 0.25 U/mL HRP, 0.08 U/mL l-glutamate oxidase, 0.5 U/mL l-glutamate–pyruvate transaminase, and 200 μM l-alanine by adding: 50 μL of the Amplex® Red reagent stock solution

   - 12.5 μL of the HRP stock solution

   - 80 μL of the l-glutamate oxidase stock solution

   - 25 μL of the l-glutamate–pyruvate transaminase stock solution (prepared in Step 1.6)

   - 5 μL of the l-alanine stock solution

   - 4.83 mL of 1X reaction buffer

6. This 5 mL volume is sufficient for ~100 assays. Note that final concentrations of each component will be twofold lower in the final reaction volume.

7. Begin the reactions by adding 50 μL of the Amplex® Red reagent/HRP/glutamate oxidase/glutamate–pyruvate transaminase/alanine working solution to each microplate well containing the samples (cell media) and controls.

8. Incubate the reactions for 30 minutes or longer at 37°C, protected from light. Because the assay is continuous (not terminated), fluorescence may be measured at multiple time points to follow the kinetics of the reactions.

9. Measure the fluorescence in a fluorescence microplate reader using excitation in the range of 530–560 nm and emission detection at ~590 nm.

10. For each point, correct for background fluorescence by subtracting the values derived from the no–glutamic acid control.

Glutamate oxidase assay

The following protocol provides a guideline for using the Amplex® Red Glutamic Acid/Glutamate Oxidase Assay Kit to measure l-glutamate oxidase activity. The volumes recommended here are sufficient for ~100 assays, each containing a volume of 100 μL.

1. Dilute the l-glutamate oxidase-containing samples in 1X reaction buffer. A volume of 50 μL will be used for each reaction.

2. Prepare a positive control by diluting the 5 U mL^{-1} l-glutamate oxidase stock solutions into 1X reaction buffer to produce a 0.04 U mL^{-1} l-glutamate oxidase solution. Use 1X reaction buffer without l-glutamate oxidase as a negative control. A volume of 50 μL will be used for each reaction.

3. Prepare a second positive control by diluting the 20 mM H_2O_2 working solution to 10 μM in 1X reaction buffer.

4. Pipet 50 μL of the diluted samples and controls into separate wells of a microplate.

5. Prepare a working solution of 100 μM Amplex® Red reagent containing 0.25 U mL^{-1} HRP, 0.5 U mL^{-1} l-glutamate–pyruvate transaminase, 40 μM l-glutamic acid, and 200 μM l-alanine by adding:

   - 50 μL of the Amplex® Red reagent stock solution

   - 12.5 μL of the HRP stock solution

   - 25 μL of the l-glutamate–pyruvate transaminase stock solution

   - 1 μL of the l-glutamic acid stock solution

   - 5 μL of the l-alanine stock solution

   - 4.91 mL of 1X reaction buffer

   This 5 mL volume is sufficient for ~100 assays. Note that final concentrations of each component will be two-fold lower in the final reaction volume.

6. Begin the reactions by adding 50 μL of the Amplex® Red reagent/HRP/glutamate–pyruvate transaminase/glutamic acid/alanine working solution to each microplate well containing the samples (round glass coverslips with layers of immobilized L-glutamate oxidase) and controls (round glass coverslips with no L-glutamate oxidase immobilized).

7. Incubate the reactions for 30 minutes or longer at 37° C, protected from light. Because the assay is continuous (not terminated), fluorescence may be measured at multiple time points to follow the kinetics of the reactions.

8. Measure the fluorescence in a fluorescence microplate reader using excitation in the range of 530–560 nm and emission detection at ~590 nm.

A.4.   Nanoport Bonding

1. Prepare the bonding surfaces of both the port and the substrate (glass slide) by cleaning with isopropyl alcohol.

2. Invert the NanoPort flat bottom.

3. Insert the gasket seal into the recess in the bottom of the port.

4. Center and place the adhesive ring on the substrate (glass slide) surrounding the access hole. Then place the NanoPort over the adhesive ring.

5. Clamp the port to the substrate (glass slide). Place clamped ports in the oven at a temperature of 330-350° F/ 165-177° C for one hour to develop a complete bond between the port and the substrate (glass slide).

The above procedure is obtained from Upchurch Scientific®.

The Amplex® Red Glutamic Acid/Glutamate Oxidase Assay Kit provides an ultrasensitive method for continuously detecting glutamic acid or for monitoring glutamate oxidase activity in a fluorescence microplate reader or fluorometer. In the assay, L-glutamic acid is oxidized by glutamate oxidase to produce α-ketoglutarate, NH3 and H_2O_2. L-Alanine and L-glutamate–pyruvate transaminase are included in the reaction to regenerate L-glutamic acid by transamination of α -ketoglutarate, resulting in multiple cycles of the initial reaction and a significant amplification of the H_2O_2 produced. The hydrogen peroxide reacts with 10-acetyl-3, 7-dihydroxy phenoxazine (Amplex® Red reagent) in a 1:1 stoichiometry in the reaction catalyzed by horseradish peroxidase (HRP) to generate the highly fluorescent product, resorufin. Resorufin has absorption and fluorescence emission maxima of approximately 571 nm and 585 nm, respectively.

APPENDIX B

CELL PROTOCOLS

B.1.　　　Preparation of CRL-2303 Media

1. Add 125 ml of DMEM to the sterile filtration unit.

2. Add 25 ml of (5%) Fetal Bovine Serum to the sterile filtration unit.

3. Add 1.25 ml of (5%) penicillin/streptomycin to the sterile filtration unit.

4. Add 111.25 ml of DMEM to the sterile filtration unit.

5. Turn on the vacuum till entire the liquid run down to the container.

6. Turn off the vacuum, and then remove the filtration unit from the container.

7. Place and close the cap on the container.

8. Label the media container by CRL-2303, date, maker's name.

9. Store the container in the refrigerator.

B.2.　　　Thawing CRL-2303

1. Warm the required amount of media in the dish or flask in which we would culture the cells in the incubator for about 15 minutes.

2. For thawing CRL 2303 culture vial (stored in liquid nitrogen), remove the vial from the liquid nitrogen.

    Note: Wear the protection eye wear and safety gloves while dealing with liquid nitrogen.

3. Thaw the vial of frozen cells in water bath for about three to five minutes.

4. Add the thawed cells to the culture dish/flask without titrating but just by sucking up.

5. Use the media from the flask/dish to wash the cryo-vial.

6. Suck up all the media and cells and add to dish/flask.

7. Keep it in the incubator.

B.3. Replating the Cells

1. Keep the media in ice until it is time to use.

2. Defrost trypsin in water bath and mix it to even colored solution.

3. Prepare 1X PBS solution out of 10X PBS by taking one ml of 10X PBS into a tube and mixing it with nine ml of distilled water.

4. Once all the arrangements are done, get the flask of cells from incubator.

5. Using pipette remove all the media from the flask and empty it into a jar for liquid wastes.

6. Let the solution cover the surface completely and almost immediately remove the solution and dump it into jar.

7. Take trypsin using a pipette and pour into the flask of cells

8. Cap the flask and start gently shaking the solution in the flask for about 10-15 minutes until the whole layer of cells detach from the surface.

9. Once all the cells are deplated, remove the whole liquid using a pipette and pour into a new tube labeled "cells".

10. Add some media to this liquid.

11. Wash the emptied flask with serum and empty the flask.

12. Now take the tube of cells and centrifuge it for about seven minutes at 150 RCF (relative centrifugal force) and at a temperature of 5 °C.

13. After seven minutes we acquire a pellet of cells at the bottom of the centrifuged tube.

14. Remove the media from this tube without sucking up the cells and dump it into the jar.

15. Add fresh media and vortex the solution until the cells are evenly distributed without any lumps.

16. Now take the new flask/dish in which we want to replate the cells and fill the media in it.

17. Once again mix the tube containing cells and take the required amount of solution into a pipette and pour in the new media filled flask.

18. Mark the flask with the name of cells/media, passage number, date replated/fed, initials of the person who fed/ who replated the dish.

19. Close the dish and let the surface be covered with the whole solution and observe under the microscope.

20. Then take the flask and keep it in the incubator.

21. For flask make sure that the caps are slightly loose so that there is vent for CO_2.

B.4.   Counting the Cells

1. Take two separate small centrifuge tubes.

2. Add 20 µl of trypan blue to each tube.

3. Add 20 µl of thoroughly mixed cells to each tube. Mix the cells and trypan blue very well.

4. Distribute 10 µl from one tube to one side of the hemacytometer, such that the whole surface is covered. Then add 10 µl from the other tube to the opposite side of the hematocytometer.

5. The liquid should be injected into the notch under the glass plate.

6. Take the hemacytometer and count the cells under a microscope.

   • Hemacytometer has a 25 cellular grid on each side.

- When there are a lot of cells, such as cancer cell line, usually we count a diagonal five squares for the number of cells on each side and average the count. In case of low cell counts like astrocytes, we count the entire grid of 25.

7. Then calculate the total number of cells as

- (Average number of cells) x 2 x 5 x 10000 = No. of cells per ml

- The No. of cells per ml x Total ml of cellular liquid = Total No. of cells.

8. After counting the no. of total cells we decide how many cells can be cultured on a dish.

9. Make sure to clean the hemacytometer surface immediately which avoids the blue stain that will be caused by trypan blue.

B.5.   Freezing of Cells

1. Add 5% of dimethyl sulphoxide (DMSO) slowly dropwise to cell suspension and mix it well by inverting tube slowly (DMSO is quite traumatic for cells so mix it very slowly).

2. Add proper amount of cell suspension with DMSO to cryo preservative tube slowly, avoid bubbles during addition (bubbles may cause contamination).

3. Keep cryo-preservation tube in freezing device with 250 ml 100% isopropyl alcohol in it (change isoproponal after every five runs). Tight the cap of the device properly and keep it in -80 °C for four hours/overnight.

4. After four hours/overnight freezing in freezing device at -80 °C, move the cryo-preservation tube to liquid nitrogen.

B.6.   Poly-L-lysine Protocol

1. Use 1:1 ratio of poly-l-lysine to sterile water, or use recycled.

2. Use enough mixture to coat coverslip and let sit for at least one hour (room temp.)
    or as long as overnight (at 4 °C).

3. With draw the mixture and wash the coverslip with 1x PBS, and the coverslip is
    ready for plating the cells.

B.7.   Preparation of Locke's Solution

1. Reagents for 250 ml solution

    *   2250 mg of sodium chloride (NaCl) (154 mM)

    *   104.4 mg of potassium chloride (KCl) (5.6 mM)

    *   75.6 mg of sodium bicarbonate (NaHC03) (3.6 mM)

    *   84.5 mg of calcium chloride (CaCl2.2H20) (2.3 mM)

    *   252.3 mg of glucose (5.6 mM)

    *   1.25 ml of 1M stock 4-(2-hydroxyethyl)-l-piperazine ethanesulfonic acid
        (HEPES) (pH 7.4) (5 mM)

    *   Water (Purified) 248.75 ml

2. Add the components together in the following manner:

    *   Dissolve the components in 100 ml of purified water and add to the vacuum
        filtration unit.

    *   Add 100 ml of purified water to the vacuum filtration unit.

    *   Add water with dissolved components.

    *   Add 1.25 ml of 1M stock Hepes.

    *   Add remaining amount of purified water.

- Place cap on unit. Carefully turn on the vacuum.

- Allow all the liquid to pass through the filter. Turn off the vacuum before bubbles form.

- Twist the top of the vacuum unit off carefully. Screw the sterile cap onto the container of the media.

- Label as Locke's' solution with date and lab name. Store in refrigerator at 4°C.

B.8.   Calcein Staining

1. The loading solution for staining contains 200 fold propidium iodide (PI), 2000 fold pluronic acid and 1000 fold calcein AM.

2. Recipe for 9.5 ml of loading solution.

    - 9.5 ml of Locke's solution

    - Add 4.75 μl of pluronic acid- vortex after addition.

    - Add 9.5 μl of calcein AM- vortex after addition.

    - Add 47.5 μl of PI stock solution (1 mg/ml)-vortex after addition.

3. After removing media from the dish, add equivalent amount of loading solution and incubate for 25 minutes. Now the dish is ready for imaging.

B.9.   DAPI Staining for Living Cells

1. The reagents required are stock solution of DAPI (stored in -80 °C, 14.27 mM in DI water) and Locke's solution.

2. A 1 to 100 fold dilution with the stock is performed (Take three μl of stock and dilute with 297 μl of Locke's).

3. The above 300 μl solution is added to three ml of media in a dish (1 to 10 fold dilution).

4. Once DAPI is added, place the dish in incubator for 10 minutes (may be more). Now dish is ready for imaging.

B.10. MTT Assay Procedure for a 24-wellplate

It takes 400 μl of a solution to completely cover the bottom of a well in a 24 well plate. This being considered, 9.6 mL of MTT would be needed to treat an entire plate. To allow a safety buffer volume, 11 mL will be prepared.

1. Dilute MTT to 5.0 mg/mL in Locke's solution then follow a 4x dilution for a final concentration of 1.25 mg/mL for this 13.75mg of MTT powder needs to be added to 11 mL of Locke's solution.

2. Media is removed from cells. Do not wash.

3. Add 400 μl of MTT solution to each well.

4. Let MTT incubate for at least one hour. In viable cells the yellow solution will yield blue crystals.

5. Remove MTT solution.

6. Add 250 μl of 91 % Isopropanol. This will lift the crystals but not the cells.

7. Transfer 200 μl of the Isopropanol with dissolved crystals into wells of a 96 well plate. Dispose of the remaining liquid.

8. Cells should be covered with 400 uL of PBS to preserve them.

9. Measure the plate reader to a wavelength of 595.

B.11.   Fluo3/AM Imaging

1. Warm Locke's solution and retrieve Fluo dye and Pluronic acid (PA) from -80 °C

   and place in ice bath.

2. Withdraw the two ml of locke's and place in tube and label loading solution (LS).

3. Bring PA to room temperature and add two µl to LS at 1000x dilution.

4. Cap and vortex. Vortexing give LS a soapy look.

5. Bring Fluo3 to room temperature and add four µl to LS at 500x dilution.

6. Cap and vortex.

7. Withdraw media from cells and discard.

8. Add LS to cells gently.

9. Incubate the dish for 30 minutes.

10. Withdraw LS from dish and load fresh warm locke's and incubate for 30 minutes.

11. The dish with cells is ready for imaging.

12. Potassium Chloride (KCL) - 50 mM, Glutamate - 4 mM, and Ionomycin - 2 µM

   can elicit a calcium response and is added to the dish.

APPENDIX C

DATA ANALYSIS

C.1   MATLAB program for base line correction of the measured signal.

Interactive find peaks script with peak-zoom feature, for pre-defined data in x, y.

Load a typical data set into the vectors x, y, then run this m-file and adjust the five sliders

to determine what values of the parameters give the most reliable peak detection. Peak

number and position, height, and width of each peak are returned in the matrix P.

```
formatcompact

global x

global y

globalSlopeThreshold

globalAmpThreshold

globalSmoothWidth

globalFitWidth

globalPeakNumber

global P

close

figure(1)

% Graph the signal in red

h=figure(1);

plot(x,y,'m')

h2=gca;axis([x(1) x(length(x)) min(y) max(y)]);

title('Vary the sliders to see how the parameters effect peak finding performance')

% Initial values of variable parameters
```

```
WidthPoints=10;  % Average number of points in half-width of peaks (CHANGE

TO FIT YOUR SIGNAL)

SlopeThreshold=WidthPoints^-2;

AmpThreshold=0.1*max(y);

SmoothWidth=WidthPoints/2;  %SmoothWidth should be roughly equal to 1/2

the peak width (in points)

FitWidth=WidthPoints/2; % FitWidth should be roughly equal to 1/2 the peak

widths(in points)

ifFitWidth<3,FitWidth=3;end

PeakNumber=0;

% Find and number the peaks on the graph

% type warning off MATLAB:polyfit:RepeatedPointsOrRescale

P=findpeaks(x,y,SlopeThreshold,AmpThreshold,SmoothWidth,FitWidth);

xlabel(['SlopeT = ' num2str(SlopeThreshold) '   AmpT = '

num2str(AmpThreshold) '   SmoothWidth = ' num2str(SmoothWidth) '

FitWidth = ' num2str(FitWidth) ])

text(P(:, 2),P(:, 3),num2str(P(:,1)))  % Number the peaks found on the graph

 % Maximum ranges of the sliders (change as needed)

SlopeMax=100;

SlopeMin=10^-6;

AmpMax=max(y);

AmpMin=min(y);

SmoothWidthMax=100;
```

FitWidthMax=100;

MaxPeaks=40;

% Draw the sliders

rtslid(h,@SlopeTSlider,h2,1,'Scale',[log10(SlopeMin)log10(SlopeMax)],'Def',log

10(SlopeThreshold),'Back',[0.9 0.9 0.9],'Label','SlopeT','Position',[0.03 0.5 0.03

0.35]);

rtslid(h,@AmpTSlider,h2,0,'Scale',[AmpMinAmpMax],'Def',AmpThreshold,'Bac

k',[0.9 0.9 0.9],'Label','AmpT','Position',[0.03 0.04 0.03 0.35]);

rtslid(h,@BGSlider,h2,0,'Scale',[0 1],'Def',0,'Back',[0.9 0.9

0.9],'Label','BG','Position',[0.94 0.9 0.03 0.04]);

rtslid(h,@SmoothSlider,h2,0,'Scale',[0 2],'Def',log10(SmoothWidth),'Back',[0.9

0.9 0.9],'Label','Smooth','Position',[0.94 0.32 0.03 0.2]);

rtslid(h,@FitSlider,h2,0,'Scale',[log10(3)

log10(FitWidthMax)],'Def',log10(FitWidth),'Back',[0.9 0.9

0.9],'Label','Fit','Position',[0.94 0.04 0.03 0.2]);

rtslid(h,@PeakSlider,h2,0,'Scale',[0 MaxPeaks],'Def',0,'Back',[0.9 0.9

0.9],'Label','Peak','Position',[0.94 0.6 0.03 0.22]);

And the new x and y will give the baseline corrected data. The program is obtained from Tom O'Haver (toh@umd.edu) (http://www.wam.umd.edu/~toh) at The University of Maryland at College Park.

C.2   Configuring the Digital Multimeter with NI LabVIEW Signal Express

The below specifications are obtained from the User's Guide, Agilent 34420A

Nano Volt/Micro Ohm Meter.

<u>RS-232 Interface Configuration</u>

Configure the RS-232 interface using the parameters specified below. Use the

front panel I/O MENU to select the interface to RS-232 and enter. Use the front panel I/O

MENU to select the baud rate, parity, and number of data bits.

1. Baud Rate: 9600

2. Parity and Data Bits: None/ 8 data bits

3. Number of Start Bits: 1 bit (fixed)

4. Number of Stop Bits: 2 bits (fixed)

<u>Connection to a Computer</u>

To connect the meter to a computer or terminal, a proper interface cable is

needed. Most computers and terminal are DTE (Data Terminal Equipment) devices.

Since the meter is also a DTE device, a DTE-to-DTE interface cable must be used. These

cables are also called null-modem, modem-eliminator, or crossover cables. The interface

cable must also have the proper connector on each end and the internal wiring must be

correct. Connectors typically have nine pins (DB-9 connector) or 25 pins (DB-25

connector) with a "male" or "female" pin configuration. A male connector has pins inside

the connector shell and a female connector has holes inside the connector shell.

<u>DTR/DSR Handshake Protocol</u>

The meter is configured as a DTE (Data Terminal Equipment) device and uses the

DTR (Data Terminal Ready) and DSR (Data Set Ready) lines of the RS-232 interface to

handshake. The meter uses the DTR line to send a hold-off signal. The DTR line must be TRUE before the meter will accept data from the interface. When the meter sets the DTR line FALSE, the data must cease within 10 characters.

<u>Settings for LabVIEW</u>

Install the software's below in a computer with RS-232 port and connect the cable to the meter and computer. Software's needed for installations are listed below and must be installed in the sequence.

1. Latest Agilent I/O Libraries.

2. LabVIEW.

3. NI DAQmx.

4. NI Visa.

5. Ni Device Drivers.

6. Signal Express.

7. Hp34420a driver from NI (www.ni.com).

In the measurement and automation explorer, set the COM port baud rate, parity, and number of data bits specifications similar to the settings in the meter (Section D.2.1) and save the configuration. On IVI Drivers, go to General settings and select Don't Simulate with from the popup menu and save the configuration. Open NI Signal Express and in Add Step select IVI DMM and set the COM port and Hp 34420A Driver to acquire data. Click RUN to continuously monitor the data. To see a Scope Chart, Right Click on the graph and select Scope Chart from Update Mode. Now the instrument is ready to record signals for analysis.

REFERENCES

[1]   P. Bittigau, and C. Ikonomidou, "Topical Review: Glutamate in Neurologic Diseases," *Journal of Child Neurology,* vol. 12, no. 8, pp. 471-485, November 1, 1997, 1997.

[2]   M. R. Hynd, H. L. Scott, and P. R. Dodd, "Glutamate-mediated excitotoxicity and neurodegeneration in Alzheimer's disease," *Neurochemistry International,* vol. 45, no. 5, pp. 583-595, 2004.

[3]   D. E. Bergles, and C. E. Jahr, "Glial contribution to glutamate uptake at Schaffer collateral-commissural synapses in the hippocampus," *The Journal of Neuroscience : the Official Journal of the Society for Neuroscience,* vol. 18, no. 19, pp. 7709-16, 1998.

[4]   P. P. Hsu, and D. M. Sabatini, "Cancer Cell Metabolism: Warburg and Beyond," *Cell,* vol. 134, no. 5, pp. 703-707, 2008.

[5]   P. Seguela, A. Haghighi, J. J. Soghomonian *et al.,* "A novel neuronal P2x ATP receptor ion channel with widespread distribution in the brain," *The Journal of Neuroscience : the Official Journal of the Society for Neuroscience,* vol. 16, no. 2, pp. 448-55, 1996.

[6]   M. Orlowska-Majdak, "Microdialysis of the brain structures: application in behavioral research on vasopressin and oxytocin," *Acta Neurobiol Exp (Wars),* vol. 64, no. 2, pp. 177-88, 2004.

[7]   H. Vitten, and J. S. Isaacson, "Synaptic transmission: Exciting times for presynaptic receptors," *Current Biology,* vol. 11, no. 17, pp. R695-R697, 2001.

[8]   E. R. Kandel, "The Molecular Biology of Memory Storage: A Dialogue Between Genes and Synapses," *Science,* vol. 294, no. 5544, pp. 1030-1038, 2001.

[9]   N. C. Danbolt, "Glutamate uptake," *Progress in Neurobiology,* vol. 65, no. 1, pp. 1-105, 2001.

[10]   H. S. Waagepetersen, U. Sonnewald, O. M. Larsson *et al.,* "Multiple compartments with different metabolic characteristics are involved in biosynthesis of intracellular and released glutamine and citrate in astrocytes," *Glia,* vol. 35, no. 3, pp. 246-252, 2001.

143

[12] "Alzheimer's Facts and Figures Report,"
      http://www.alz.org/alzheimers_disease_facts_and_figures.asp, [September 2,
      2011, 2011].

[13] P. G. Haydon, and G. Carmignoto, "Astrocyte control of synaptic transmission
      and neurovascular coupling," *Physiological Reviews*, vol. 86, no. 3, pp. 1009-
      1031, 2006.

[14] S. Vesce, D. Rossi, L. Brambilla *et al.*, "Glutamate Release from Astrocytes in
      Physiological Conditions and in Neurodegenerative Disorders Characterized by
      Neuroinflammation," *International Review of Neurobiology*, 2007, pp. 57-71.

[15] A. Araque, G. Carmignoto, and P. G. Haydon, "Dynamic signaling between
      astrocytes and neurons," *Annual Review of Physiology*, 2001, pp. 795-813.

[16] M. Nedergaard, B. Ransom, and S. A. Goldman, "New roles for astrocytes:
      Redefining the functional architecture of the brain," *Trends in Neurosciences*, vol.
      26, no. 10, pp. 523-530, 2003.

[17] H. Sontheimer, "A role for glutamate in growth and invasion of primary brain
      tumors," *Journal of Neurochemistry*, vol. 105, no. 2, pp. 287-295, 2008.

[18] Y. Hu, K. M. Mitchell, F. N. Albahadily *et al.*, "Direct measurement of glutamate
      release in the brain using a dual enzyme-based electrochemical sensor," *Brain
      Research*, vol. 659, no. 1-2, pp. 117-125, 1994.

[19] M. D'Onofrio, A. Arcella, V. Bruno *et al.*, "Pharmacological blockade of
      mGlu2/3 metabotropic glutamate receptors reduces cell proliferation in cultured
      human glioma cells," *Journal of Neurochemistry*, vol. 84, no. 6, pp. 1288-1295,
      2003.

[20] S. A. Lyons, W. J. Chung, A. K. Weaver *et al.*, "Autocrine glutamate signaling
      promotes glioma cell invasion," *Cancer Research*, vol. 67, no. 19, pp. 9463-9471,
      2007.

[21] S. Yoshida, and S. Plant, "Mechanism of release of Ca2+ from intracellular stores
      in response to ionomycin in oocytes of the frog Xenopus laevis," *The Journal of
      Physiology*, vol. 458, no. 1, pp. 307-318, December, 1992.

[22] B. Alberts, *Molecular Biology of the Cell*, 4th ed., New York: Garland Science,
      2002.

[23] S. K. Marie, and S. M. Shinjo, "Metabolism and brain cancer," *Clinics (Sao
      Paulo)*, vol. 66 Suppl 1, pp. 33-43, 2011.

[24]   F. W. Scheller, R. Hintsche, D. Pfeiffer *et al.*, "Biosensors: Fundamentals, applications and trends," *Sensors and Actuators B: Chemical*, vol. 4, no. 1-2, pp. 197-206, 1991.

[25]   O. Niwa, R. Kurita, T. Horiuchi *et al.*, "Continuous Monitoring of <FONT SIZE='-2'>L</FONT>-Glutamate Released from Cultured Rat Nerve Cells with a Microfabricated On-Line Sensor at a Slow Flow Rate," *Electroanalysis*, vol. 11, no. 5, pp. 356-361, 1999.

[26]   J. Castillo, A. Blöchl, S. Dennison *et al.*, "Glutamate detection from nerve cells using a planar electrodes array integrated in a microtiter plate," *Biosensors and Bioelectronics*, vol. 20, no. 10, pp. 2116-2119, 2005.

[27]   R.-a. Doong, and H.-m. Shih, "Glutamate optical biosensor based on the immobilization of glutamate dehydrogenase in titanium dioxide sol-gel matrix," *Biosensors and Bioelectronics*, vol. 22, no. 2, pp. 185-191, 2006.

[28]   K. Hayashi, R. Kurita, T. Horiuchi *et al.*, "Selective detection of -glutamate using a microfluidic device integrated with an enzyme-modified pre-reactor and an electrochemical detector," *Biosensors and Bioelectronics*, vol. 18, no. 10, pp. 1249-1255, 2003.

[29]   W. H. Oldenziel, G. Dijkstra, T. I. F. H. Cremers *et al.*, "*In vivo* monitoring of extracellular glutamate in the brain with a microsensor," *Brain Research*, vol. 1118, no. 1, pp. 34-42, 2006.

[30]   W. H. Oldenziel, G. Dijkstra, T. I. F. H. Cremers *et al.*, "Evaluation of Hydrogel-Coated Glutamate Microsensors," *Analytical Chemistry*, vol. 78, no. 10, pp. 3366-3378, 2006.

[31]   O. Niwa, T. Horiuchi, and K. Torimitsu, "Continuous monitoring of L-glutamate released from cultured nerve cells by an online sensor coupled with micro-capillary sampling," *Biosensors and Bioelectronics*, vol. 12, no. 4, pp. 311-319, 1997.

[32]   A. Hirano, and M. Sugawara, "Receptors and enzymes for medical sensing of L-glutamate," *Mini Rev Med Chem*, vol. 6, no. 10, pp. 1091-100, Oct, 2006.

[33]   W. J. Albery, M. G. Boutelle, and P. T. Galley, "The dialysis electrode-a new method for *in vivo* monitoring," *Journal of the Chemical Society, Chemical Communications*, no. 12, pp. 900-901, 1992.

[34]   M. C. Walker, P. T. Galley, M. L. Errington *et al.*, "Ascorbate and Glutamate Release in the Rat Hippocampus After Perforant Path Stimulation: A "Dialysis Electrode" Study," *Journal of Neurochemistry*, vol. 65, no. 2, pp. 725-731, 1995.

[35] S. Asai, Y. Iribe, T. Kohno *et al.*, "Real time monitoring of biphasic glutamate release using dialysis electrode in rat acute brain ischemia," *NeuroReport,* vol. 7, no. 5, pp. 1092-1096, 1996.

[36] T. Kohno, S. Asai, Y. Iribe *et al.*, "An improved method for the detection of changes in brain extracellular glutamate levels," *Journal of Neuroscience Methods,* vol. 81, no. 1-2, pp. 199-205, 1998.

[37] K. Nakajima, T. Yamagiwa, A. Hirano *et al.*, "A glass capillary microelectrode based on capillarity and its application to the detection of L-glutamate release from mouse brain slices," *Analytical sciences : the international journal of the Japan Society for Analytical Chemistry,* vol. 19, no. 1, pp. 55-60, 2003.

[38] E. Zilkha, T. P. Obrenovitch, A. Koshy *et al.*, "Extracellular glutamate: on-line monitoring using microdialysis coupled to enzyme-amperometric analysis," *Journal of Neuroscience Methods,* vol. 60, no. 1-2, pp. 1-9, 1995.

[39] O. Niwa, K. Torimitsu, M. Morita *et al.*, "Concentration of extracellular l-glutamate released from cultured nerve cells measured with a small-volume online sensor," *Analytical Chemistry,* vol. 68, no. 11, pp. 1865-1870, 1996.

[40] J. Castillo, A. Blochl, S. Dennison *et al.*, "Glutamate detection from nerve cells using a planar electrodes array integrated in a microtiter plate," *Biosensors and Bioelectronics,* vol. 20, no. 10, pp. 2116-2119, 2005.

[41] Y. Kasai N Fau - Jimbo, K. Jimbo Y Fau - Torimitsu, and K. Torimitsu, "Electrochemical monitoring of glutamate release at multiple positions in a rat hippocampal slice," no. 0910-6340, 2002.

[42] N. V. Kulagina, L. Shankar, and A. C. Michael, "Monitoring Glutamate and Ascorbate in the Extracellular Space of Brain Tissue with Electrochemical Microsensors," *Analytical Chemistry,* vol. 71, no. 22, pp. 5093-5100, 1999.

[43] B. Wolf, M. Brischwein, W. Baumann *et al.*, "Microsensor-aided measurements of cellular signalling and metabolism on tumor cells. The cell monitoring system (CMSÂ®)," *Tumor Biology,* vol. 19, no. 5, pp. 374-383, 1998.

[44] A. M. Otto, M. Brischwein, E. Motrescu *et al.*, "Analysis of Drug Action on Tumor Cell Metabolism Using Electronic Sensor Chips," *Archiv der Pharmazie,* vol. 337, no. 12, pp. 682-686, 2004.

[45] B. Z. Chowdhry, A. E. Beezer, and E. J. Greenhow, "Analysis of drugs by microcalorimetry: Isothermal power-conduction calorimetry and thermometric titrimetry," *Talanta,* vol. 30, no. 4, pp. 209-243, 1983.

[46] R. B. Kemp, "Developments in cellular microcalorimetry with particular emphasis on the valuable role of the energy (enthalpy) balance method," *Thermochimica Acta,* vol. 219, no. 0, pp. 17-41, 1993.

[47] T. Maskow, J. Lerchner, M. Peitzsch *et al.,* "Chip calorimetry for the monitoring of whole cell biotransformation," *Journal of Biotechnology,* vol. 122, no. 4, pp. 431-442, 2006.

[48] E. A. Johannessen, J. M. R. Weaver, L. Bourova *et al.,* "Micromachined Nanocalorimetric Sensor for Ultra-Low-Volume Cell-Based Assays," *Analytical Chemistry,* vol. 74, no. 9, pp. 2190-2197, 2002.

[49] J. Lerchner, A. Wolf, G. Wolf *et al.,* "A new micro-fluid chip calorimeter for biochemical applications," *Thermochimica Acta,* vol. 445, no. 2, pp. 144-150, 2006.

[50] N. Xia, T. P. Hunt, B. T. Mayers *et al.,* "Combined microfluidic-micromagnetic separation of living cells in continuous flow," *Biomed Microdevices,* Sep 25, 2006.

[51] N. Crews, C. Wittwer, R. Palais *et al.,* "Product differentiation during continuous-flow thermal gradient PCR," *Lab on a Chip,* vol. 8, no. 6, pp. 919-24, Jun, 2008.

[52] M. J. Muehlbauer, E. J. Guilbeau, and B. C. Towe, "Applications and stability of a thermoelectric enzyme sensor," *Sensors & Actuators: B. Chemical,* vol. 2, no. 3, pp. 223-232, 1990.

[53] Y. Zhang, and S. Tadigadapa, "Calorimetric biosensors with integrated microfluidic channels," *Biosensors and Bioelectronics,* vol. 19, no. 12, pp. 1733-1743, 2004.

[54] W. Lee, W. Fon, B. W. Axelrod *et al.,* "High-sensitivity microfluidic calorimeters for biological and chemical applications," *Proceedings of the National Academy of Sciences,* vol. 106, no. 36, pp. 15225-15230, Sep 8, 2009.

[55] S. M. Tangutooru, V. L. Kopparthy, G. G. Nestorova *et al.,* "Dynamic thermoelectric glucose sensing with layer-by-layer glucose oxidase immobilization," *Sensors and Actuators B: Chemical,* pp no. 637-641, 2012.

[56] P. Bataillard, E. Steffgen, S. Haemmerli *et al.,* "An integrated silicon thermophile as biosensor for the thermal monitoring of glucose, urea and penicillin," *Biosens Bioelectron,* vol. 8, no. 2, pp. 89-98, 1993.

[57] G. G. Nestorova, and E. J. Guilbeau, "Thermoelectric method for sequencing DNA," *Lab on a Chip,* vol. 11 no. 10, pp. 1761-1769, 2011.

[58]   X. Yang, L. Hua, H. Gong *et al.*, "Covalent immobilization of an enzyme (glucose oxidase) onto a carbon sol-gel silicate composite surface as a biosensing platform," *Analytica Chimica Acta,* vol. 478, no. 1, pp. 67-75, 2003.

[59]   C. Pizarro, M. A. Fernández-Torroba, C. Benito *et al.*, "Optimization by experimental design of polyacrylamide gel composition as support for enzyme immobilization by entrapment," *Biotechnology and Bioengineering,* vol. 53, no. 5, pp. 497-506, 1997.

[60]   S. Cosnier, "Biomolecule immobilization on electrode surfaces by entrapment or attachment to electrochemically polymerized films. A review," *Biosensors and Bioelectronics,* vol. 14, no. 5, pp. 443-456, 1999.

[61]   M. J. Muehlbauer, E. J. Guilbeau, B. C. Towe *et al.*, "Thermoelectric enzyme sensor for measuring blood glucose," *Biosensors and Bioelectronics,* vol. 5, no. 1, pp. 1-12, 1990.

[62]   Y. Lvov, K. Ariga, I. Ichinose *et al.*, "Assembly of Multicomponent Protein Films by Means of Electrostatic Layer-by-Layer Adsorption," *Journal of the American Chemical Society,* vol. 117, no. 22, pp. 6117-6123, 2002.

[63]   S. Kar, and M. A. Arnold, "Fiber-optic ammonia sensor for measuring synaptic glutamate and extracellular ammonia," *Analytical Chemistry,* vol. 64, no. 20, pp. 2438-2443, 1992.

[64]   Y. Lvov, K. Ariga, M. Onda *et al.*, "A careful examination of the adsorption step in the alternate layer-by-layer assembly of linear polyanion and polycation," *Colloids and Surfaces A: Physicochemical and Engineering Aspects,* vol. 146, no. 1-3, pp. 337-346, 1999.

[65]   Y. Lvov, *Protein Architecture: Interfacial Molecular Assembly and Immobilization Biotechnology,* p., pp. 125-136, NY: Marcel Dekker Publ, 2000.

[66]   T. H. Park, and M. L. Shuler, "Integration of cell culture and microfabrication technology," *Biotechnol Prog,* vol. 19, no. 2, pp. 243-53, Mar-Apr, 2003.

[67]   S. N. Bhatia, M. L. Yarmush, and M. Toner, "Controlling cell interactions by micropatterning in co-cultures: Hepatocytes and 3T3 fibroblasts," *Journal of Biomedical Materials Research,* vol. 34, no. 2, pp. 189-199, 1997.

[68]   S. Britland, E. Perez-Arnaud, P. Clark *et al.*, "Micropatterning Proteins and Synthetic Peptides on Solid Supports: A Novel Application for Microelectronics Fabrication Technology," *Biotechnology Progress,* vol. 8, no. 2, pp. 155-160, 1992.

[69]   B. Lom, K. E. Healy, and P. E. Hockberger, "A versatile technique for patterning biomolecules onto glass coverslips," *J Neurosci Methods,* vol. 50, no. 3, pp. 385-97, Dec, 1993.

[70]   M. Mrksich, C. S. Chen, Y. Xia *et al.,* "Controlling cell attachment on contoured surfaces with self-assembled monolayers of alkanethiolates on gold," *Proc Natl Acad Sci U S A,* vol. 93, no. 20, pp. 10775-8, Oct 1, 1996.

[71]   M. Mrksich, L. E. Dike, J. Tien *et al.,* "Using Microcontact Printing to Pattern the Attachment of Mammalian Cells to Self-Assembled Monolayers of Alkanethiolates on Transparent Films of Gold and Silver," *Experimental Cell Research,* vol. 235, no. 2, pp. 305-313, 1997.

[72]   S. Takayama, J. C. McDonald, E. Ostuni *et al.,* "Patterning cells and their environments using multiple laminar fluid flows in capillary networks," *Proceedings of the National Academy of Sciences,* vol. 96, no. 10, pp. 5545-5548, May 11, 1999.

[73]   S. Takayama, E. Ostuni, X. Qian *et al.,* "Topographical Micropatterning of Poly(dimethylsiloxane) Using Laminar Flows of Liquids in Capillaries," *Advanced Materials,* vol. 13, no. 8, pp. 570-574, 2001.

[74]   S. Takayama, E. Ostuni, P. LeDuc *et al.,* "Subcellular positioning of small molecules," *Nature,* vol. 411, no. 6841, pp. 1016, Jun 28, 2001.

[75]   S. B. Carter, "Haptotactic islands: a method of confining single cells to study individual cell reactions and clone formation," *Exp Cell Res,* vol. 48, no. 1, pp. 189-93, Oct, 1967.

[76]   Y. Jimbo, H. P. Robinson, and A. Kawana, "Simultaneous measurement of intracellular calcium and electrical activity from patterned neural networks in culture," *IEEE Trans Biomed Eng,* vol. 40, no. 8, pp. 804-10, Aug, 1993.

[77]   A. Folch, B.-H. Jo, O. Hurtado *et al.,* "Microfabricated elastomeric stencils for micropatterning cell cultures," *Journal of Biomedical Materials Research,* vol. 52, no. 2, pp. 346-353, 2000.

[78]   S. W. Rhee, A. M. Taylor, C. H. Tu *et al.,* "Patterned cell culture inside microfluidic devices," *Lab on a Chip,* vol. 5, no. 1, pp. 102-107, 2005.

[79]   T. M. Squires, and S. R. Quake, "Microfluidics: Fluid physics at the nanoliter scale," *Reviews of Modern Physics,* vol. 77, no. 3, pp. 977-1026, 2005.

[80]   Y. Xia, and G. M. Whitesides, "SOFT LITHOGRAPHY," *Annual Review of Materials Science,* vol. 28, no. 1, pp. 153-184, 1998.

[81] H. Becker, and U. Heim, "Hot embossing as a method for the fabrication of polymer high aspect ratio structures," *Sensors and Actuators A: Physical,* vol. 83, no. 1-3, pp. 130-135, 2000.

[82] S. J. Pearton, C. R. Abernathy, F. Ren *et al.,* "Dry and wet etching characteristics of InN, AlN, and GaN deposited by electron cyclotron resonance metalorganic molecular beam epitaxy," *Journal of Vacuum Science & Technology A: Vacuum, Surfaces, and Films,* vol. 11, no. 4, pp. 1772-1775, 1993.

[83] D. A. Bartholomeusz, R. W. Boutte, and J. D. Andrade, "Xurography: rapid prototyping of microstructures using a cutting plotter," *Journal of Microelectromechanical Systems,* vol. 14, no. 6, pp. 1364-1374, 2005.

[84] C. Loesberg, J. C. van Miltenburg, and R. van Wuk, "Heat production of mammalian cells at different cell-cycle phases," *Journal of Thermal Biology,* vol. 7, no. 4, pp. 209-213, 1982.

[85] J. r. Nittinger, L. Tejmar-Kolar, and P. Furst, "Microcalorimetric investigations on human leukemia cells-Molt 4," *Biology of the Cell,* vol. 70, no. 3, pp. 139-142, 1990.

[86] R. van Wijk, J. Souren, D. H. J. Schamhart *et al.,* "Comparative Studies of the Heat Production of Different Rat Hepatoma Cells in Culture," *Cancer Research,* vol. 44, no. 2, pp. 671-673, February 1, 1984.

[87] S. E. Hoffner, R. W. Meredith, and R. B. Kemp, "Estimation of heat production by cultured cells in suspension using semi-automated flow microcalorimetry," *Cytobios,* vol. 42, no. 166, pp. 71-80, 1985.

[88] G. G. Nestorova, and E. J. Guilbeau, "Thermoelectric method for sequencing DNA," *Lab on a Chip,* vol. 11, no. 10, pp. 1761-1769, 2010.

[89] N. A. Kotov, "Layer-by-layer self-assembly: The contribution of hydrophobic interactions," *Nanostructured Materials,* vol. 12, no. 5-8, pp. 789-796, 1999.

[90] Y. Lvov, and F. Caruso, "Biocolloids with Ordered Urease Multilayer Shells as Enzymatic Reactors," *Analytical Chemistry,* vol. 73, no. 17, pp. 4212-4217, 2001.

[91] G. Z. Sauerbrey, "Use of quartz crystal vibrator for weighting thin films on a microbalance" *Physics,* vol. 155, pp. 206-222, 1959.

[92] J. R. Tennant, "Evaluation of the Trypan Blue Technique for Determination of Cell Viability," *Transplantation,* vol. 2, no. 6, pp. 685-694, 1964.

[93] Y. Su, R. Whan, C. Empsen *et al.*, "Microscopy: Science, Technology, Applications and Education," *Multidimensional Live Cell Imaging of Cancer-Mediated Events*, pp. 2050-2061: Formatex Research Center, 2010.

[94] S. Hamada, and S. Fujita, "DAPI staining improved for quantitative cytofluorometry," *Histochemistry*, vol. 79, no. 2, pp. 219-26, 1983.

[95] L. D. Plant, J. P. Boyle, I. F. Smith *et al.*, "The production of amyloid beta peptide is a critical requirement for the viability of central neurons," *Journal of Neuroscience*, vol. 23, no. 13, pp. 5531-5, Jul 2, 2003.

[96] V. Parpura, and P. G. Haydon, "Physiological astrocytic calcium levels stimulate glutamate release to modulate adjacent neurons," *Proceedings of the National Academy of Sciences of the United States of America*, vol. 97, no. 15, pp. 8629-8634, July 18, 2000.

[97] J. P. Kao, A. T. Harootunian, and R. Y. Tsien, "Photochemically generated cytosolic calcium pulses and their detection by fluo-3," *Journal of Biological Chemistry*, vol. 264, no. 14, pp. 8179-84, May 15, 1989.

[98] W. B. Stallcup, "Sodium and calcium fluxes in a clonal nerve cell line," *Journal of Physiology*, vol. 286, pp. 525-40, Jan, 1979.

[99] J. Shaikh Mohammed, M. A. DeCoster, and M. J. McShane, "Micropatterning of Nanoengineered Surfaces to Study Neuronal Cell Attachment *in Vitro*," *Biomacromolecules*, vol. 5, no. 5, pp. 1745-1755, 2004.

[100] T. Sordel, F. Kermarec-Marcel, S. Garnier-Raveaud *et al.*, "Influence of glass and polymer coatings on CHO cell morphology and adhesion," *Biomaterials*, vol. 28, no. 8, pp. 1572-1584, 2007.

[101] F. Incropera, and D. DeWitt, *Fundamentals of Heat and Mass Transfer, 5th Edition*: Wiley, 2001.

[102] B. C. Towe, and E. J. Guilbeau, "A vibrating probe thermal biochemical sensor," *Biosensors and Bioelectronics*, vol. 11, no. 3, pp. 247-252, 1996.

[103] S. K. Kanakamedala, "Passive micromixers and organic electrochemical transistors for biosensor applications," Dissertation, Biomedical Engineering; Electrical Engineering; Nanotechnology, Louisiana Tech University, Ruston, 2011.